Master Thesis, Department of Geosciences

Repeatability and Detectability Requirements for 4D CSEM

Sensitivity analysis, inversion-based analysis and interpretation of 4D CSEM data to determine the minimum detectable depletion in hydrocarbon reservoir

Amir Babakhani

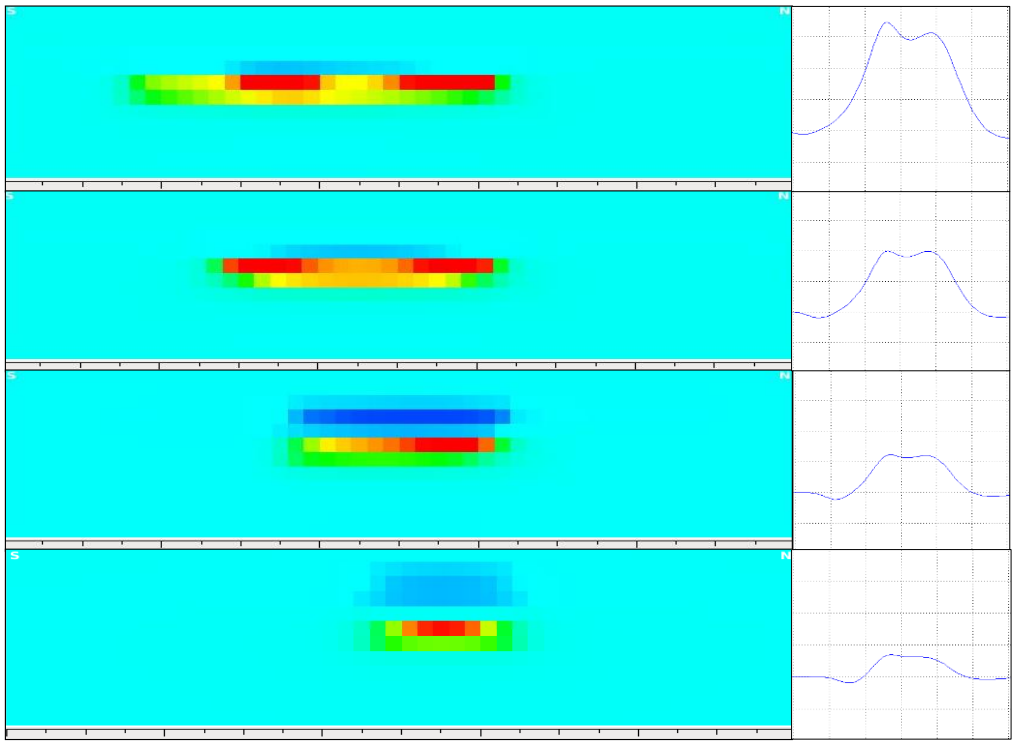

UNIVERSITY OF OSLO

FACULTY OF MATHEMATICS AND NATURAL SCIENCES

Repeatability and Detectability Requirements for 4D CSEM Surveys

Sensitivity analysis, inversion-based analysis and interpretation of 4D CSEM data to determine the minimum detectable depletion in hydrocarbon reservoir

Amir Babakhani

Master Thesis in Geosciences

Discipline: Geophysics

Department of Geosciences

Faculty of Mathematics and Natural Sciences

University of Oslo

June, 2015

Acknowledgments

Many thanks to my supervisor Professor Leiv Jacob Gelius who guided me through the start of the project .Special thanks to my co-supervisor Dr Daniil Shantsev for his contribution and fruitful discussions during this study. He is also much appreciated for providing me access to the EMGS's data and software.

I am indebted to Professor Valerie Maupen who reviewed and emendated the thesis. I would like also to acknowledge the support and help I received from my family, friends and colleagues at the department of Geoscience; university of Oslo, particularly Rohaldin Miri, Mohammad KoochakZadeh and Sigurd Eide for their continuous support and encouragement.

Amir Babakhani
May 31, 2015

Abstract

It has already been demonstrated that marine controlled source electromagnetic (CSEM) method can have sufficient sensitivity for time-lapse applications and can detect variations in a hydrocarbon reservoir due to production over a few years. A key question for 4D studies is repeatability of the base and monitoring surveys. So far all published analyses of repeatability requirements 4D CSEM include only evaluation of the direct effects of the acquisition parameters on the electromagnetic data. This implies that the analysis of 4D data is performed in the data domain by looking at differences in the measured fields. At the same time, the most efficient method to extract value from CSEM data is by inversion for subsurface resistivity. Therefore, we are going to determine the repeatability requirements for 4D CSEM surveys in the model domain, by looking at differences in the inversion results. We consider two of the main causes leading to non-repeatability of the 4D EM data: change of water conductivity and variation of receiver positions from the base to monitoring surveys the minimum detectable depletion (MDD) of a hydrocarbon reservoir in time-lapse CSEM operations.

A controlled (synthetic) test data associated with two reservoir models is generated. A sensitivity analysis was carried out on a 2.5D base model to determine the MDD of the assumed hydrocarbon reservoir for different values of frequency. The results showed the MDD is approximately 2% when the water conductivity changed by 4.5% from base to the monitoring survey. The MDD is ~5%, when the receiver positions changed by 100 m along the receiver lines. Then, different 2.5D inversions were run on the inline electrical data for cases of full and depleted reservoirs. Also, inversions were run for the full reservoir case, while changing the water conductivity or receiver positions. The background resistivity was constrained within ±25% of the true value in the base-survey inversion and then fixed, in the monitoring-survey inversion. We also assumed a 10% error for the background resistivity of the start model, and this did not affect the MDD value significantly. Analysis of average reservoir resistivity derived from inversions indicated that MDD was approximately 1%, i.e. allows one to detect two times smaller changes in the reservoir as compared to the standard sensitivity analysis in the data domain in terms of variation of water conductivity and five times in terms of variation of receiver positions.

Table of Contents

List of Figures

List of Tables

Chapter 1 Introduction

1.1 Controlled-Source Electromagnetic (CSEM)

The Controlled Source Electromagnetic (CSEM) method is geophysical exploration technique which employs electromagnetic remote-sensing technology to specify the existence and extent of hydrocarbon reservoirs. The CSEM method introduced as a tool for hydrocarbon reservoir detection more than a decade ago (Ellingsrud et al., 2002) and estimates the resistivity of geological structures through the measurement of induced electric and magnetic fields. To discover HC reservoirs, the seismic methods are the common choice, however the interpretation of seismic data in marine environments is challenging. Utilizing exclusively the seismic method, recognition of fluid content in the host rocks is not easy as the sensitivity of the seismic velocity wave and density to variations in fluid saturation is very poor. In addition, in marine environments, it is very common to have layers with very high resistivity similar to HC layers or even higher in resistivity (i.e. tight limestone carbonate reefs, volcanic cover and salt), which are very unlikely to be detected by seismic techniques. Since discrimination of pore fluid content will be closer (Wang et al., 2008), the application of CSEM for oil exploration and also monitoring purposes has rapidly increased. Moreover, as the electromagnetic data are more sensitive to hydrocarbons than the seismic data, the CSEM method serves as a complementary method to seismic.

Due to close relation between fluid saturation and electric conductivity, the CSEM method can discriminate between brine and resistive layers in the subsurface (Lien and Mannseth, 2008). To detect the resistivity of a layer, the relative increment of the lateral magnetic component of electromagnetic signal will record through several resistors located at the seafloor. In addition, there is a transmitter which emits a periodic signal with different values of frequencies (Zach et al., 2009).

Another marine electromagnetic technique which is currently in use for hydrocarbon exploration is magnetotelluric (MT) method. MT is very sensitive to large conductive features making it useful in mapping background resistivity as well as location of large structures, such as basement, salt and carbonates. Using this method, the investigation of depth from 300 m to hundreds of kilometers will be possible. The natural variations of electromagnetic field over several days (Barker et al., 2012) give the Magnetotelluric data. While the MT method

uses natural electromagnetic variations of source, CSEM uses a controlled (known) variation of source (Pankratov and Geraskin, 2010). The MT method has been used for many years onshore, allowing for the progress of the theory behind the methods. MT data quality depends on source signal strength, duration of survey, noise, water depth, successful measurements of electric and magnetic data, effectiveness of robust processing and etc. (Gelius, 2010).

1.2 CSEM Applications

The marine controlled-source electromagnetic (CSEM) is a marine geophysical method and is carried out for mapping the resistivity and it can possibly identify hydrocarbon reservoirs supported by seismic surveying data. The seismic technique is susceptible on delineating geological structures and is commonly used to develop geological models of structure and stratigraphy, while the CSEM method depends on the existence of transverse resistivity anomalies defined by Rt =Δ ρ. Δz (Orange et al., 2009) where ρ is resistivity and Δz is thickness of the reservoir. The seismic and CSEM methods are sensitive to different medium attributes where the Figure 1.1 shows this difference. The seismic method detects changes in density and wave velocity, while the CSEM method detects changes in the electric conductivity or its inverse, resistivity (Constable, 2006).

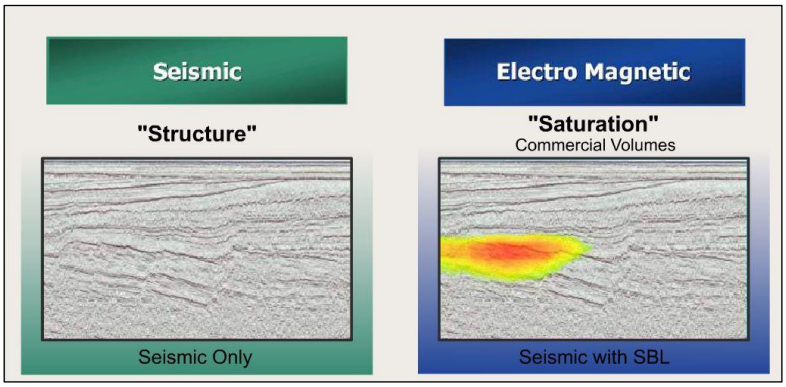

Figure 1. 1: CSEM and seismic can be regarded as complementary methods (Gelius, 2010).

One of the reasons that advantages of CSEM compared to seismic is that it can easily distinguish water from oil as a pore fluid (Constable, 2006). Generally, the method is more sensitive to saturations than seismic. The use of marine CSEM has been motivated by the particular sensitivity of seismic method to trace amounts of gas in the pore fluid ("fizz-gas"). Figure 1.2 shows the case of monitoring a brine-gas reservoir.

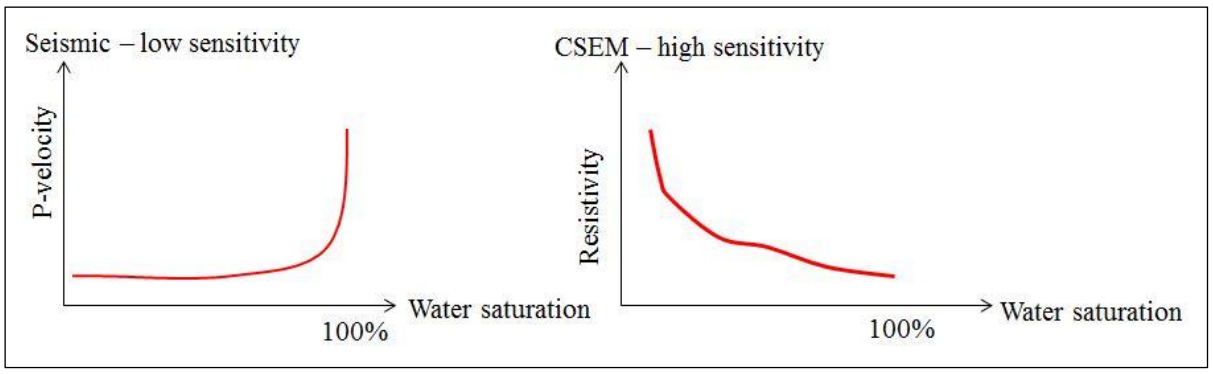

Figure 1. 2: Sensitivity to water saturation (Gelius, 2010).

As has been shown in Figure 1.2, the resistivity changes smoothly with increasing the water saturation, whereas the seismic method has no resolving power. The reservoir resistivity depends on different factors as shown in Figure 1.3. As an example, the resistivity decreases with increasing water content and increases with increasing hydrocarbon content.

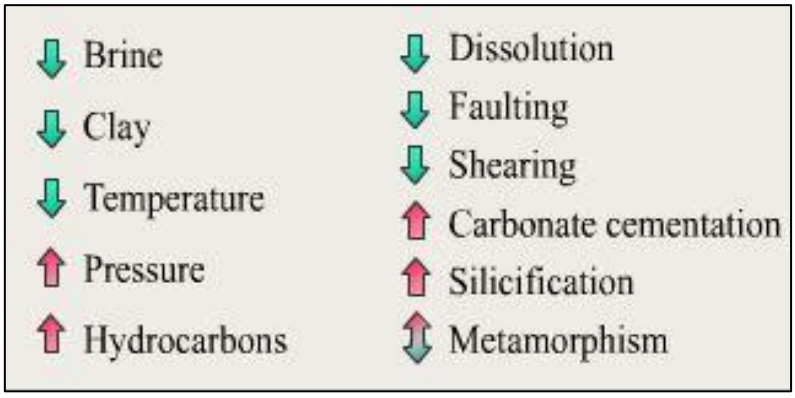

Figure 1. 3: Sensitivity to reservoir resistivity (Gelius, 2010).

Figure 1.4 shows schematics of a CSEM survey with a vessel towing the horizontal electric dipole (HED) antenna and with measurement nodes deployed on the bottom. In addition, the contribution from MT is included. This movable horizontal electric dipole (HED) is used as a transmitter and emits periodic and alternating current that operates with a frequency between 0.1 and 10 Hz. This transmitter is towed 10 to 50 m above the seabed to maximize the energy that goes to the seafloor rocks and sediments and minimize coupling with the air. An array of stationary EM receivers deployed on the sea bottom and records the time-varying source signal. Typically, these receivers include electric and magnetic sensors.

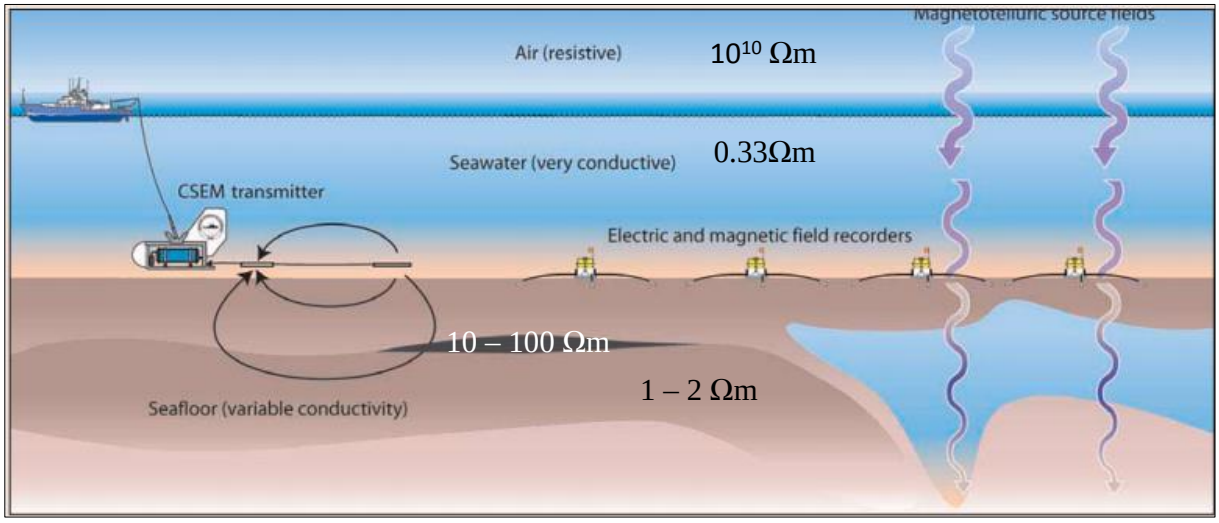

Figure 1. 4: Schematic diagram of a typical marine CSEM survey, modified from (Constable, 2006).

The possible main contributions associated with a CSEM are shown in Figure 1.5. In the following, we assume deep water (about 300 m and above). In case of shallow water (less than 200 m) the air wave starts to dominate small and intermediate offsets. The direct wave is dominated at short offset which is wave number 1 in the following figure. Then, wave number 2 (Figure 1.5) comes which is the guide wave from the reservoir and dominates intermediate offsets (e.g. subsurface energy). The guide wave is attenuated much less while inside the reservoir than an EM wave propagating in the surrounding medium. Finally, wave number 3 represents the air wave which propagates in the air and reaches down to the receivers. Actually, in case of deeper water the guided mode can be detected at an offset typically about 2-3 times the depth of target. At such an offset, the direct mode will have been so attenuated by diffusion through the water layer that the guided mode will start to dominate. By increasing the offset, the contribution from the airwaves will start to be significant and eventually dominate. But in case of shallow water the airwave will also dominate at smaller and intermediate offsets and mask more or less the guided-more responses. Briefly speaking, the effect of air wave in CSEM method is very important and can influence the data recorded from the field.

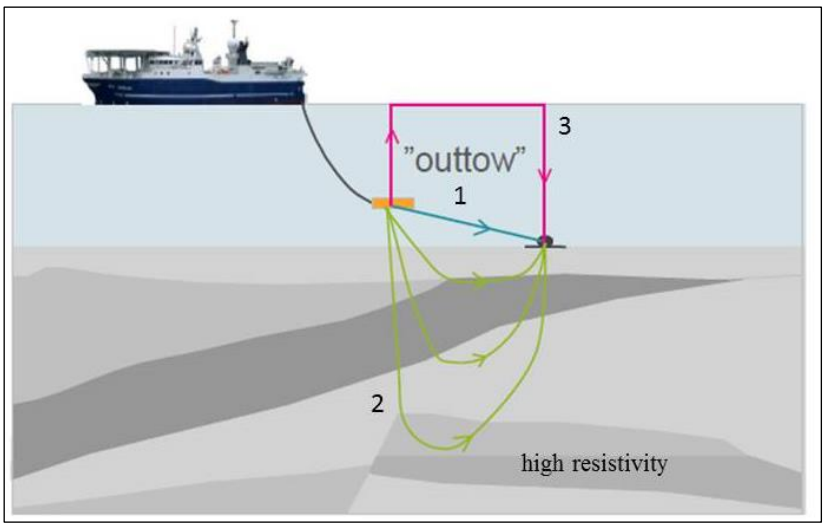

Figure 1. 5:Main contribution in CSEM, modified from (Linus Boman, 2014).

The Figure 1.6 shows the magnitude versus offset (MVO) curve. This figure shows the comparison between inline electric data (Ex) when the data has been recorded in 1D and 2D domain. A large offset range (15 km) has been considered in this figure. Since the CSEM data is profoundly lessened through the subsurface spread, the MVO curve is typically plotted in logarithmic scale (i.e. $\log_{10}$) with a dynamic scope of e.g. 10^{-15} to 10^{-5} V/Am^2 (Park et al., 2010). The bends on the both sides of Figure 1.6 show the effect of airwave. On the right side, the break indicates the existing of a resistive layer. Other factors which can influence CSEM can be near-surface effect, overburden pressure, water conductivity and perturbation of receivers. In this thesis, the focus is mostly on the effect of changing of water conductivity and receiver positions.

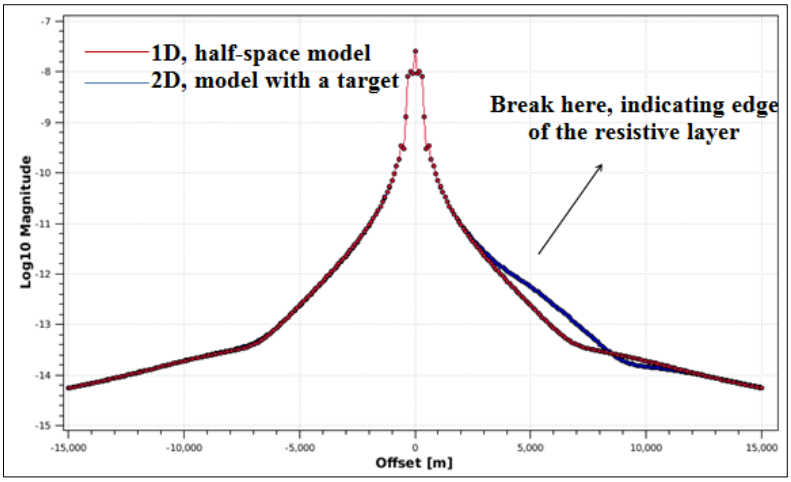

Figure 1. 6: The magnitude versus offset (MVO) electric data for one receiver.

1.3 Brief History

Much of the early marine EM technology grew in the 1950s and 1960s. But utilizing the method in hydrocarbon exploration dates back to the beginning of the twentieth century (Constable, 2006). The academic institutes and production industries were interested in submarine and mine detection by using low frequency waves to discover the geological structure under the deep water. In the early 1960s, a group of Charles Cox and Jean Filloux developed the materiel for MT and CSEM soundings. Between 1961 and 1965, they worked on deep seafloor and developed both electric and magnetic field records in 4000 m water at a distance of 650 km from coast (Filloux, 1967). At 1967, The Scripps Institution of Oceanography (SIO), the University of Toronto, the University of Cambridge and Southampton developed a marine MT system which was able to record electric fields at full water depth by using the frequency below 10^{-3} Hz (Filloux, 1967). The developed MT method takes a planar geometry to the EM fields that propagate downward to the Earth's surface and therefore MT is a useful tool for regional mapping. The data from electric and magnetic fields have been recorded. The electrical properties of the geology for a particular area can be found from these fields. Later, in 1980 Cox proposed the use of electric and magnetic waves to study seafloor geology (Constable, 2010).

Although, the exploration at deep water started in the late 1990s, and the production started in the early 21st century, but before that, the former Soviet Union had used the electromagnetic method for oil and gas exploration on land (Fonarev, 1982).

CSEM data is acquired in the time-domain and transformed in the frequency-domain for advanced processing, inversion and interpretation. The receiver times series can be transformed from the frequency-domain via a discrete time short time Fourier transform (STFT). After processing to the frequency-domain, the fields are used to make an impedance tensor, which allows getting the interpretation of electrical conductivity as a function of depth as well as position for arrays of stations. For CSEM exploration it has been developed a deep-towed Horizontal Electric Dipole (HED) transmitter which can be detected by either inline or broadside configuration(Constable, 2006).

Over the years, the Marine EM Labs have developed the HED source transmitter, receiver instrumentation and software for the CSEM method, where these receivers are able to record

the frequencies between 0.0001 to 100 Hz. In CSEM method the receivers are deployed first and will be on the sea floor while the transmitter is towed 30 - 100m above the receivers.

This method developed as academic tools to study the oceanic lithosphere and mantle between 1980-1990's. An effective and perfect investigation of the CSEM method has been down by Chave (1991) which is still credible (Mehta et al., 2005). And some of the institutes which have dealt with this method are University of Southampton and Schripps, University of Toronto and Woods Hole (Gelius, 2010).

Recently, improvements in toll, computational power, modeling and inversion have allowed for commercial development of the marine CSEM method production industry and marine hydrocarbon detection are interesting in this method and that's why that the method has received support. A number of companies are now providing this service. Some of the companies which had cooperation with academic centers and universities in this time were Statoil and ExxonMobil and then in 2002 this method has followed and developed by ElectroMagnetic GeoServices ASA (EMGS) and some small companies like Atlas Iron Limited (AGO) (Gelius, 2010).

1.4 Time-lapse method (4D)

The 4^{th} dimension is reflecting that a measurement has been repeated several times. Changes in response between the measurements are denoted 4D response (or time lapse response). Typically, the main objective in a 4D study is not to optimize the individual measurements with respect to 3D imaging, but to optimize the imaging of changes that have occurred over time.

1.4.1 4D Seismic

4D reservoir monitoring technique is based on analysis of repeated 3D seismic vintages over a definite time span. Studying the attributes differences caused by changes in pore fluid and pore pressure associated with drainage of reservoir under production gives possibility to detect changes of significant importance concerning the reservoir depletion process, helping an optimal decision making on the economics of a producing field. By repeating surveys over the time, the production of reservoir can be followed and depletion of hydrocarbon detected

(Mussett and Khan, 2000). An example has been shown in Figure 1.7 where seismic image changes continuously by injection of CO_2 into the reservoir over the time.

The 4D seismic / time-lapse method, involves acquisition, processing, and interpretation of repeated surveys over a producing hydrocarbon field. Production of hydrocarbon, injection of water or gas into the reservoir alters the physical properties of the reservoir. Comparing the datasets acquired within the time of injection or production provides a processing product, the so called "time-lapse difference dataset", exhibiting the physical changes occurred within the reservoir (Schlumberger, 2014).

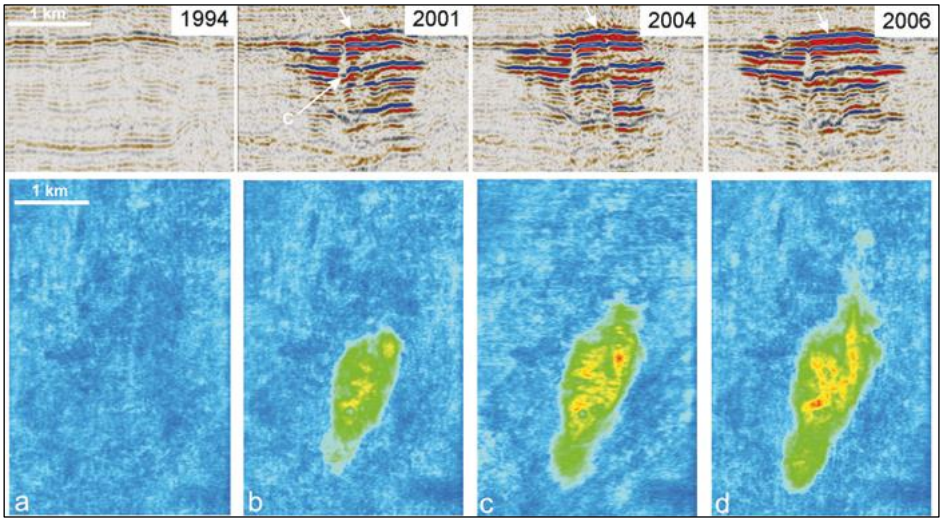

Figure 1. 7: 4D seismic images showing vertical sections (along the top) and maps of the expanding plume in 1994, 2001, 2004 and 2006 (along the bottom) (Chadwick, 2015).

Data harmonization is of great importance for a successful monitoring process. As the data quality is dependent on survey orientation and processing procedures, any errors may alter the final difference volumes, causing inaccuracies in the final product. Hence, different elimination between the datasets is an essential part of the work (Gelius, 2010).

As the accuracy in repeatability is a corn-stone of the method, a carefully designed processing flow will help compensate for the complications in exactly repeating two / several seismic datasets. This will enhance the signal to noise ratio and increases the resolution of the real events, suppressing the ghost / multiples inherent in the acquisition process. Known applications of the 4D seismic methods can be summarized as monitoring the spatial extent of the injected water front used for secondary recovery, imaging bypassed oil, determining flow properties of sealing or leaking faults and detecting changes in oil-water contact (Gelius,

2010). The difference in acquisition and processing is the difference between two seismic surveys, while this difference is sensitive to changes in reservoir rock as well. How a 4D project can be successful, it actually depends on both detectability and seismic repeatability. A schematic illustration of the key factors influencing detectability and repeatability is presented in Figure 1.8.

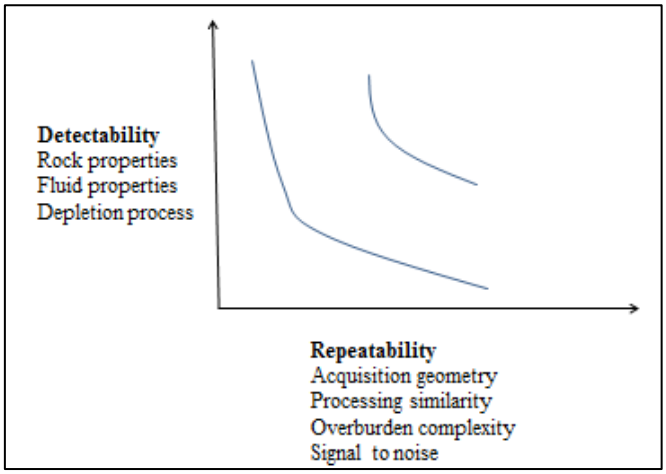

Figure 1. 8: Factors that influence both detectability and seismic repeatability (After Johansson ExxonMobile).

Decisive factors that influence repeatability include acquisition geometry differences such as sail line orientation and heading source-receiver, spacing, streamer feather and coverage due to obstructions, near-surface conditions resulting in statics and receiver coupling variations, sea level changes, sea state and swell noise, water temperature and salinity, residual multiple energy, ambient and short generated noise, geological factors such as shallow gas and steep geological dip. Major factors which influence detectability include rock properties, fluid properties, reservoir depletion and how the combination and fabric affect seismic parameters.

1.4.2 4D CSEM

The technical feasibility of 4D CSEM, i.e. time-lapse CSEM, and its potential as a reservoir mentoring tool is investigated regarding quantitative mapping of resistivity within larger reservoirs. Time-lapse surveys for production and water flood monitoring, including distinguishing between the different flood shapes, is already technically feasible, as improvements in navigation and processing are likely to increase accuracy in survey repeatability (Coruh, 1988).

The accuracy of the results is likewise dependent of good quality 3D dataset, both seismic and CSEM, with robust inversion algorithms, integrated porosity information and water saturation data from CSEM inversions constrained by well logs, to reduce uncertainties in input data and its depth conversion which will affect rock property volumes (Schlumberger, 2014). Time-lapse CSEM data containing two or more repeated surveys recorded over a producing reservoir is combined to detect and estimate production-induced changes in the subsurface rock and fluid properties, similar to the seismic method. An example has been shown in Figure 1.9. This figure shows the 4D CSEM changes for the four scenarios after one year of water injection. : (a) reference case, (b) Case X, in which subsurface aquifer water is injected into a highly saline formation water (c) Case Y, in which low salinity water is injected into the formation water and (d) Case Z, in which seawater is injected into formation water. According to this figure, the 4D CSEM amplitude change is clear.

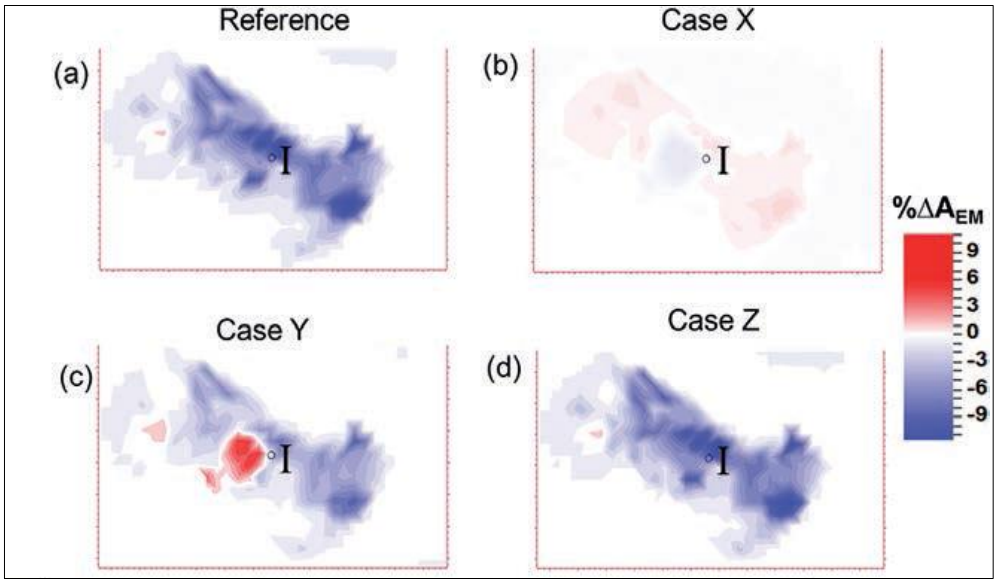

Figure 1. 9: Time lapse CSEM amplitude changes for the four scenarios after 12 months of water injection (Salako et al., 2015).

Any changes in attributes, e.g. rock resistivity are often associated with changes in fluid saturation assuming a non-compacting isothermal reservoir. Several authors have addressed this technique. Presented time-lapse transient EM surveys over a shallow underground gas storage reservoir with high porosity demonstrated that the data is repeatable enough to detect the reservoir and monitor the movement of gas-water content due to gas pumping and/or extraction during summer and winter. Lien and Mannseth (2008) conducted a feasibility study of time-lapse CSEM data to monitor the water flooding of an oil reservoir. Utilizing 3D

integral equation modeling, they found that time-lapse induced some changes into the present measurement errors (Lien and Mannseth, 2008). Wang et al. (2008) tested the sensitivity of the marine CSEM method to reservoir heterogeneities. They found out that the electromagnetic response resolves poorly lateral variations in lithology (porosity and shaliness) and should be combined with seismic for such purposes.

However, in the case of reservoir monitoring in connection with EOR (Enhanced oil recovery), the electric response was in general much more sensitive to saturation changes than the seismic method as expected (Wang et al., 2008). Orange et al. (2009) further expanded the work by Lien and Mannseth (2008) by utilizing a 2D finite element modeling to simulate time-lapse CSEM data in response to several simplified water flooding scenarios, including lateral, bottom flooding and partial depletion. Through a set of 2D modeling studies, they showed that a repeatability of 1-2% is required to detect the small time-lapse signals (Orange et al., 2009). Zach et al. (2009) conducted 3D time-lapse modeling by perturbing conductivity over a large reservoir (10 x 10 km^2) and reported anomalies of 30% to 50% changes in relative amplitudes of the base and the monitoring surveys. They noted that these relatively strong signal as well as different shapes of fronts could be monitored. They evaluated the 4D capability of the acquisition mode at the time of publication and discussed about the possible sources of non-repeatability and they were included source navigation and waveform, ocean bottom receiver position and orientation and also the cultural changes between repeat acquisitions (Zach et al., 2009) . Here, it is noteworthy that the ocean water conductivity is also a source of non-repeatability as Zach et al. (2009) could point to this important effect. Black et al. (2009) modeled time-lapse CSEM response over a realistic geologic model, although they assumed a simplified flood geometry without fluid flow simulation and rock physics modeling. The study showed that marine CSEM data is able to locate the position of oil-water contact if the field is normalized for the background bathymetry and salt dome effects. No reservoir simulation and rock physics modeling was performed, but a direct perturbation of electrical-conductivity is assumed (Black et al., 2011). In 2009, PGS (Petroleum Geo-Services) published a time domain EM repeatability experiment over the North Sea Harding filed. Utilizing Archie's equation, fluid flow simulation and resistivity modeling for clay-free sandstone were combined by integral equation modeling to simulate EM data. The study concludes that the production-induced changes in reservoir resistivity would be observable providing a signal to noise ratio of greater than 100 (Shahin et al., 2010).

1.5 Motivation of this thesis

The marine Controlled-Source Electromagnetic (CSEM) method is a promising and well-established method for hydrocarbon exploration (Eidesmo et al., 2002, Wang et al., 2008). The CSEM resistivity data in conjunction with seismic could produce a reasonable picture of underground hydrocarbon reservoirs. It has already been demonstrated that the CSEM has sufficient sensitivity to detect changes in a hydrocarbon reservoir caused by production over a few years (Zach et al., 2009). A key question for 4D is the repeatability requirements of the base and monitoring surveys. Some of the non-repeatability sources for the time-lapse surveys are source altitude, tilt, path offset, and feathering (Zach et al., 2009). For example, from a recent dataset in the Gulf of Mexico, the error due to source navigation (part of a survey was towed twice over the same receiver drop) resulted in time-lapse repeatability within 3-5% (Zach et al., 2009). It is well documented in the literature that the greatest acquisition uncertainty of CSEM is related to the receiver orientation, which introduced a systematic error of up to 3-5 degrees in azimuth and tilt. With more accurate receiver orientation measurements and also using the seabed monuments, the sources of non-repeatability for time-lapse surveys could be mitigated. So far, all analyses of the repeatability requirements include only evaluation of the direct effects of the acquisition parameters on the EM data. This implies that the analysis of 4D data is performed in the data domain by looking at differences in the measured fields. At the same time, the most efficient method to extract value from CSEM data is by inversion for subsurface resistivity. Therefore, our intention in this study is to determine the repeatability and detectability requirements for 4D CSEM surveys that could allow reservoir monitoring and changing of water conductivity based on inversion of EM data. To achieve this first controlled (synthetic) test data associated with two reservoir models are generated and then the subsurface models recovered by conducting 2.5D inversions. Consider that there are other effects which influence CSEM recorded data. Water properties are very important factors which they change continuously over the time and result in differences in the monitoring surveys data in comparison with the base survey. In addition, the differences in receiver positions of CSEM surveys over the time may cause significant variation in the data. In this thesis, the effects of these parameters on 4D CSEM results are tried to be fully understood by applying different approaches including sensitivity analysis and inversion-based analysis.

Chapter2 Theoretical Considerations

2.1 EM relation and CSEM

The physics behind the CSEM method is founded on Maxwell's equations which describe the mutual interaction between electric and magnetic fields excited by an electric source current. Maxwell's Equation is composed of Ampere's and Faraday's law and in differential form can be expressed as:

$$\nabla \times H = \sigma E + \frac{\partial(\varepsilon E)}{\partial t} \tag{2.1}$$

$$\nabla \times E = -\frac{\partial(\mu H)}{\partial t} \tag{2.2}$$

Where:

E is electric field (V/m)

H is magnetic field (A/m)

J is source current density (A/m^2)

σ is conductivity (S/m) where, $\rho = \sigma^{-1}$ (resistivity, Ωm)

μ is magnetic permeability (N/A^2)

ε is dielectric permittivity (F/m)

Then an electric field can be generated by a time varying magnetic field, which describes Faraday's law, where E (V/m) is electric field and B (Tesla, V.s/m^2) is the magnetic field as shown in Figure 2.1.

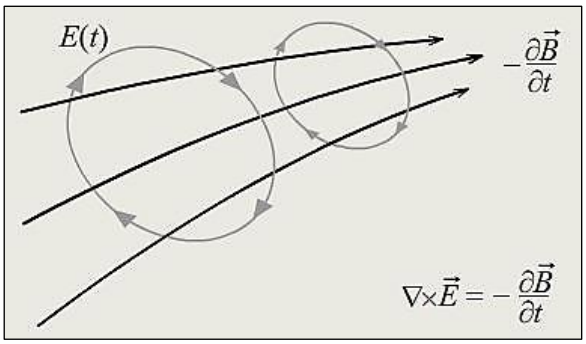

Figure 2. 1: Faraday's law of induction (Gelius, 2010).

This law can be written as:

$$\nabla \times E = -\frac{\partial B}{\partial t} = -\mu \frac{\partial H}{\partial t} \tag{2.3}$$

The Ampere's law explains that a magnetic field can be generated by a time varying electric field. The vector D (C/m^2) showing in Figure 2.2, is the electric displacement field and the J (A/m^2) vector is the total current density.

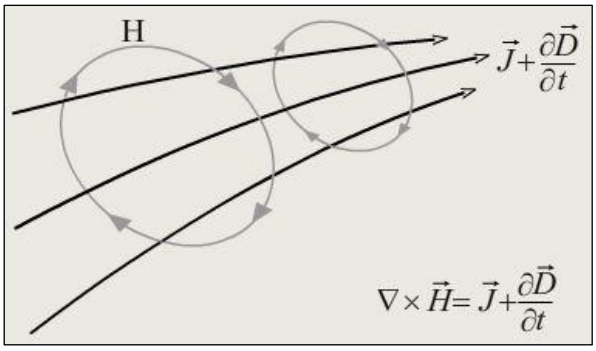

Figure 2. 2: Ampere's generalized law (Gelius, 2010).

And this law can be written as well as:

$$\nabla \times H = J + \frac{\partial D}{\partial t} = \partial E + \frac{\partial E}{\partial t}\varepsilon \tag{2.4}$$

As the name implies, in marine controlled source electromagnetic method, the electromagnetic waves are used. Therefore, it is necessary to apply the electromagnetic wave equation. The electric and magnetic vectors in an electromagnetic wave are perpendicular to each other and the direction of propagation, as shown in Figure 2.3. A differentiation of Ampere's law with respect to the time, give us the electromagnetic wave equation.

$$\nabla \times \frac{\partial}{\partial t} H = \sigma \frac{\partial E}{\partial t} + \varepsilon \frac{\partial^2 E}{\partial t^2} \tag{2.5}$$

And by combination with Faraday's law:

$$\frac{-1}{\mu} \nabla \times (\nabla \times E) = \sigma \frac{\partial E}{\partial t} + \varepsilon \frac{\partial^2 E}{\partial t^2} \tag{2.6}$$

Finally, when $\nabla E = 0$ and $\nabla \times (\nabla \times E) = (\nabla E)\nabla - \nabla^2 E$;

The electromagnetic wave equation for a monochromatic plane- wave will be:

$$\nabla^2 E - \mu\sigma \frac{\partial E}{\partial t} - \mu\varepsilon \frac{\partial^2 E}{\partial t^2} = 0 \qquad (2.7)$$

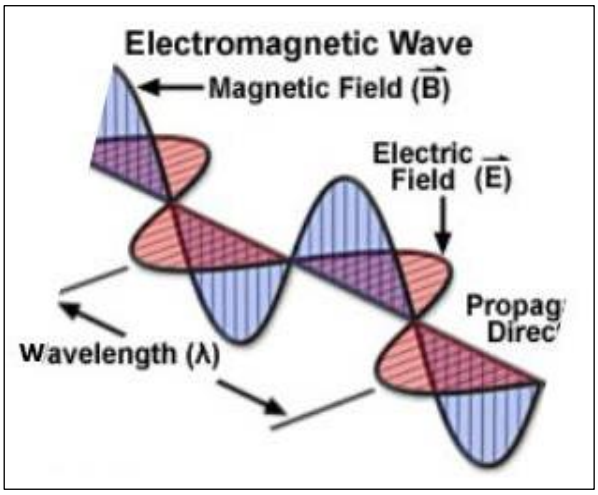

Figure 2. 3: The electric and magnetic vectors in an electromagnetic wave are perpendicular to each other and the direction of propagation (Abramowitz, 2014).

Then, by using Fourier transform which is a mathematical transformation employed to transform signals between time domain and frequency domain with respect to the time in the wave equation, equation (2.8) will be obtained where the CSEM data is acquired in the time-domain and transformed into the frequency-domain. CSEM measurements are mostly processed in the frequency domain, but both the time and frequency domains can be used for land applications (Wirianto et al., 2010).

$$\nabla^2 E = (i\sigma\mu\omega - \varepsilon\mu\omega^2)E = -k^2 E \qquad (2.8)$$

Where ω is angular frequency and k is complex wavenumber. A monochromatic plane-wave $E=E_0 \exp[-i(\omega t-kx)]$ solution of the diffusion-equation gives the wavenumber identity. Moreover, as already pointed out, low frequency is used in CSEM method. Then, it implies that the following approximation can be shown which describes the diffusing of the waves by considering conductivity:

$$\sigma \rangle\rangle \omega\varepsilon$$

$$\omega \to 0: \quad \nabla^2 E = i\sigma\mu\omega E \;\leftrightarrow\; \nabla^2 E - \sigma\mu \frac{\partial E}{\partial t} = 0 \qquad (2.9)$$

To find the complex wavenumber, k, equation (2.10) applies:

$$k = k_R + i\,k_I \tag{2.10}$$

Then the propagating and attenuation of a wave can be described by the equation (2.11) where it applies an exponential function:

$$e^{ikx} = e^{i(\alpha+i\alpha)x} = e^{i\alpha x}.e^{-\alpha x} \tag{2.11}$$

Where $k_R + ik_I = \alpha + i\alpha$ and $e^{i\alpha x}$ describes the propagating of the wave and the second term which is $e^{-\alpha x}$, describes the attenuation of the wave. Consider that $\alpha = \sqrt{\pi\sigma\mu f}$.

According to these equations:

$$k = \sqrt{i\omega\sigma\mu} = (i+1)\sqrt{(\omega\sigma\mu)/2} = (i+1)\alpha \tag{2.12}$$

Then the skin (penetration) depth can be applied here:

$$e^{-\alpha\delta} \equiv e^{-1} \Rightarrow \alpha\delta = 1 \Rightarrow \frac{1}{\alpha} = \delta = \sqrt{\frac{1}{\sigma\,\mu_0\,\pi\,f}} \approx 503.3\sqrt{1/\sigma\,f} = 503.3\sqrt{R/f} \tag{2.13}$$

Generally, the using of low frequency can be described by looking at skin depth δ, equation (2.14), which explains the travel distance after which the magnitude of the EM signal is recorded by a factor of 1/e = 0.37.

$$\delta = \sqrt{\frac{\rho}{\mu_0 \pi f}} \tag{2.14}$$

In terms of marine CSEM method, three different values of resistivity (R) will typically be used. The resistivity for sea water, overburden sediments and hydrocarbon reservoir which is 0.30 Ωm, 1-2 Ωm and 10-100 Ωm, respectively. Table 2.1 shows an example of skin depth values for different resistivity values using law frequency.

Form Table 2.1 it is clear that by decreasing of frequency values and increasing of resistivity, the skin depth increases as well. That means the skin depth varies with frequency and consequently, the better detection of geological structures in marine environments will be possible. Because of a more rapid attenuation of the EM fields, the skin depth of the signal would be reduced when the higher frequencies are used (Lien and Mannseth, 2008).

Table 2. 1: Calculated skin depth for different values of resistivity with different frequencies.

R (Ωm)	f (Hz)	δ (m)
0.30	0.1	871.7400
2.00	0.1	2250.820
50.0	0.1	11254.13
0.30	1.0	275.6600
2.00	1.0	711.7800
50.0	1.0	3558.870
0.30	10	87.17000
2.00	10	225.0800
50.0	10	1125.410

The marine CSEM method provides information about the subsea resistivity structure, a property separating water from gas and oil-filled reservoirs. The CSEM method uses a high powered horizontal electric dipole (HED) to transmit a low frequency (0.1<f<10 Hz) and dipolar EM fields can be detected at the seafloor receivers employing either inline or broadside configuration (Wang et al., 2009).

Considering Figure 2.4a, we can find that in broadside form, the electric current dose not cross any conductivity boundaries and the flow direction is normal to the plane of the figure. At the same time, Figure 2.5 shows that the electric filed is perpendicular to the propagation direction. It means there are horizontal current loops. This mode is called transverse electric (TE) mode. Figure 2.4b shows the geometric response of broadside configuration.

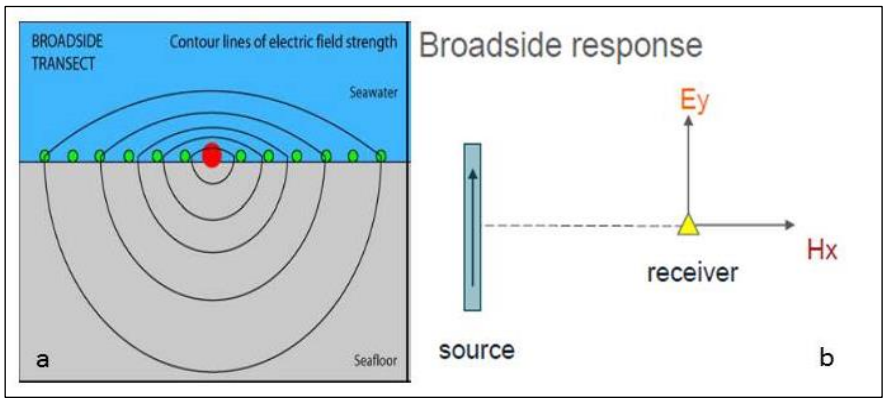

Figure 2. 4: a) in broadside form, the electric current dose not cross any conductivity boundaries (Gelius, 2010) b) the geometric response of broadside configuration.

Figure 2.5 shows that the electric field is parallel to the propagation direction of the magnetic waves. In this mode, which is called transverse magnetic (TM) mode, we have vertical current loops, and Figure 2.6b supports this claim. Figure 2.6a shows the form of inline configuration.

It shows that the electric current cross boundaries between region of different conductivity values.

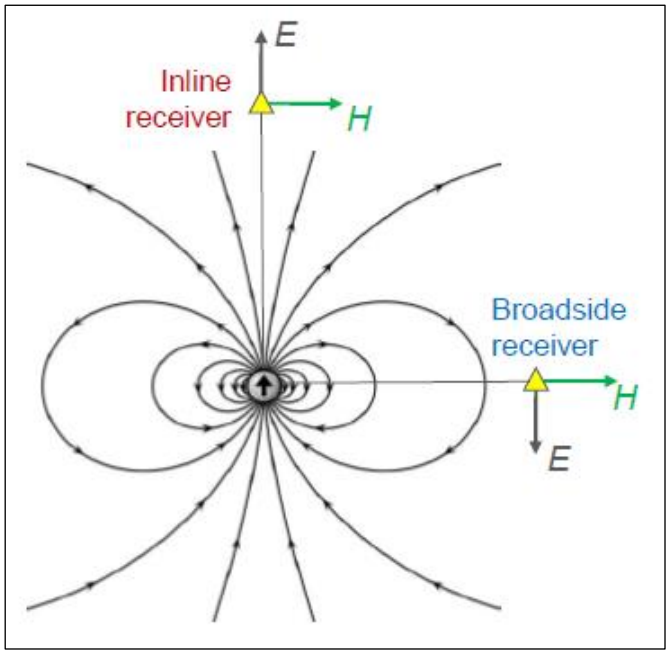

Figure 2. 5: Inline versus broadside.

Generally, the measurement of current depends on the conductivity of material and how the electric field varies. Therefore, the ohm's law, $\vec{J} = \sigma \vec{E}$, should applies here. When the large vertical electric field is excited inside the resistor, with specific conductivity value, we will be able to detect the thin resistors. And by using horizontal field line tend to flow around this resistor we can detect if the resistor is thick or thin.

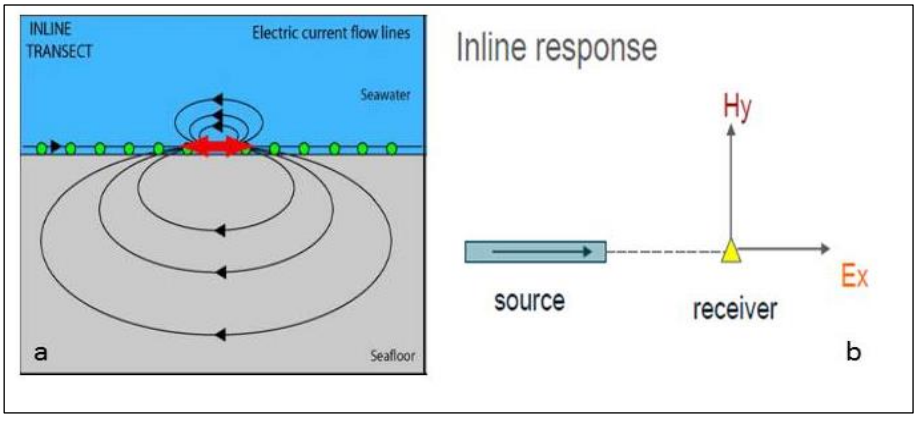

Figure 2. 6: a) shows the form of inline configuration (Gelius, 2010) b) the geometric response of inline configuration.

Inline measurements are very sensitive to the presence of resistive layers, while the broadside has limited sensitivity to thin resistors (Morten et al., 2011). Because the broadside data is measured at receivers on a line perpendicular to the dipole source. The conclusion is that CSEM is sensitive to the vertical resistivity in a thin resistor.

2.2 Archie's low

The EM waves go across the hydrocarbon-layer. These waves will propagate in all direction and the receivers recorded signals from such environment. Changes in the received signal as the source are towed through the array of receivers to record the bulk electrical resistivity of the seafloor. If the thickness is known, the bulk resistivity of a reservoir is controlled by the attributes and repartition of fluids within it. However, the Electrical properties of a rock depend on the pore geometry and fluid distribution.

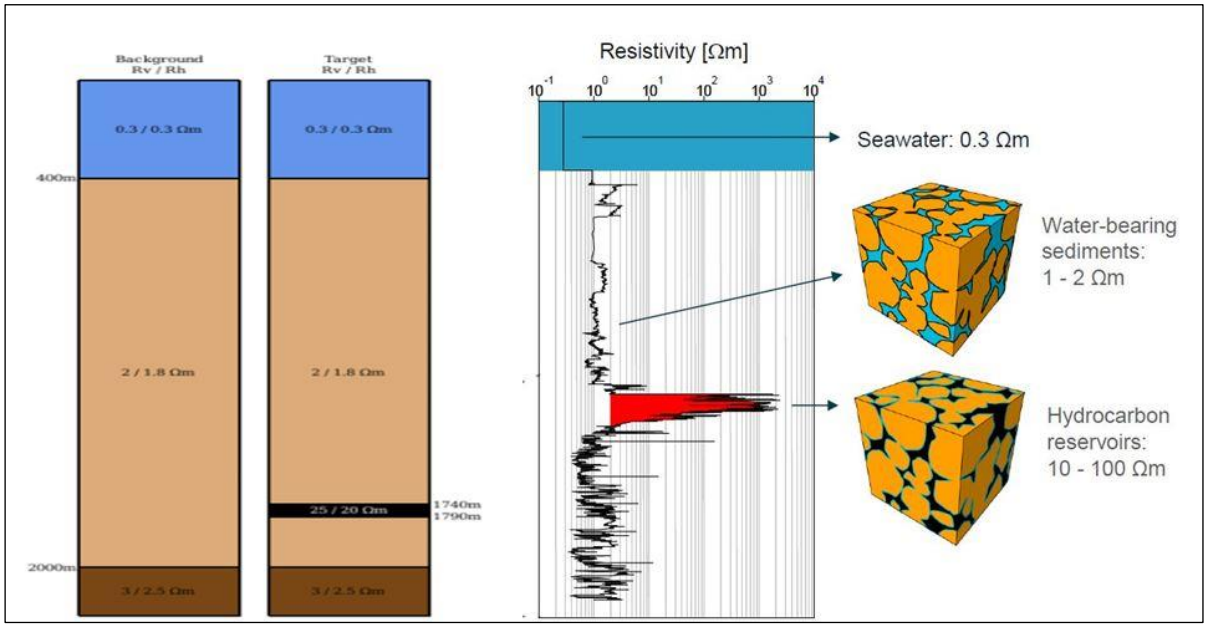

Figure 2. 7: Resistivity of seawater, sediments and HC (Linus Boman, 2014).

Assuming the resistivity of seawater to be 0.30 Ωm, the overlying / underlying sediments to be 1-2 Ωm and the hydrocarbon resistivity to be in the range of 10-100 Ωm as shown in Figure 2.7, then the Ohms law and Archies' law for clean sandstones can be applied. We can consider the resistivity of different rocks, air and water according to Figure 2.8.

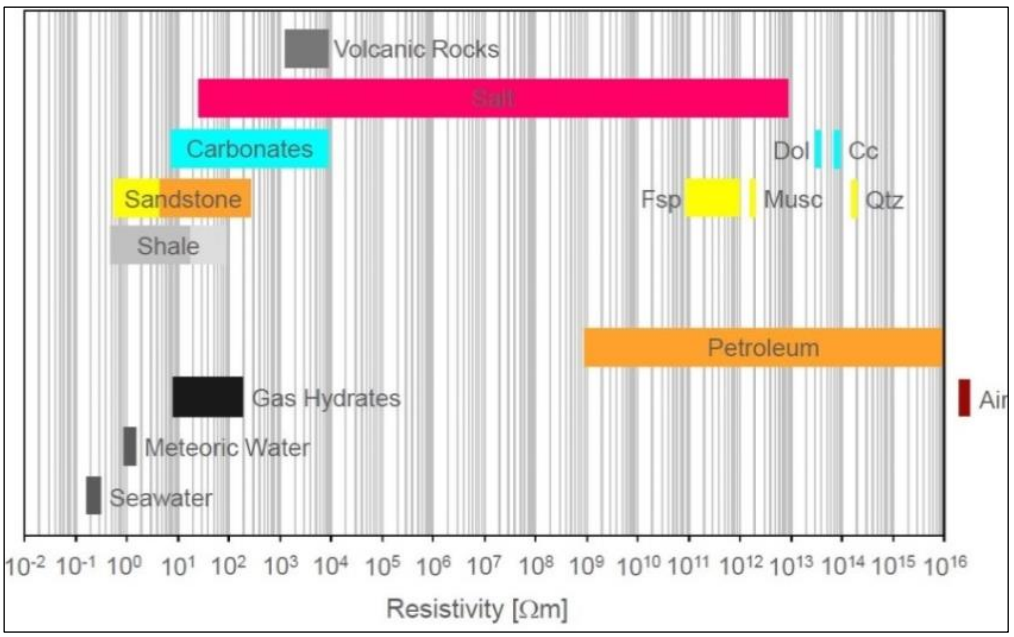

Figure 2. 8: Resistivity of different rocks, air and water (Boman, 2014).

By using Ohm law, the potential difference will be found, when we have measured current, I and a calculated resistance, r:

$$V = I\,r \tag{2.15}$$

And in addition it will be used the Darcy's law to find the electric current, I in a homogeneous medium for example brine, as can be described by:

$$\frac{I}{A} = \sigma_w \frac{V}{L} \tag{2.16}$$

Where A is the area of medium, L is the length of medium and σ_w is the conductivity of homogeneous medium. And then water resistivity defines as, $R_w = r_w A/L$, which gives us the resistance with respect to the water phase.

$$r_w = \frac{R_w L_a}{A_p} \tag{2.17}$$

where the L_a is the length of tortuosity and A_p is the porous phase. So the resistance with respect to fluid-filled, porous rock:

$$r_o = \frac{R_o L}{A} \tag{2.18}$$

Consider that resistivity is the inverse of conductivity. Then it will be show that formation resistivity factor, water resistivity and rock resistivity are related by the following expression over wide ranges of porosity which shows that the resistivity of fully water-saturated sediment (R_o) is closely proportional to the resistivity of the pore fluid (R_w):

$$F = \frac{R_o}{R_w} \tag{2.19}$$

Where:

F = formation factor
R_o = resistivity of rock filled with water, Ωm
R_w = resistivity of water, Ωm

Archie's law is an empirical law and the original model of that for brine saturated rock is given as:

$$F = \phi^{-m} \tag{2.20}$$

Where ø is porosity and m is the cementation exponent of the rock (usually 1.7-2.3). We have several versions of this law that try to put the effects of water-gas, water-oil, mixed fluids in the pores and air water mixes in the unsaturated zone. Then the version of Archie's Law typically used in the hydrocarbon industry for brine and gas filled sandstones is given by:

$$F = K\phi^{-m} \tag{2.21}$$

Where K is formation resistivity factor coefficient (usually 1.0-1.2) and is unity when F=1 and ø =1**.** From a physical perspective, the values of parameters K and m depend on the interconnectivity of the pore spaces, which in turn depends on lithology, cementation, and grain size distribution (Hearst et al., 2000).

If formation includes hydrocarbon saturation the hydrocarbon resistivity index I_R is independent of water saturation S_W; $I_R = (S_w)^{-n}$, where n is the saturation index(usually 1.7-2), then the conductivity will be:

$$\sigma = (FI_R)^{-1}\sigma_w \qquad (2.22)$$

Relationships among these quantities indicate that the resistivity decreases with increasing porosity and increases with increasing petroleum content. Resistivity measurements are also dependent upon pore geometry, formation stress, composition of rock, interstitial fluids**,** and temperature. Resistivity is, therefore, a valuable tool for evaluating the producibility of a formation (Tiab and Donaldson, 2011).

In terms of detectability in CSEM method, actually there is not so much literature / references available due to novelty of the subject. described that the temperature coefficients of electrical conductivity for shaly sands are greater than those for aqueous salt solutions and increase systematically with increasing clay content of the sands, compared at the same equilibrating brine concentration. Thus, shaly sand formation resistivity factors are temperature independent (Waxman and Thomas, 1974). They created a model and in this model the effective conductivity is split in two terms, one due to brine (Archie type) and one due to the clay double-layer. Wang and Gelius (2007) showed that different clay distributions, keeping the volume fraction of clay constant, give rise to very different effective conductivities of the reservoir rock, and hence EM response. And they concluded that the salinity of brine in a sand-shale reservoir rock also affects the EM response considerably.

It can be conclude that rock and fluid property alterations in the reservoir are the main factors, as well as hydrocarbon leakage into resistive layers, where brine replaces the oil/ gas phase. This will cause resistivity to decrease within the resistive layers, bringing about a partial depletion effect. The phenomenon has been studied by Orange et al. (2009). Concluding that the distal edge of the reservoir is the best location for assigning source and receiver measurements, and despite the prevailed depleting condition / reduced production, the reservoir's physical properties can be measured in CSEM response overtime.

Chapter 3 Software, EM modeling and Inversion

3.1 Software

3.1.1 SBLwiz

SBLwiz is an interactive user interface developed by EMGS for use in quality control and processing of CSEM data. It has been designed to be a user friendly interface for working with CSEM raw data and performs advanced processing such as forward modeling, 2.5 inversion and 3D inversion (Espeland, 2014). SBLwiz runs on 64-bit Linux and much of the numerical processing is performed by separate binary command-line modules that use files as input and output. Processing in SBLwiz is generally done by running workflow jobs. There are several workflows defined for processing, modelling and inversion. Separate executables and libraries are used under the hood. All installed with a single installer. The survey data generally consists of many data files at various stages of processing plus support files containing survey layout, navigation, source information, waveforms, positions, angles, etc.

3.2 Modeling

3.2.1 2.5D Modeling

The base model for our simulations is one dimensional (1D) modelling where the geological resistive layer has a finite thickness and is infinite in the other dimensions. If there is no sensitivity in 1D, the survey is not feasible. For most practical purposes the target's size cannot be assumed infinite (Orange et al., 2009). Unlike the 1D model, the geological resistive layer in 2D models is finite in two dimensions. Unfortunately, 2D method has not always capability to produce a clear image of the geology. Because in this methods the vessel tows a single streamer and the data set occurs along a line of receivers. The diffractions and constructed from offline geologic structures can distort 2D data and because of this the interpretation is difficult. In 3D modeling, the target is assumed to be finite in all three dimensions. However, the 3D modeling could be very expensive and demands enormous processing time. Therefore, the approach which has been used in this study is based on 2.5D modeling as it is fast and accurate. The 2.5D modeling is based on the Maxwell's equations, where the electric and magnetic data apply. In CSEM acquisition, optimization and interpretation of the 2.5D modeling is frequently used. Figure 3.1 shows comparison between a 3D and 2.5D model, where in the 2.5D model, the target has been shown in 2D while the source and receivers has been shown in 3D (Tehrani and Slob, 2013).

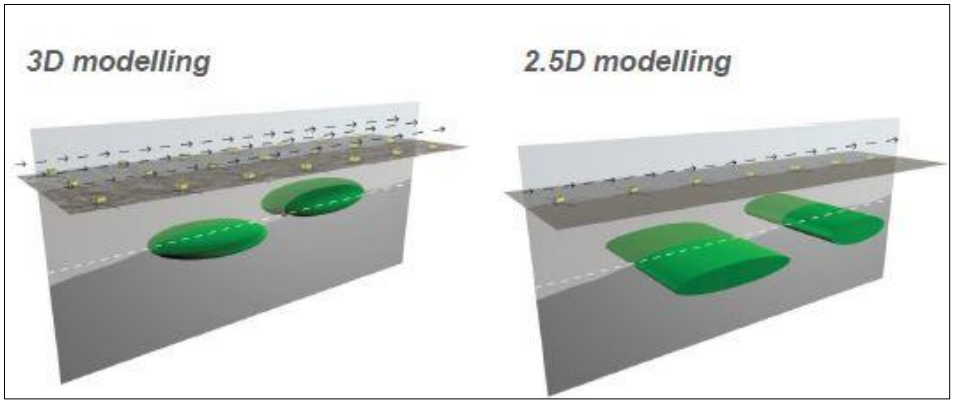

Figure 3. 1: Comparison between a 3D and 2.5D model (Linus Boman, 2014).

Figure 3.2 shows a simple diagram of the input and output data which have been used in this thesis. This figure shows that the input data depends on several factors, which determine the final output of the interpretations. The output data are electric and magnetic data.

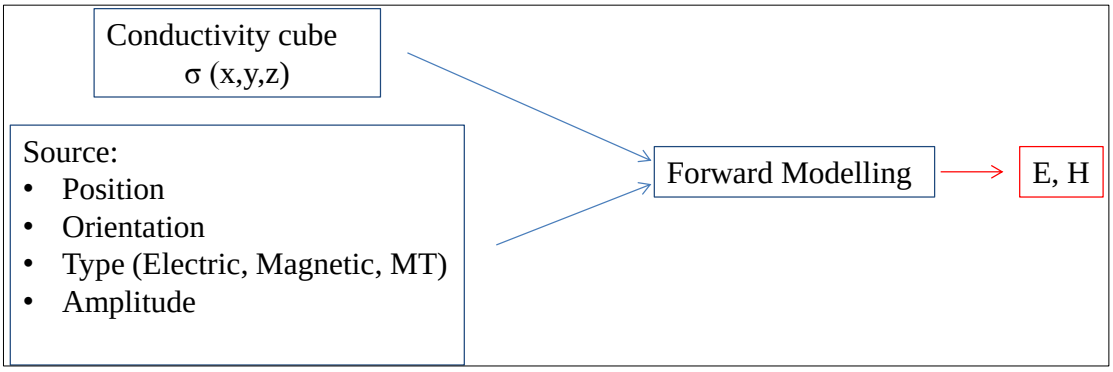

Figure 3. 2: A simple image of the input and output modelling.

Using of modelling leads to feasibility of sensitivity study, survey design, engine for inversion and at least post inversion modeling and interpretation. Two different types of modelling codes have been used here.

3.2.2 1D modelling code

Features for 1D modelling codes include frequency-wave number domain formulation, models anisotropy, models inline and broadside sources (Løseth, 2007). 1D modelling code uses for sensitivity tools like EM, SBLwiz and to plane layer models. This code is forward engine for 1D inversion as well. As an example, Figure 3.3 shows a normalized electric

magnitude vs offset in terms of 1D modelling. This ratio can be found by dividing the electric data recorded from an area with the target to data of the half-space area.

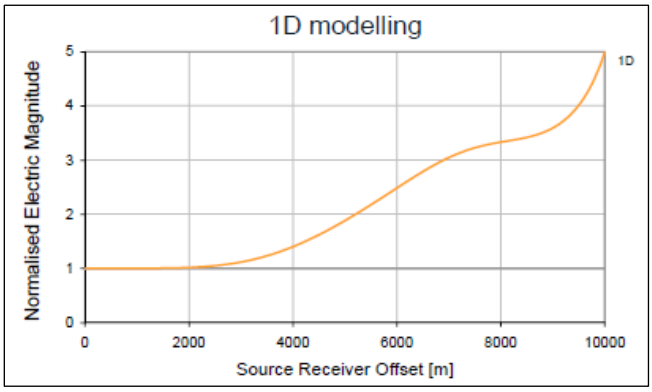

Figure 3. 3: An example from 1D modelling code (Hansen, 2014).

3.2.3 2.5D modelling code

The real 3D subsurface is approximated by a 2D section in which the resistivity varies along the towline and in depth, but is constant in the cross-line direction. Accuracy of 2.5D approximation is promising and very small variations can be detected in the interpretations. As shown in Figure 3.4, very small differences (< 4%) have been detected. This example shows that maximum error can be found by dividing the electric data field recorded from a 2D model to corresponding data from a 3D model.

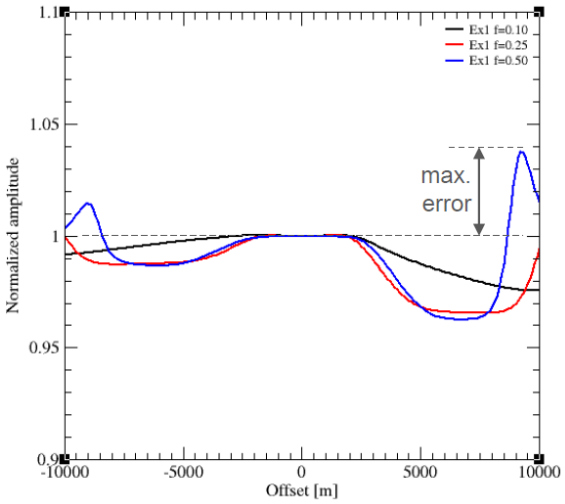

Figure 3. 4: 2.5D approximation normalized by the exact 3D result for a 3.5 wide reservoir (Hansen, 2014).

In this thesis a finite model is created. The conductivity models discretized into small cells and electric and magnetic field are calculated in each cell. Figure 3.5 shows features of the model which has been used. The numbers of cells in X-direction are 491 cells where the size of each cell in this direction is 100 m. In contrast, the numbers of cells in Z-direction are 81 where the size of each cell in this direction is 80 m.

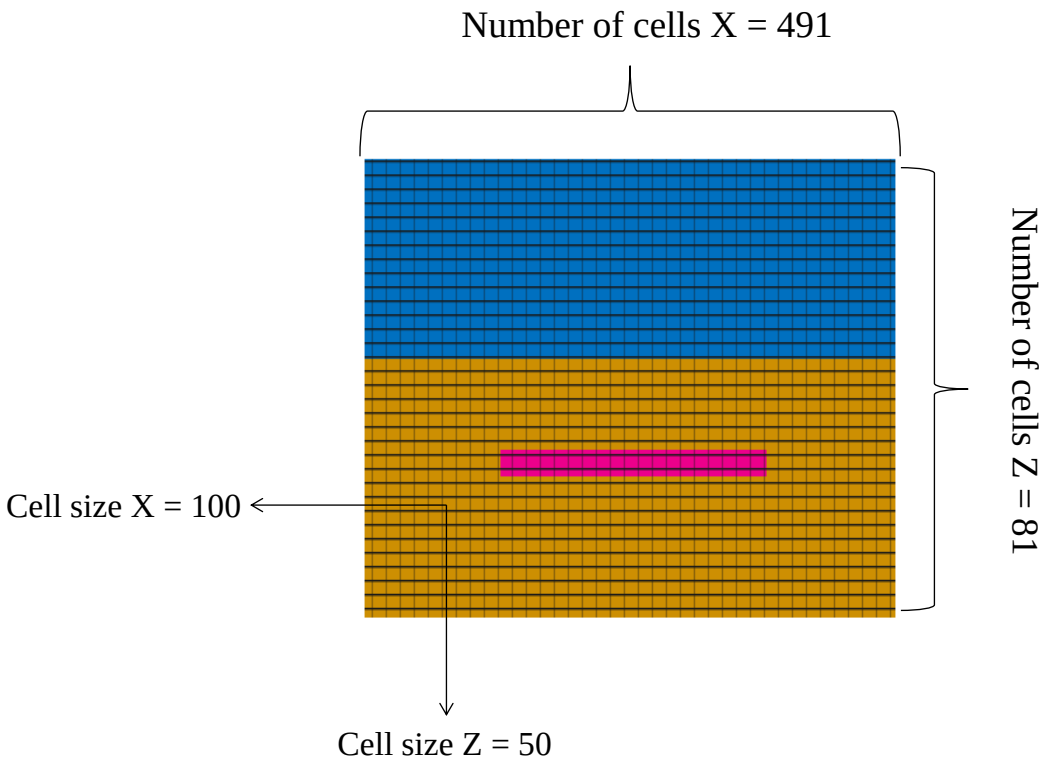

Figure 3. 5: Discretized conductivity model used in this thesis.

3.3 Inversion

Inversion of the data for a resistivity model may provide better results. The goal of inversion is to determine a subsurface resistivity model that reproduces the observed data within the data uncertainty. In addition, the inversion method provides more accurate geological information about a specified area. Figure 3.6 shows a simple relationship between modeling and inversion. This figure shows that having the resistivity model, the modeled data could be taken and vice versa. In this thesis the inline electric field is inverted and the output is a resistive model.

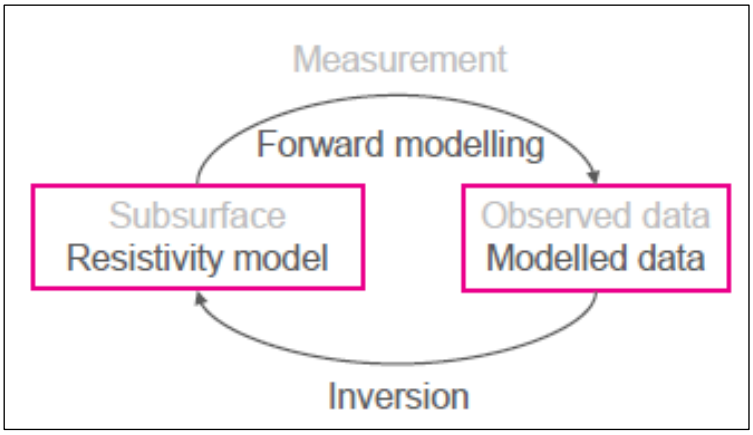

Figure 3. 6: A simple relationship between modeling and inversion. (Hansen, 2014).

The following relationship (3.1) is used to compare monitoring data with base data.

$$\left|\frac{E_{monitor}-E_{base}}{E_{monitor}}\right|\times 100\% \qquad (3.1)$$

Where $E_{monitor}$ is inline electric field for monitoring model and E_{base} is inline electric field for base model. If this value is close to zero, it means that variation of the recorded data for two different surveys is not considerable.

The following objective function has been minimized during inversion to quantify the error misfit function. This equation implies that the good data fit is when $E_D \approx 0$ (Hansen, 2014).

$$E_D(m)=\frac{1}{N_D}\sum\left|\frac{F_{obs}-F_{\mathrm{mod}}(m)}{\Delta F}\right|^2 \qquad (3.2)$$

Where:

E_D is the error (or misfit) function.

N_D is the number of inputs.

F can be electric or magnetic field data. Here F_{obs} is observed data and F_{mod} is modelled data, m is model parameters (σ, ρ) and Δ represents the uncertainty of data.

There are several challenges with CSEM inversion including complex bathymetry, shallow water, small prospects, depth to target, high resistivity overburden and proper background

model (Gelius, 2010). These challenges will be discussed in this study later. The inversion works at this study are based on 1D, 3D and 2.5D inversion approaches.

In the 1D inversion, a 1D resistivity model will be used where the data are taken from one receiver. However, 1D inversion is not suitable for accurate determination of resistors depth. In 3D inversion, a 3D resistivity model and 3D EM fields are used. In addition, azimuth and inline data are incorporated as well. In 3D modeling there is no geometric limitation, but slow due to complexity of modeling and large number of unknowns. And in 2.5D inversion a 2D resistivity model and EM from 3D field will be used. Here, only inline data uses. Since synthetic data is generated using 2.5D modeling, bathymetry variations or strong 3D effects transversal to the line can cause problems.

In general, a CSEM inversion algorithm attempts to find a conductivity distribution which produces synthetic data matching the observed data. The misfit between observed and synthetic data for a given model is measured by defining a data error functional. A small value of this functional indicates that the misfit between observed and synthetic data is small. The objective of the inversion algorithm is thus to find a model which minimizes the error functional. Since the error functional is non-linear, the inversion algorithm is typically an iterative algorithm, starting from an initial guess for the solution, and then successively updating the model until convergence. Because of this the existence, uniqueness and stability of the solution are not guaranteed. For this reason, prior information on what constitutes a plausible model is needed to reduce these problems. This prior information is typically in the form of "minimum structure" requirements on the solution, so that the obtained solution will be the simplest one which matches the data. This process is known as regularization.

3.3.1 2.5D inversion

In 2.5D inversion, it is assumed that the receiver and source positions are located along a line, and conductivity varies little in the horizontal direction and perpendicular to the towline. In addition to the input data files, a number of inversion parameters are also needed to be specified. Several input model files are used in the SBLwiz 2.5D Inversion. The following is a summary and brief description of all input parameters in this thesis. In addition, the commands which have been used in this thesis are listed in Appendix B.

Inputs:

- Receivers

Receivers list of data *files* to include the inversion. Each file should contain data for the EM field components of interest in the frequency domain.

- Vertical initial model

  The initial model used by the inversion, specified by the initial model parameter, should be a reasonable model of the conductivity of the background. Often a simple half space model will suffice, but it is important that the sea floor is accurately modeled, especially in shallow water cases. Reasonable values for the conductivities of the water and the formation should be given, such that the initial data misfit between observed and synthetic data calculated from the initial model is not too large. It is good practice to imprint the water column with conductivity values obtained from the acquisition in order to improve the accuracy of the forward modelling.

- Model mask

  To provide the mapping between the conductivity of the model grid cells and the inversion parameters, a model mask must be provided .The mask is given as a model file which must have the same grid dimensions as the initial model. The use of model masks is primarily done for two reasons: first, to allow spatial constraints on the resulting model, either by fixing the conductivity of certain parts of the model to a given value or to enforce homogeneity of certain regions. And second, to reduce the number of inversion parameters by the use of upscaling, since a large number of inversion parameters results in a very time consuming inversion. The maximum allowed number of inversion parameters is 15.000.

- Minimum conductivity model

  Vertical conductivity model file used to constrain the minimum conductivity values.

- Maximum conductivity model

  Vertical conductivity model file used to constrain the maximum conductivity values.

- Regularization strength model

  Model specifying the spatial variation of the regularization strength.

Parameters:

- EMF list

  There are separated list of field components to include in the inversion. Ex and Hy.

- Frequencies

There are separated list of frequencies to include the inversion.

- Offsets

  There are separated list of smallest and largest to include in the inversion. One value must be specified for each frequency.

- Vertical receivers positions

  Sets the receiver positions in the synthetic data using the sea floor found in the input model and the given rule.

- Regularization strength

  This parameter determines the overall strength of the regularization.

- Weights noise mode

  This is a noise mode option for the data weights.

Chapter 4 Results, Interpretation and Discussion

4.1 Target depletion and sensitivity analysis

Having production in a resistive layer, brine replaces the oil /gas phase. Therefore, resistivity of the resistive layer decreases. Monitoring of resistive layers during depletion is a new application area for CSEM. Orange et al. (2009) investigated that CSEM method is sensitive to depletion. In this thesis, most of modeling approaches are inspired from this work. First, their work is reviewed and similar results were reproduced. The goal is to achieve minimum detectable depletion (MDD) in the all analysis. They investigated effect of target depletion and relative difference in inline electric field for different stage of depletions. According to their model, sea water conductivity is assumed 3.030 S/m and frequencies were set to 0.1, 0.25, 0.5, 0.75, 0.85 and 1 Hz. The source altitude which has been assumed above seabed was 30 m. The reservoir model was 100 m thick, 5 km wide, buried 1000 m below the seafloor. The model had a resistivity of 100 Ωm, the water depth was 1500 m and resistivity of the background was 1 Ωm as shown in Figure 4.1. This figure also shows that the distances between the receivers is 2000 m. Finally, the field component is Ex.

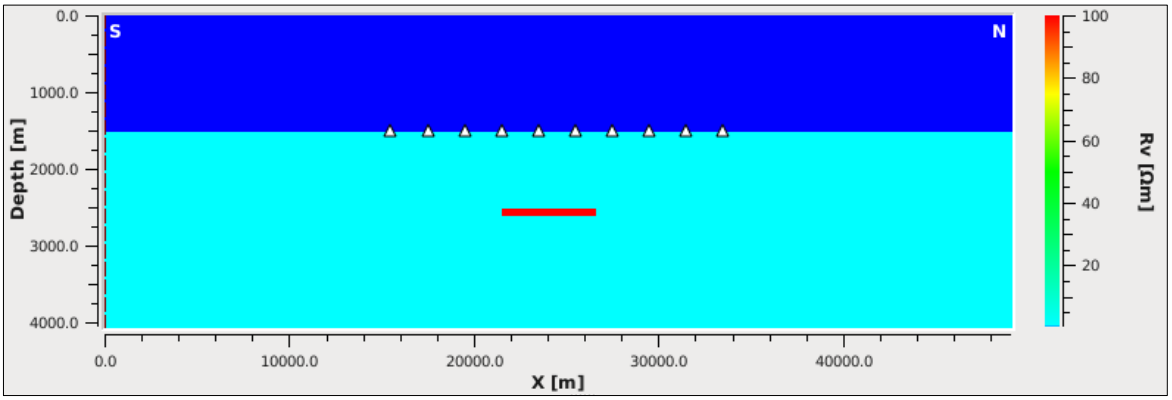

Figure 4. 1: The 2D model has been used for the simulation where the data from the third receiver, from the left, has been calculated. The distance from the left edge to this receiver is 2 km.

The inline electric field data will be recorded in two different settings; i.e. with and without target (half-space model). Basically, to show the difference between these two models AVO or MVO curves would be displayed. Figure 4.2 shows an AVO (amplitude vs source receiver offset) image where the third receiver is selected. This receiver has 2000 m distance from the target edge. The effect of presence of the target is displayed in this figure. It is clear from this figure that the lateral edge of the target shows a strong signal in the CSEM response.

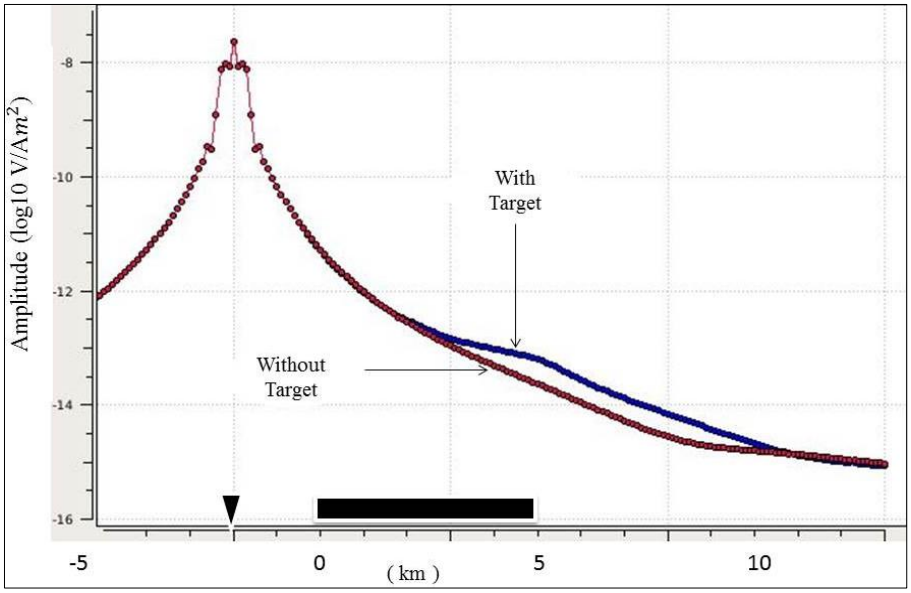

Figure 4. 2: The location of the receiver where it has 2000 m distance from the target edge, frequency = 0.1 Hz.

The investigation of sensitivity of target depletion is done by Orange et al. (2009). In fact, they only checked the effect of high depletion of reservoir as depicted in Figure 4.3. The depletion process occurs from the left and water will replace the hydrocarbon in place. The electric data fields are recorded for every steps of depletion.

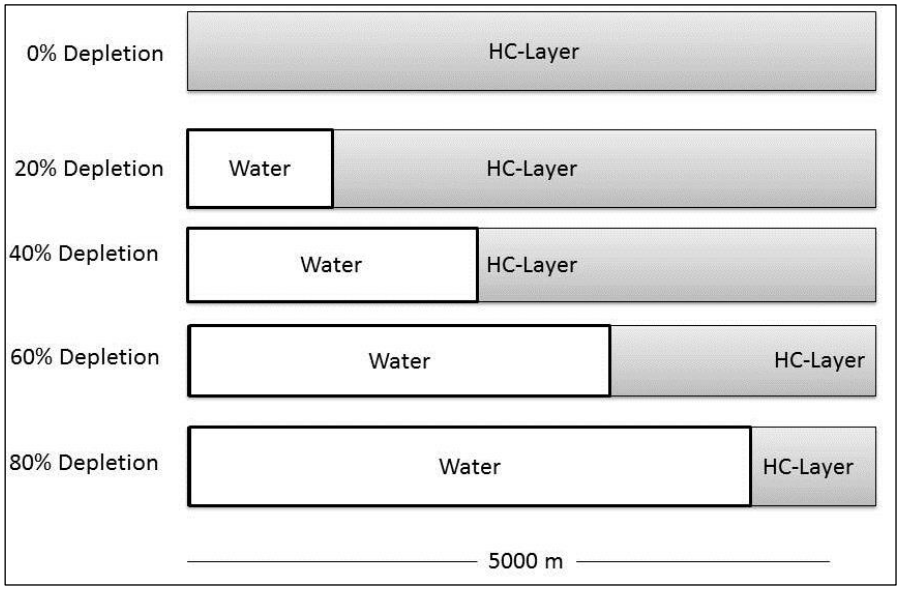

Figure 4. 3: The lateral depletion of the target step by step.

As it is shown in Figure 4.4, by increasing the depletion of the reservoir layer, the electric field ratio would decreases. It is worth mentioning that the data are analyzed by plotting the

amplitude of electric field versus source-receivers offset and then normalizing the amplitude of the electric field acquired over a possible hydrocarbon prospect with respect to the amplitude of electric field measured over a similar non-hydrocarbon bearing area. Having hydrocarbon in a specific area, the amplitude of a measured electric field increases and the normalized value will be greater than unity for areas containing resistive anomaly and unity or less for non-hydrocarbon bearing area.

The results from Orange et al. (2009) are shown in Figure 4.4a. They showed that the distal edge of the reservoir is the best location for the source when a specific receiver is selected. The Figure 4.4b shows our results in this study for a similar molding. The results are in very good agreement with one from Orange et al. (2009), however, there are negligible differences between the two results. This very small difference is maybe because of the difference in source altitude positions in the two studies. The source altitude is regarded 30 m above seabed in this study while Orange et al. (2009) computed the inline electric fields where this position is 50 m. The modeling in this study indicates that when the source is near the 0 km the response of anomaly is very small because there is no resistive structure between the source and receiver at this offset and there is relatively shallow sensitivity at short offsets (Orange et al., 2009).

According to the work which has been done by Orange et al. (2009), the same model is created here. As we already pointed out, the goal is to achieve small minimum detectable depletion in the sensitivity analysis. In Addition, the water conductivity variations will be studied and based on that, the minimum depletion detectability will be controlled.

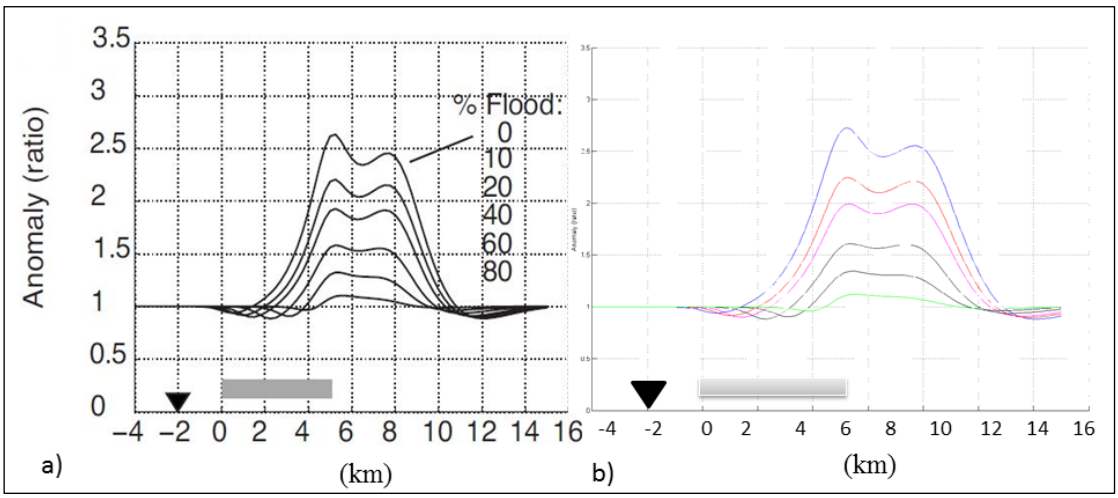

Figure 4. 4: Simulation for different percentage-depletion. The a) inline electric field Ex by (Orange et al., 2009) and b) inline electric field Ex which has been down in this thesis. Frequency =0.1 Hz.

Figure 4.5a shows the relative difference between electric field data for 0% and 20% depletion where this difference is found by the following relation:

$$relative\,difference\,in\,Ex = \left| \frac{E_{depleted} - E_{full}}{E_{depleted}} \right| \qquad (4.1)$$

Figure 4.5b, c and d show the relative difference between electric field data for 0%, 40%, 60% and 80% depletion, respectively. These figures show that by increasing the depletion, these relative differences in Ex increase as well. To detect the minimum detectable depletion, the small depletion scenarios are required. The reason is that the CSEM approach is able to detect less than 20% depletion. This purpose has been improved by Orange et al. (2009).

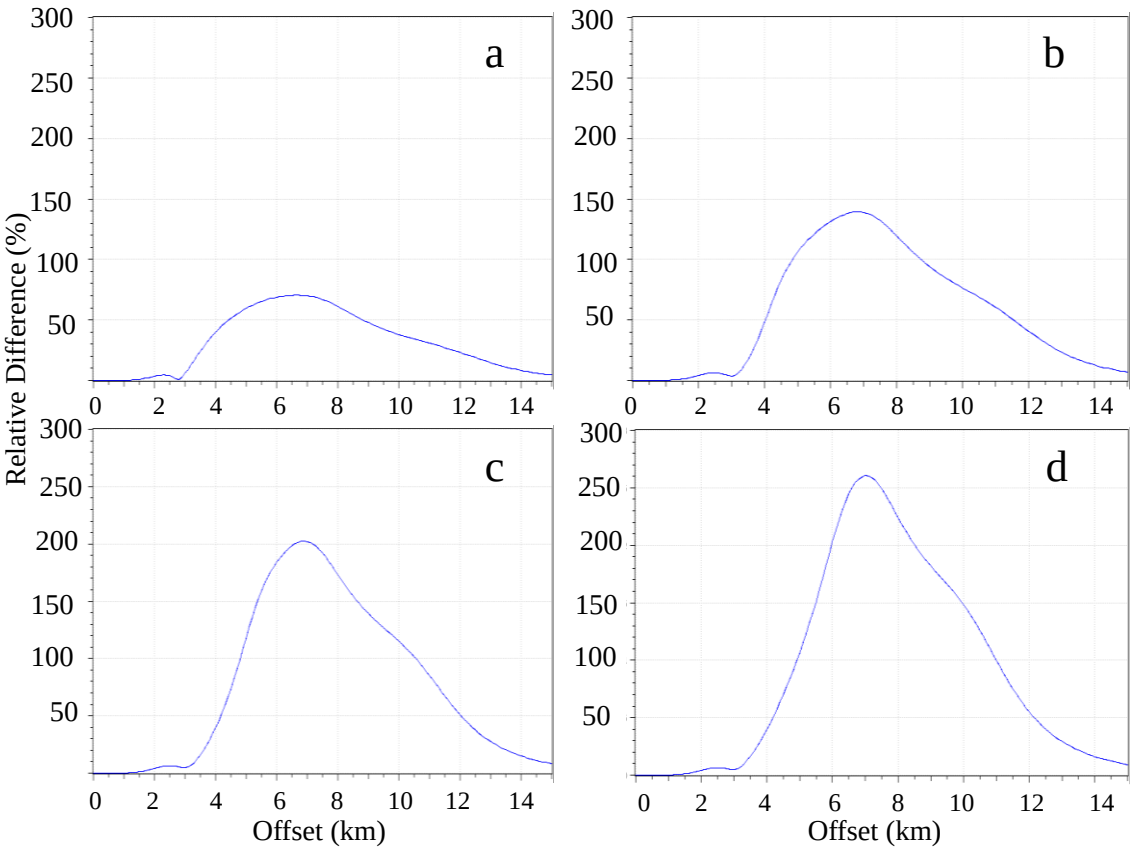

Figure 4. 5: The relative difference between electric field data (Ex) when this difference is between a) 0% & 20% b) 0%& 40% c) 0% & 60% d) 0%& 80 % of depletion, frequency =0.1 Hz.

Then, the small depletion scenarios will be investigated in this section. Figure 4.6 shows the relative difference in electric field versus offset in terms of small depletion. These differences have been found by using the relation (4.1). The peak of every curve in Figure 4.6 shows the

relative difference in electric field for different percentage depletion. According to this figure the Table 4.1 is generated. This table shows that between every step of small depletion there is approximately 7-8% changes in relative difference in electric field.

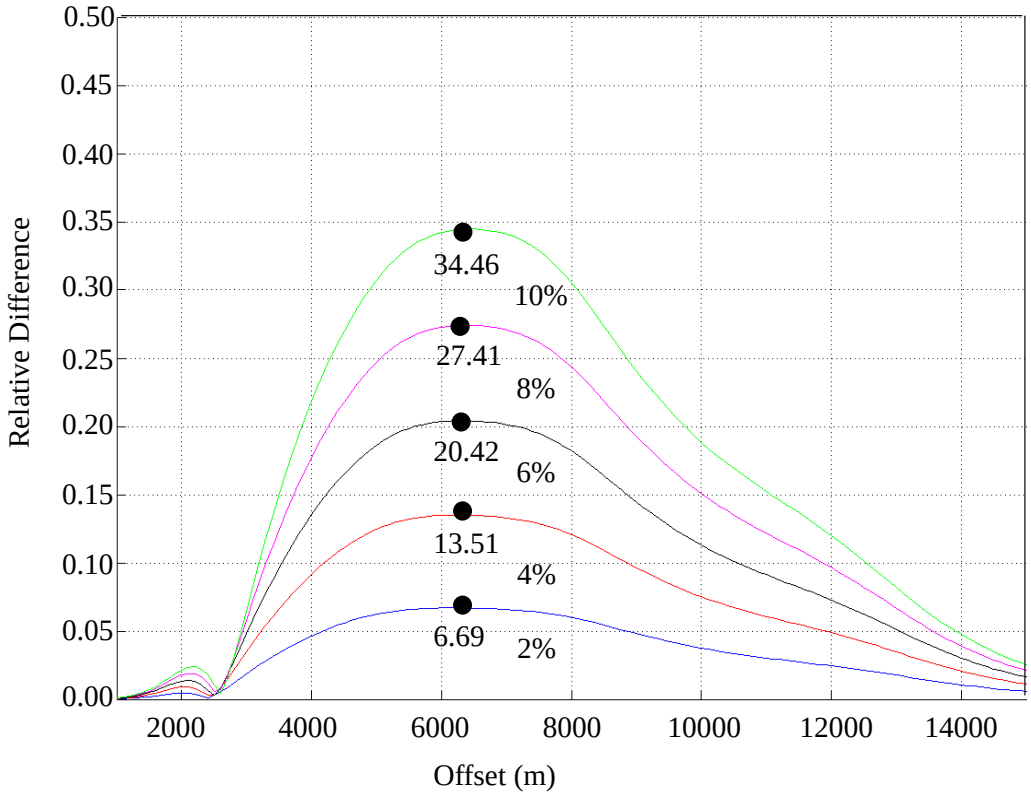

Figure 4. 6: Relative difference in Ex versus offset for small depletion scenarios, by using the relation (4.1), frequency =0.1 Hz.

Table 4. 1: The exact amount of relative difference in Ex for small depletion, where the relation (4.1) is used.

Depletion (%)	Relative Difference (%)
2	6.69
4	13.51
6	20.42
8	27.41
10	34.46

4.2 Variation of water conductivity

4.2.1 Effect of water conductivity

The variation in salinity and temperature of the environment makes the variation of ocean water conductivity. As has been pointed out before, the resistivity is the inverse of conductivity. The resistivity for hydrocarbon saturated sediments is much higher than that for brine saturated sediments. It shows that brine has higher conductivity than oil and gas (Norman et al., 2008).

The conductivity of a reservoir depends mainly on four factors; salinity of seawater, temperature, water saturation and fraction of clay in solid portion (Gelius and Wang, 2008). Near the surface, the water is warmer than the deeper parts and it makes the conductivity in the sea surface greater than the deep water (Key, 2009). As already has been discussed, the resistivity of brine depends on some factors and the most important is change of temperature.

In this section, the effect of water conductivity will be investigated when the temperature and salinity of water will be changed. The equation (4.2), (Gelius and Wang, 2008), describes that the conductivity of water depends on both the salinity and temperature , where S_0 and T_0 are initial salinity and temperature, respectively.

$$\sigma_w(s,T) = \sigma_w(s_0,T_0) + \Delta\sigma_W \tag{4.2}$$

Where,

$$\Delta\sigma_w = 0.0958\,(s - s_0) + 0.00462\,(T.s - T_0.s_0) - 0.26\times10^{-5}(T^2.s - {T_0}^2.s_0) - \frac{2.24\times10^{-3}(2.36+0.099T)}{(1.0+2.8\times10^{-2}\sqrt{s})}s^{\frac{3}{2}} + \frac{2.24\times10^{-3}(2.36+0.99T_0)}{(1.0+2.8\times10^{-2}\sqrt{s_0})}{s_0}^{\frac{3}{2}}$$

This relationship between conductivity, salinity and temperature is shown in Figure 4.7. On the left frame of this figure, one can see that by increasing the salinity the water conductivity increases as well. The right frame of this figure shows that also by increasing the temperature, the water conductivity increases.

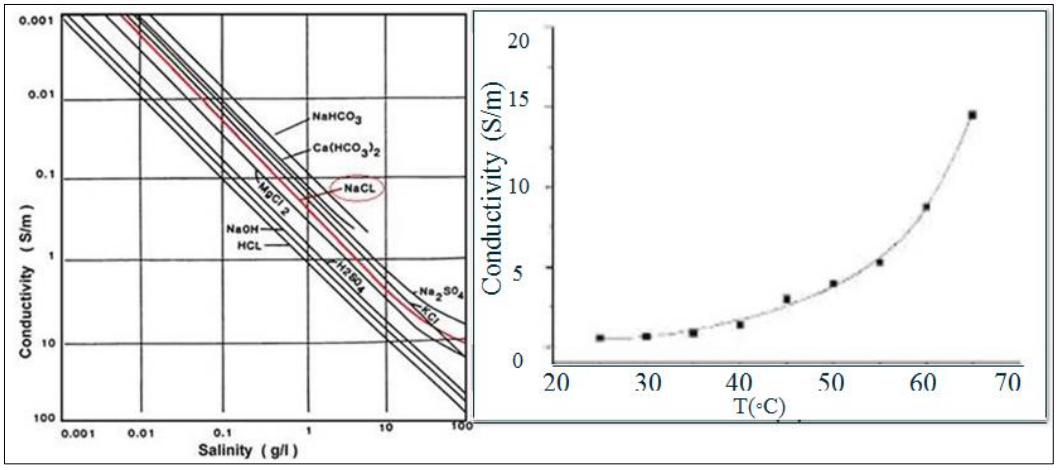

Figure 4. 7: The salinity or temperature increase, then the conductivity increases (Keller and Frischknecht, 1966).

In addition, there is a conversion table for changing conductivity into salinity (Envcoglobal, 2014) at different temperatures. The values suggested by this table can be compared with calculated $\Delta\sigma_w$ values using equation (4.2). Based on the model provided by Orange et al. (2009), the conductivity of water for the base model is 3.030 S/m (30.30 mS/cm) and then it will change to 3.175 S/m (31.75 mS/cm) i.e. there is 4.5% difference. The $\Delta\sigma_w$ is 0.145 S/m when the temperature is 5^{o}C. Table 4.2 lists the conductivity values suggested by envcoglobal (2014) for the corresponding water salinities at temperature of 5^{o}C. The difference in conductivity values listed in Table 4.2 (0.145 S/m) is the same as what has been calculated from equation (4.2).

Table 4. 2: Conversion table for changing water conductivity into salinity, the temperature is 5^{o}C.

Salinity (kppm)	**Conductivity (mS/cm)**
31×10^{-3}	30.30
33×10^{-3}	31.75

.

Figure 4.8 shows the comparison between the electric fields data for two different models for these two values of water conductivity. The difference between the inline electric fields data for these two models as is shown by the left side of Figure 4.8 is very small. An enlarged view of the image can be seen at right frame of Figure 4.8. Figure 4.8 shows a variation in response up to around 10% in normalized magnitude. This value helps us to detect minimum depletion over the time and will carefully be evaluated in the next section.

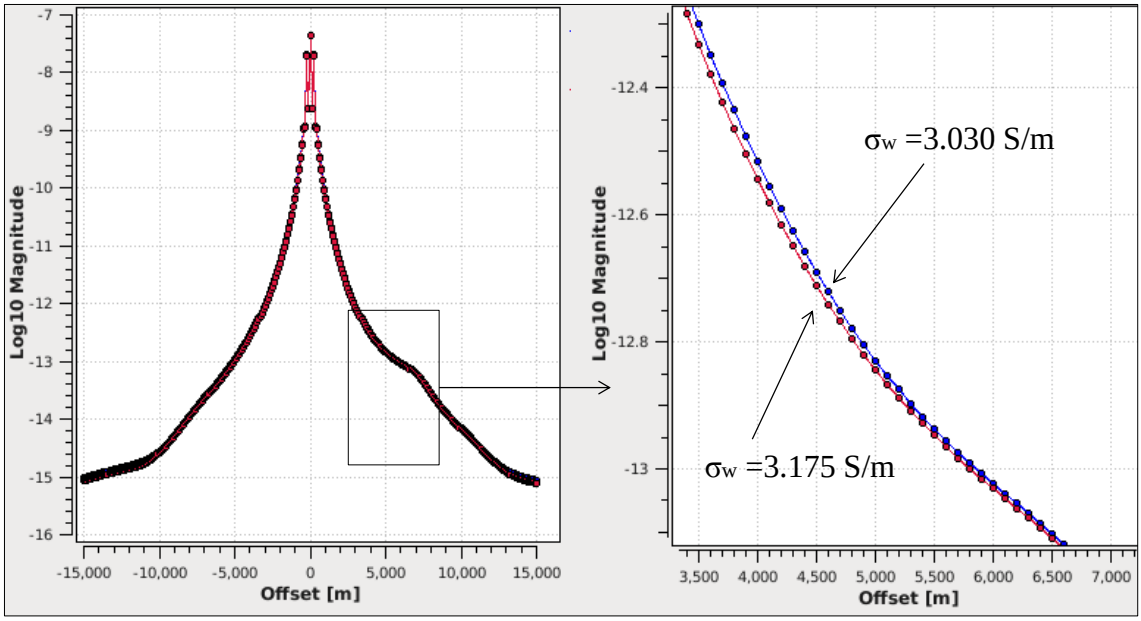

Figure 4. 8: Comparing between Ex data for a model with σw_1 =3.030 S/m and σw_2 =3.175 S/m, frequency=0.1Hz.

4.2.2 Sensitivity analysis and depletion

In this section the minimum detectable depletion will be found due to the variation of water conductivity. In section 4.2.1, we assumed that the water conductivity changes from 3.030 S/m to 3.175 S/m. It is expectable that by having 4.5% change in the water conductivity value, there will be small changes in electric field data and then some changes in the CSEM response as has been shown in Figure 4.8. The observed results indicate that there is almost 10% difference when seawater conductivity changes from 3.030 S/m to 3.175 S/m.

Effect of seawater conductivity variation influences the inline electric fields and hence it affects CSEM. Figure 4.9 shows the relative difference in the inline electric fields observed between the two scenarios with different water conductivity values calculated for two different values of frequency. This difference is found by the following relation:

$$\text{relative differnce in Ex} = \left| \frac{E_{(\sigma w2)} - E_{(\sigma w1)}}{E_{(\sigma w2)}} \right|_{peak} \quad (4.3)$$

Where $E_{(\sigma w1)}$ is inline electric data belonging the base seawater conductivity and $E_{(\sigma w2)}$ for the monitoring seawater conductivity. Based on Figure 4.9, the maximum change calculated for

each two scenarios is 8.38% when the frequency is 0.1 Hz and is 6.52% when the frequency is 1 Hz.

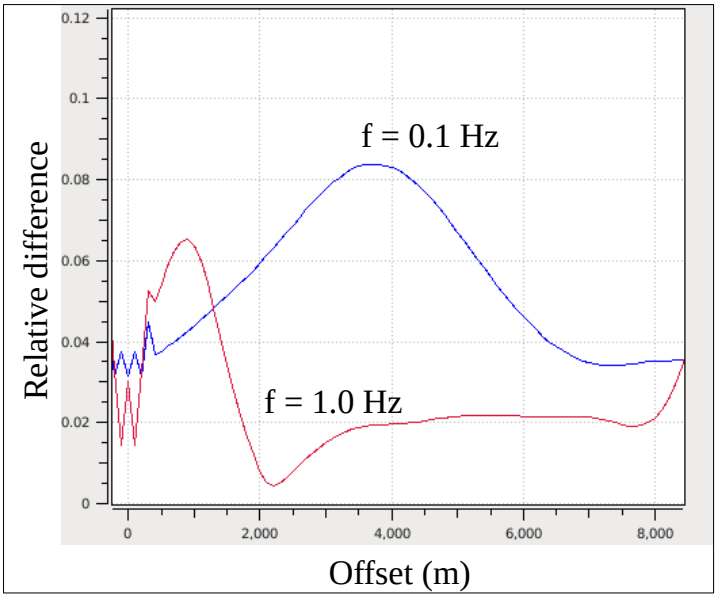

Figure 4. 9: Effect of seawater conductivity variations on CSEM for two different frequency values, getting by relation (4.3).

The minimum detectable depletion can be found via Figure 4.10 by using the 0.1 Hz frequency. This figure shows a plot of relative difference between inline electric data for every step of small depletion of CSEM response (as shown in Figure 4.6) versus depletion of the hydrocarbon reservoir. The result from Figure 4.6 indicated that by increasing the depletion of reservoir, the relative difference between inline electric fields for depleted and full reservoir increases too. These values are written inside Figure 4.10. Then by using relation (4.3) the maximum relative change of inline electric field based on variation of seawater conductivity is 8.38% when the frequency is 0.1 Hz. This value is found on the drawn line and based on that the minimum detectable depletion is approximately 2%. In practice, the depletions less than this value are difficult to detect as they situate within the red region in Figure 4.10. Then to get a much larger signal, this value is multiplied by 3, as a rule of thumb. The depletion values within the yellow region on Figure 4.10 might be detectable. Thus, the minimum depletion detectability should be more than 6% where this detectability is shown by green color in Figure 4.10. In another words, a hydrocarbon reservoir should be depleted by at least more than 6% so that the CSEM method will be able to detect this depletion when the sea water conductivity is changed by 4.5%.

Several difference values of frequency have been investigated to get the minimum detectable depletion. According to these works, Figure 4.11 is shown. This figure shows that when the frequency is optimized to 1.0 Hz, the minimum detectable depletion is approximately 2% which gives better ability comparing to the Figure 4.10 when the frequency is 0.1 HZ.

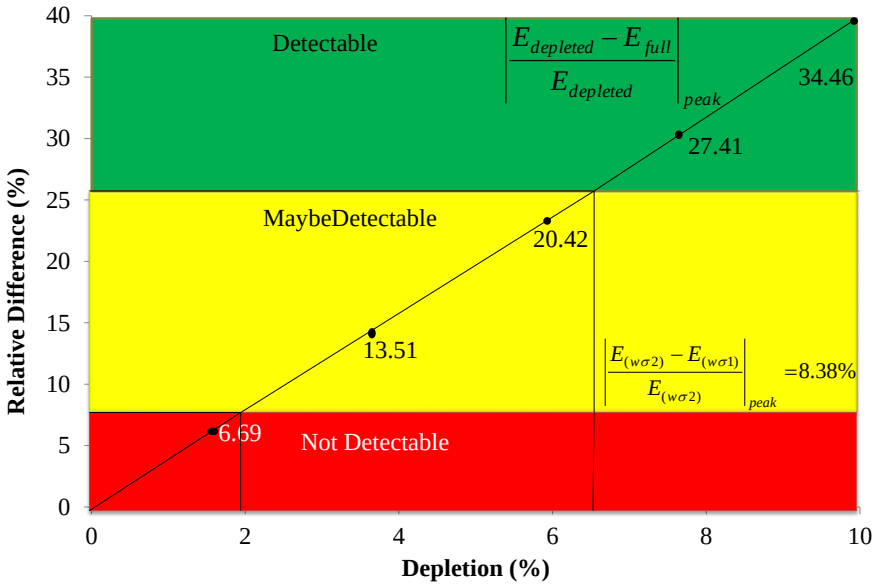

Figure 4. 10: Relative difference in Ex vs depletion, the minimum detectable depletion is than 7%, frequency = 0.1 Hz.

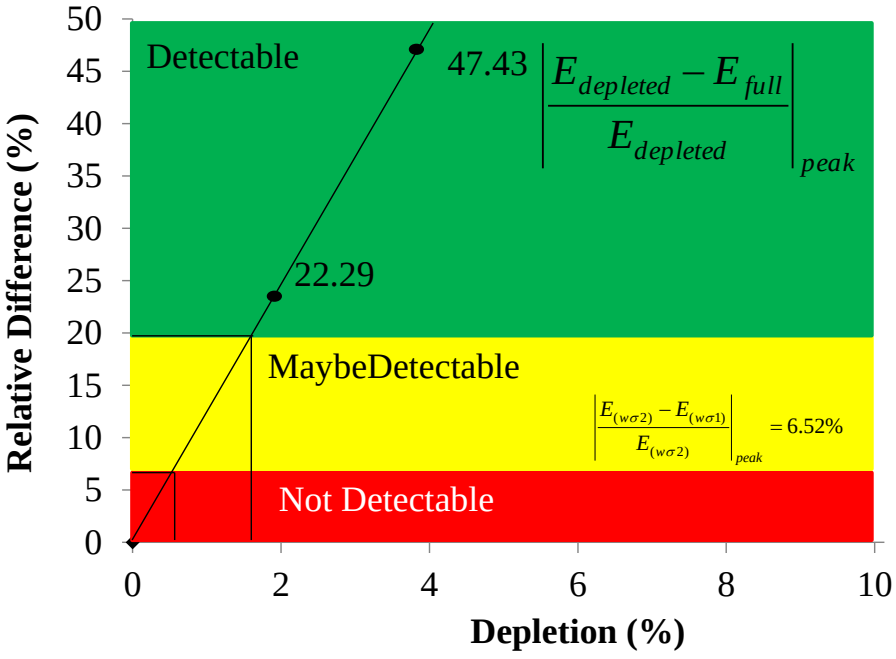

Figure 4. 11: The optimal frequency to detect the minimum depletion is 1.0 Hz and the minimum detectable depletion is less than 2%.

4.2.3 Inversion based analysis and depletion

In section 4.2.2 we studied the effect of variation of seawater conductivity in CSEM and investigated how repeatable must base and monitoring surveys be. The analysis was done in the data domain approach and we saw that variations in navigation parameters produce changes in the measured fields. This analysis should be done in the model domain approach. The most efficient method to extract value from CSEM data is by inversion for subsurface resistivity. Therefore, we needed to determine the repeatability requirements for 4D CSEM surveys that could allow reservoir monitoring and changing of water conductivity based on inversion of electromagnetic data. After every step of depletion, the changes occurring in the reservoir as a result of hydrocarbon production or injection of water or gas into the reservoir by comparing the inversion results will be determined. A typical final processing product is a time-lapse difference inversion results (Lovatini et al., 2013).

Now, a 2.5D inversion is applied to the inline electric data to recover subsurface model. Moreover, the inversion applies for several depleted models. In addition, inversions for several surveys with different values of seawater conductivity are tried as well. It is shown how to determine the repeatability requirements for 4D CSEM surveys that could allow reservoir monitoring based on inversion of EM data.

Then, the next step is investigating to get the minimum detectable depletion by using the inversion approaches. The following are studied.

- Unconstrained
- Average Anomalous Resistivity (<AR>) and Correction factor
- Constrained (conductivity limits)
- Fixed background (BG)
- Wrong BG in the start model

4.2.3.1 Unconstrained inversion

Following inputs have been used to run the inversion job and the models are shown in Figure 4.12. The true model which has displayed by Figure 4.12 is the same as the Figure 4.1. By using the SBLwiz software, it is not possible to run the inversion without a model mask. The

model mask contains information on how to parameterize the inverse problem, and is specified by the model mask file selector (emgs, 2011). Then, the model mask which has been used here is a standard mask. It will be better to remind all the inputs which have been used in this section as following: 10 Receivers, distance between receivers 2000 m, constant water depth 1500 m, resistive reservoir depth 1000 m below seafloor, resistive reservoir length 5000 m, resistive reservoir thickness 100 m, resistivity of reservoir 100 Ωm , source altitude above seabed 30 m, frequency= (0.1, 0.25, 0.5, 0.75, 0.85, 1) Hz , field components Ex and Hy, water conductivity 3.030 S/m, maximum (Line) offset 15000 m. Consider that the number and size of the cells in both X and Z directions are the same as has already been shown in Figure 3.5.

By having these inputs, the unconstrained inversion approach applies. Unconstrained inversion approach is a simple approach where inversion has no limit to invert a model. That means the inversion dose not put any limits on conductivity.

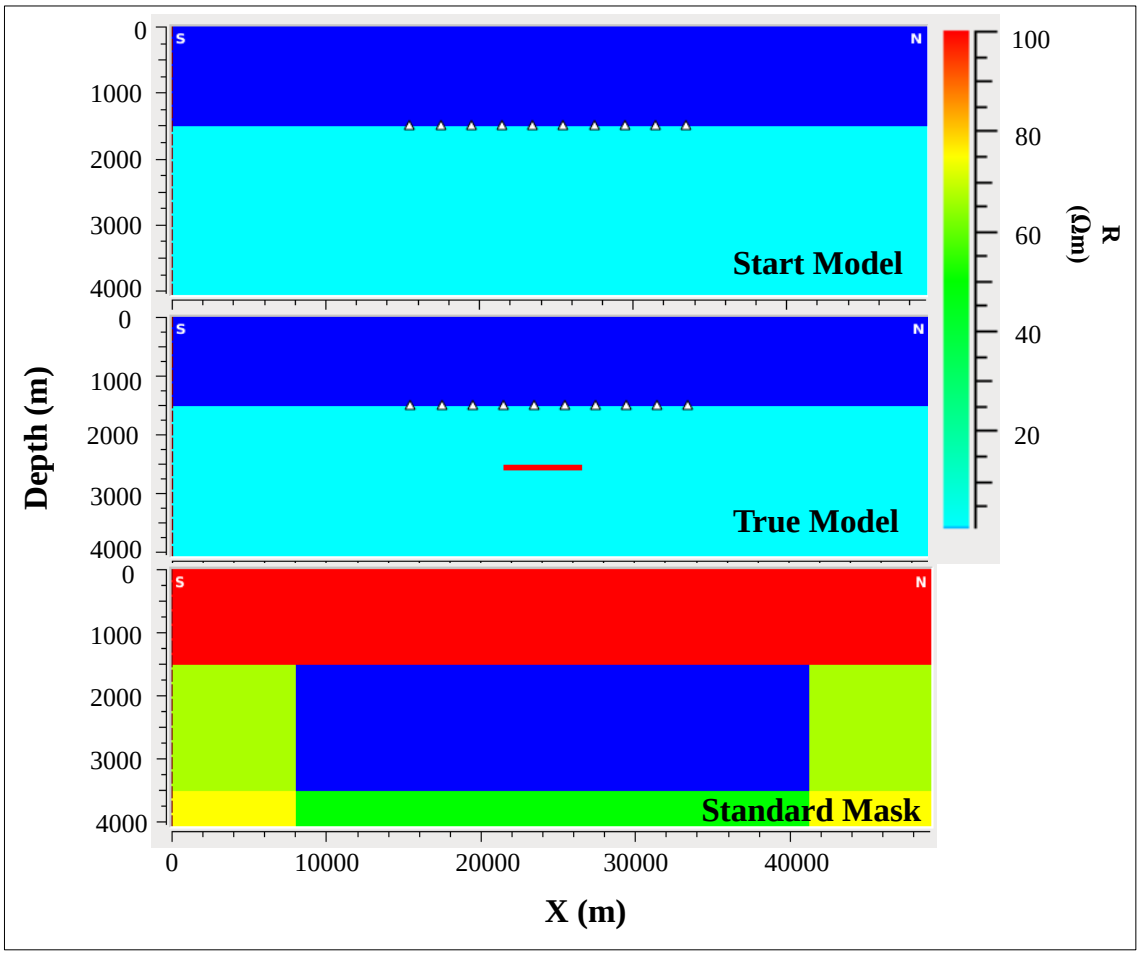

Figure 4. 12: Input models to run the unconstrained inversions.

- **High depletion**

As the sensitivity analysis results showed that minimum detectable depletion was approximately 2%, then the most focus by using the inversion approach should be between 1 to 2% depletion. In contrast, Orange et al. (2009) investigated the high depletion scenarios only in terms of data domain. Based on that, at the beginning the full reservoir model and the models with 20%, 40%, and 60% depletion are inverted. The model for full reservoir is inverted and the result of this inversion job is shown in Figure 4.13. Then, the inversion is applied for different stages of depletion as shown by Figure 4.14 which shows all the stages of depletion, corresponds to 0%, 20%, 40% and 60% depletion. This figure shows that by increasing the depletion, the resistivity decreases as well. This process is very clear. Because by increasing the depletion, the hydrocarbon will be replaced by brine and therefore resistivity decreases.

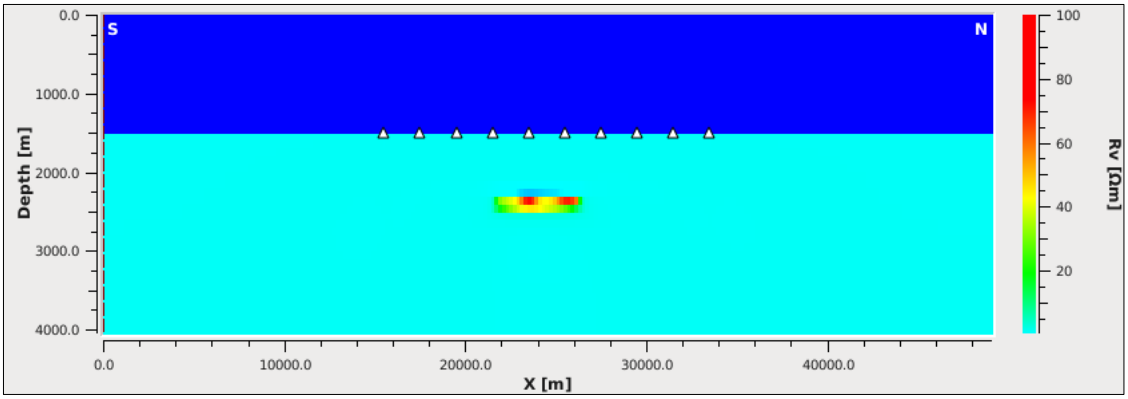

Figure 4. 13: Inversion for full reservoir, conductivity is 3.030 S/m.

It is important to know that in terms of inversion when the depletion is 80%, we cannot get the useful results as has been achieved in less depletion process. The reason is probably that the response from such a small reservoir is too small and inversion regards the data fit is good enough after just 4 or 5 iterations, which is not useful. Then it will be focused between 0 and 60% depletion.

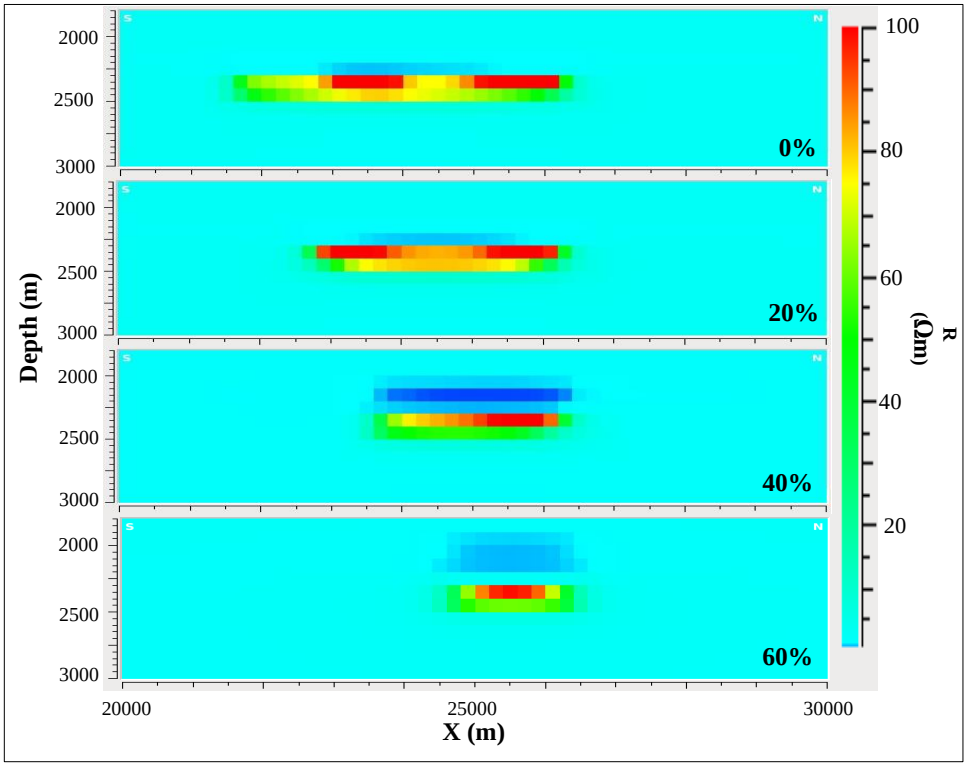

Figure 4. 14: Inversion of all the stages of depletion, corresponding to 0%, 20%, 40% and 60% depletion.

- **Small depletion**

Comparing the inversion results in terms of 0% and 20% according to the Figure 4.14 and even 10% depletion which has not been shown in this figure, it is clear that 20% depletion is very detectable. In addition, the result from sensitivity analysis based on Figure 4.11 implies that small depletion is detectable. Therefore, the inversion applies for small depletion steps and the difference between inversion results for depleted reservoir and full reservoir have been displayed in Figure 4.15. These results indicate that by applying unconstrained inversion, the minimum detectable inversion can be detected when depletion is greater than 4%. By looking at the resistivity difference between full and 2% depleted reservoir, according to the Figure 4.15, it is impossible to detect the depletion in this case. However, the red spot on the left side of 0-4% depletion indicates that by 4% depleting of the reservoir some change occur on resistivity of the reservoir. This detectability is more poor than the data domain approach. But to greater certainty, these results should be compared with the new values of seawater conductivity which changes over the time.

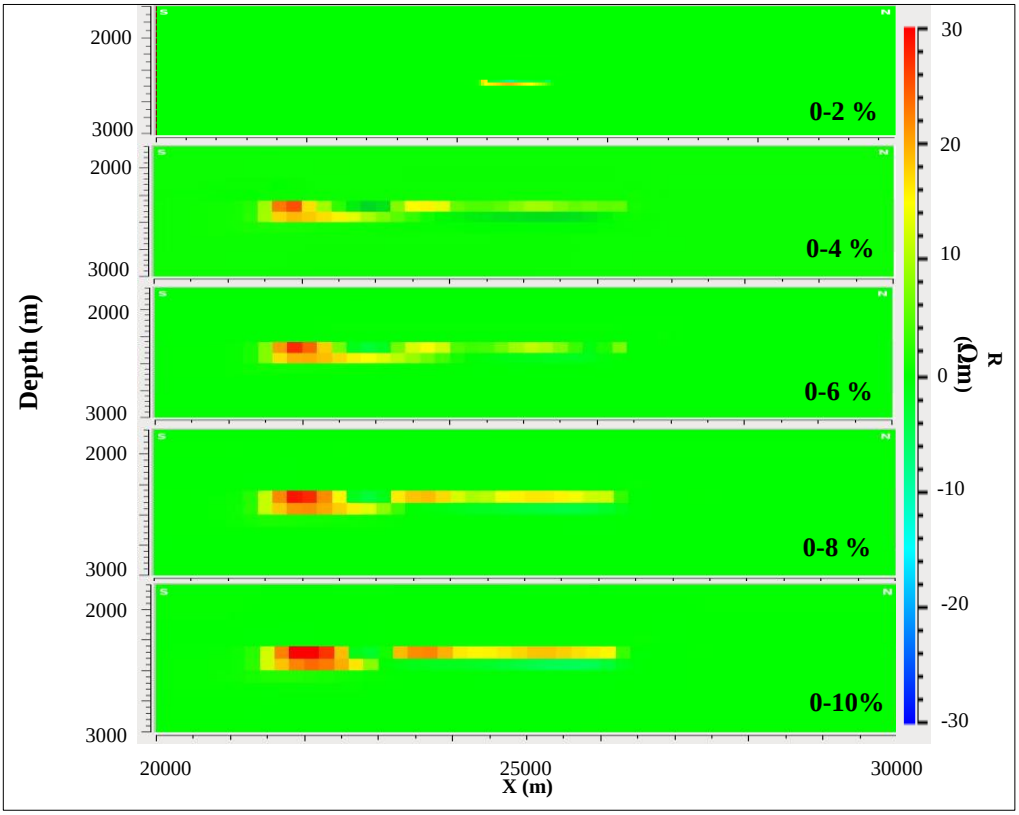

Figure 4. 15: Difference between 0-2%, 0-4%, 0-6%, 0-8% and 0-10% depletion, from top-to the bottom in this figure, respectively, conductivity =3.030 S / m.

- **Variation of seawater conductivity**

As already in data domain study has been assumed, the water conductivity varies over the time. In sensitivity analysis section, we examined the variation in response when seawater conductivity changes from the 3.030 S/m to a new value of 3.175 S/m. The inversion has already been applied on the base model when the conductivity for seawater is 3.030 S/m. The inversion is run after changing the seawater conductivity. Based on the variation of water conductivity, the inversion result for monitoring model will varies. The change of water conductivity can mask depletion anomalies if not accounted for during repeat monitoring measurements. The difference between base and monitoring inversion result is shown in Figure 4.16. Looking only at the difference between full-reservoir inversions results for two different water conductivities may be difficult to estimate the variation. The red part of the Figure 4.16 shows the positive change which occurs in the target and against, the blue part indicates the negative change in the target after inversion. Therefore, the calculation of this

variation will be difficult. However, the influence of variation of seawater conductivity is almost visible but by using just images it is not possible to compute how large this variation is.

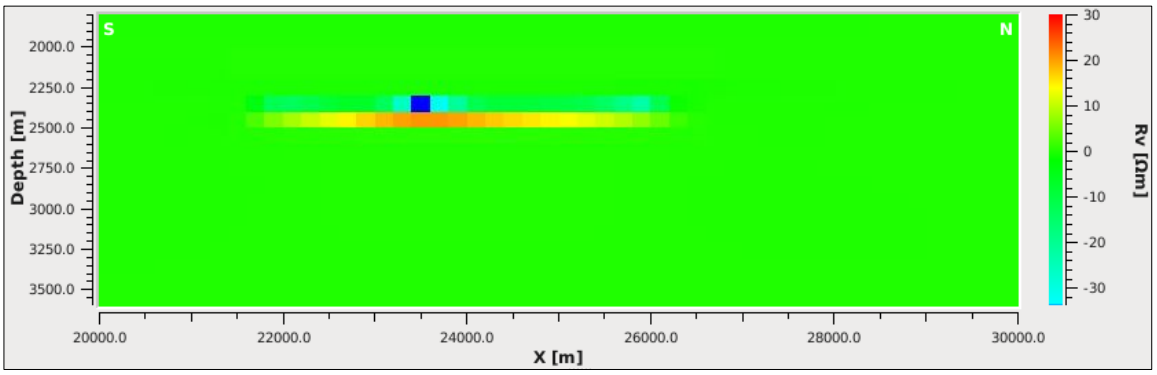

Figure 4. 16: The resistivity difference between full-reservoir inversions results for two different values of water conductivity: (σw_1 = 3.030 S/m and σw_2 = 3.175 S/m).

- **Anomalous Resistivity**

So far and by looking at the Figure 4.15, we can hopefully estimate that the minimum detectable depletion is 4%. In another hand, we assumed there is variation of seawater conductivity over the time and during depletion. Then by just looking at the images, the detection of this variation will be difficult. To handle variation in the anomaly, the average anomalous resistivity <AR> is introduced. Therefore, the calculation of anomalous resistivity is required as following:

$AR_{(x, y, z)} = R_{(box)} - R_{(Background)}$

Where, $R_{(Background)} = 1\ \Omega m$ and $R_{(box)}$ is anomalous resistivity.

Then, we have to integrate the anomalous resistivity for a specific area as following:

$$\int_{V_{box}} AR.dV = (\langle R_{box} \rangle - 1\Omega m).V_{box}$$

V_{box} covers the entire target (5000 m length, 100 m thickness) and a specific area around this layer. R_{box} is average anomalous resistivity belonging to V_{box} The <AR> after inversion depends on the depletion and thus the new values of resistivity.

In another hand, the resistivity for true model is already known. Therefore for true model:

$$\int_{V_{box}} AR.dV = (100\Omega m - 1\Omega m).V = 99\Omega m.100m.5000m = 4.95\times10^{7}\,\Omega m^{3}$$

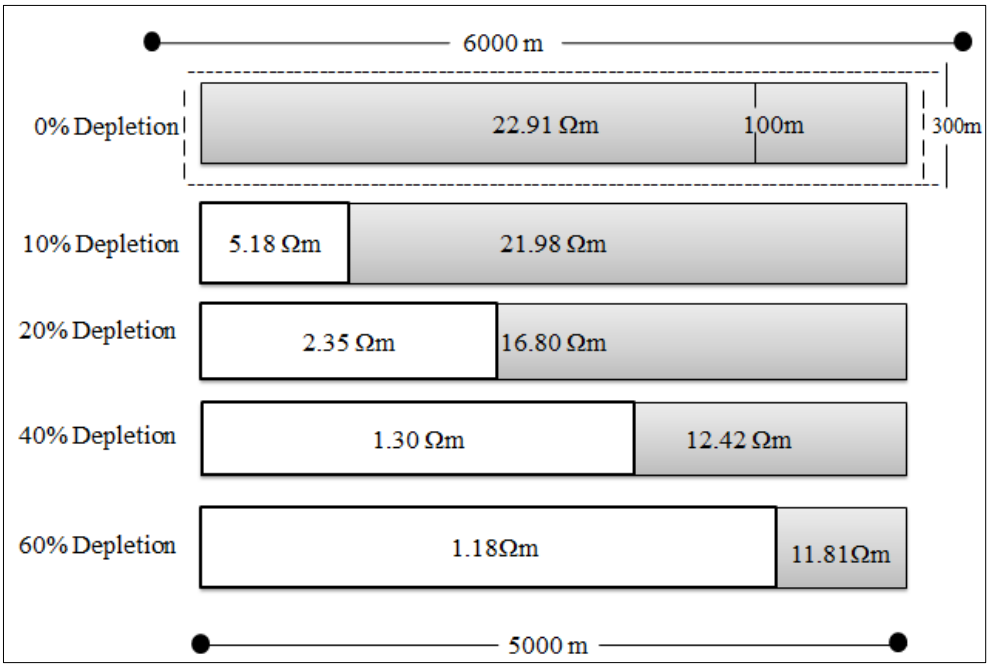

Figure 4. 17: Changing of <AR> during the depletion process.

Figure 4.17 shows the changing of average anomalous resistivity during the depletion process where by increasing the depletion, the resistivity of anomaly decreases. The average resistivity values for these part have been calculated when the depletion occurs from the left. Here, the length of anomaly is 6000 m and the thickness of that is 300 m. Therefore, to get the average anomalous resistivity some of the target's surrounding environment is also considered. The results from Figure 4.17 were far from 100 Ωm which was the resistivity for the true target. The reason is that the anomaly is very thick. To correct this misfit, a correction factor is applied. Basically, correction factor is a factor that is multiplied with the result of an equation to correct for a known amount of systemic error. One possibility is to integrate the anomalous resistivity over the volume of anomaly detected by inversion shown by equation (4.4). Ideally, it should match the integrated anomalous resistivity of the true model. For this purpose, the average anomalous resistivity (<AR>) for invert model has been calculated. And based on that, the correction factor can be described by following relationship:

$$CorrectionFactor = \frac{\int_{V_{box}} AR.dV(true)}{\int_{V_{box}} AR.dV(invert)} \quad (4.4)$$

Table 4.3 is including the computed average anomalous resistivity for every step of depletion and the calculated correction factors. This table and Figure 4.18 show that by increasing the depletion, the resistivity decreases.

Table 4. 3: The correction factors of various stages of depletion when the conductivity is 3.030 S/m.

Conductivity (S/m)	**Depletion (%)**	**Average Anomalous Resistivity <AR> (Ωm)**	**Correction Factor**
3.030	0	22.91	1.25
3.030	6	22.26	1.29
3.030	10	21.98	1.31
3.030	20	16.80	1.74
3.030	40	12.46	2.39
3.030	60	11.81	2.54

Gabrielsen et al. (2013) suggested that the correction factor is 1.28. The model which has been studied by them is different with the model used in this study and the resistivity of target they studied is 40 Ωm with varying thickness from Skrugard and Havis on the Polheim Sub-platform, located in the Norwegian North Sea, as shown in Figure 4.18. Table 4.3 shows that the results here are close to the correction factor value used by Gabrielsen et al. (2013) when the depletion is not too much and it means that these depletion scenarios generated small changes in the CSEM response. By following the results from Table 4.3, they are almost the same between 0 and 20% - the most important interval. Based on that, the variation of resistivity values are investigated in terms of small depletion and the most important results are displayed by Table 4.4. Again, the correction factors are calculated when the water conductivity is changed and the small depletions occurs. This table shows that by having small variation in the target, the correction factor values do not change a lot. That means the deviations for average anomalous resistivity in terms of small depletion are not much.

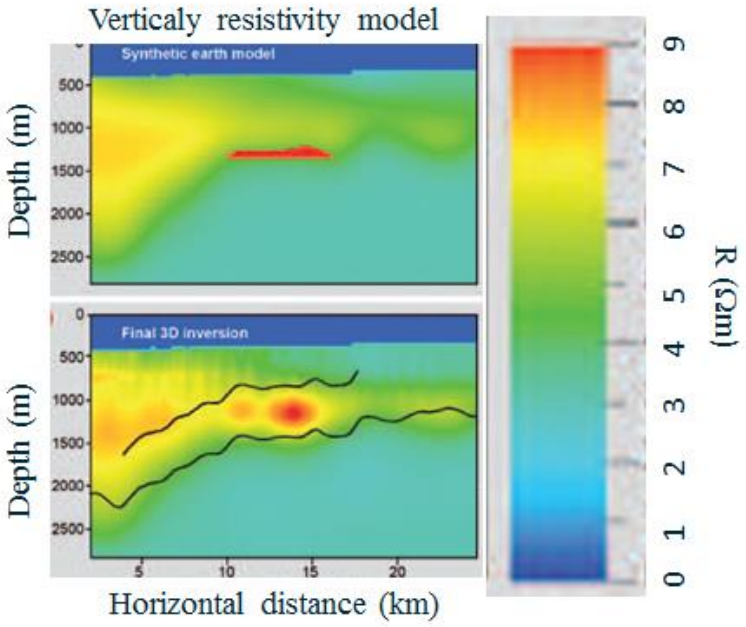

Figure 4. 18: Model used by Gabrielsen et al. (2013), Modified from (Gabrielsen et al., 2013).

Table 4. 4: The correction factors of various stages of minimum depletion for two different values of water conductivities.

Depletion (%)	Water Conductivity (S/m)	Average anomalous resistivity <AR> (Ωm)	Correction factor
0	3.030	22.91	1.25
2	3.030	22.44	1.28
4	3.030	22.35	1.28
6	3.030	22.26	1.29
8	3.030	22.17	1.29
10	3.030	21.98	1.31
20	3.030	16.80	1.74
0	3.175	22.91	1.25
6	3.175	21.31	1.35
20	3.175	15.89	1.84

Table4.4 also supports the correction factor value suggested by Gabrielsen et al. (2013).

4.2.3.2 Constrained inversion

The previous inversion results were unable to detect the minimum depletion of the target that it was expected. Thus, the inversion result is tried to be tuned here. The model which will be inverted is already shown in Figure 4.1. The constrained inversion is applied in this case. It means that the lower and upper conductivity bounds on the vertical model have been created. This estimation of the conductivity can be achieved by having some wells in the area. As we already pointed out, in terms of unconstrained inversion there is no limitation to apply inversion on the model. Table 4.5 shows that the conductivity for the true model is 1 S/m everywhere except for a small region around the reservoir where its value is 0.01S/m. The conductivity limits are slightly different. For the background the resistivity was chosen between 0.8 S/m and 1.25 S/m where the true value is 1 S/m. For the reservoir the maximum allowed resistivity is 1000 Ωm which is much above the true value of 100 Ωm. The cells in reservoir are 100 m thick i.e. there is just one layer of cells within the reservoir .All of the values which have been used in this section are shown in Table 4.5 and Figure 4.19. These models were used primarily to allow for minimum and maximum conductivity values in the background. It is important to know that, in this case, the regularization is 100 times weaker as it is shown in Figure 4.19. Therefore, this allows a very sharp conductivity contrast from background to the reservoir. As it is discussed in section 3.3.1, the regularization applies to reduce the non-uniqueness issue with inversion and also to stabilize the solution.

Table 4. 5: The different values of conductivity for sea water (σw), background (σBG) and reservoir (σR), which have been used to tune the inversions results.

	True Model (σ, S/m)	**Model with lower σ (S/m)**	**Model with higher σ (S/m)**
σ_w	3.03	2	5
σ_{BG}	1	0.8	1.25
σ_R	0.01	0.001	1.25

The result of constrained inversion for full reservoir is shown in Figure 4.20. Then, the constrained inversion is applied for depleted reservoir. However, the high depletion scenarios were not investigated in this section. Considering the obtained results from the unconstrained inversion and particularly from data domain, the minimum detectable depletion is less than 2%. Therefore, the inversion applies only for the small depletion steps. Figure 4.21 shows the difference of the resistivity between various depletion scenarios after inversion (from 0% to 10%). Comparing to the Figure 4.15, this figure shows a clear difference between inversion

results for 0% and 2% depletion. The left side of the Figure 4.21 indicates the increasing of resistivity because the depletion process again occurs from the left side of the reservoir.

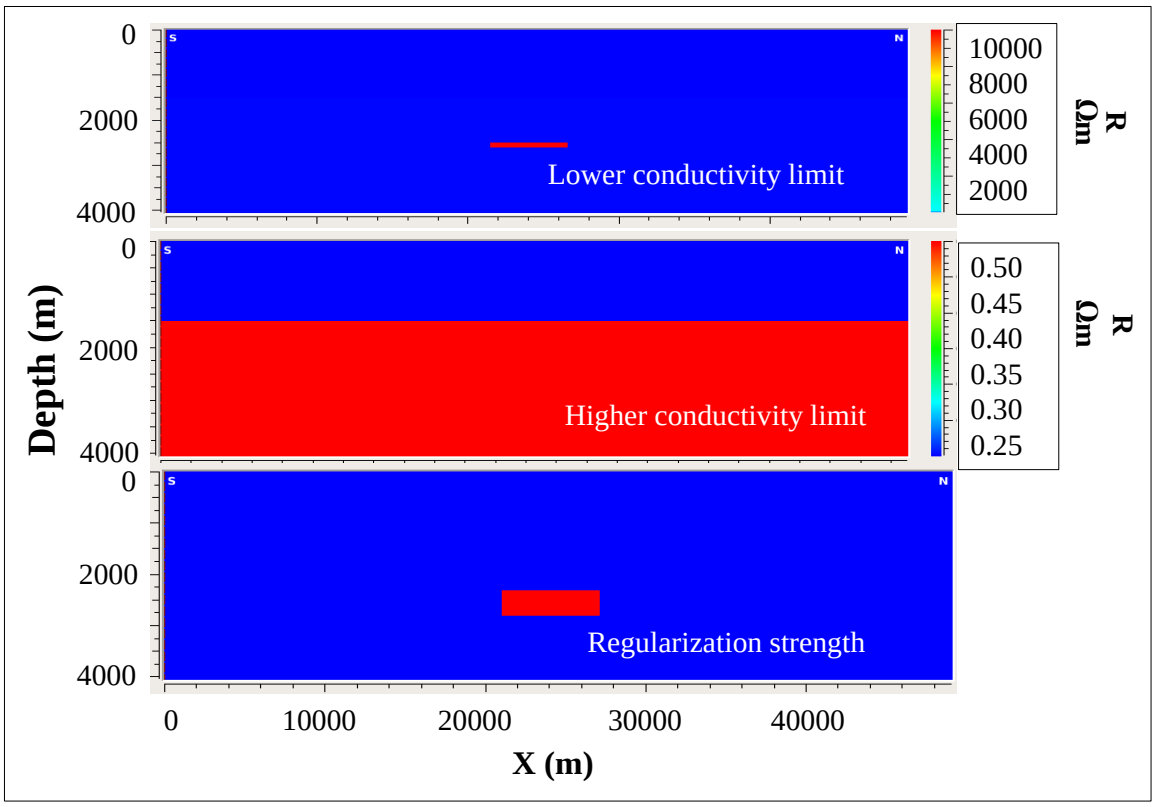

Figure 4. 19: The inputs models to run the inversions jobs for constrained inversion.

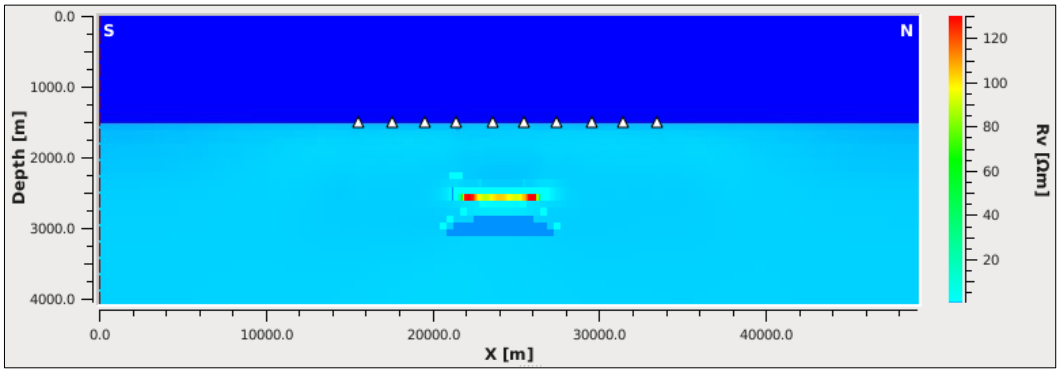

Figure 4. 20: The result of constrained inversion for full reservoir, water conductivity = 3.030 S/m.

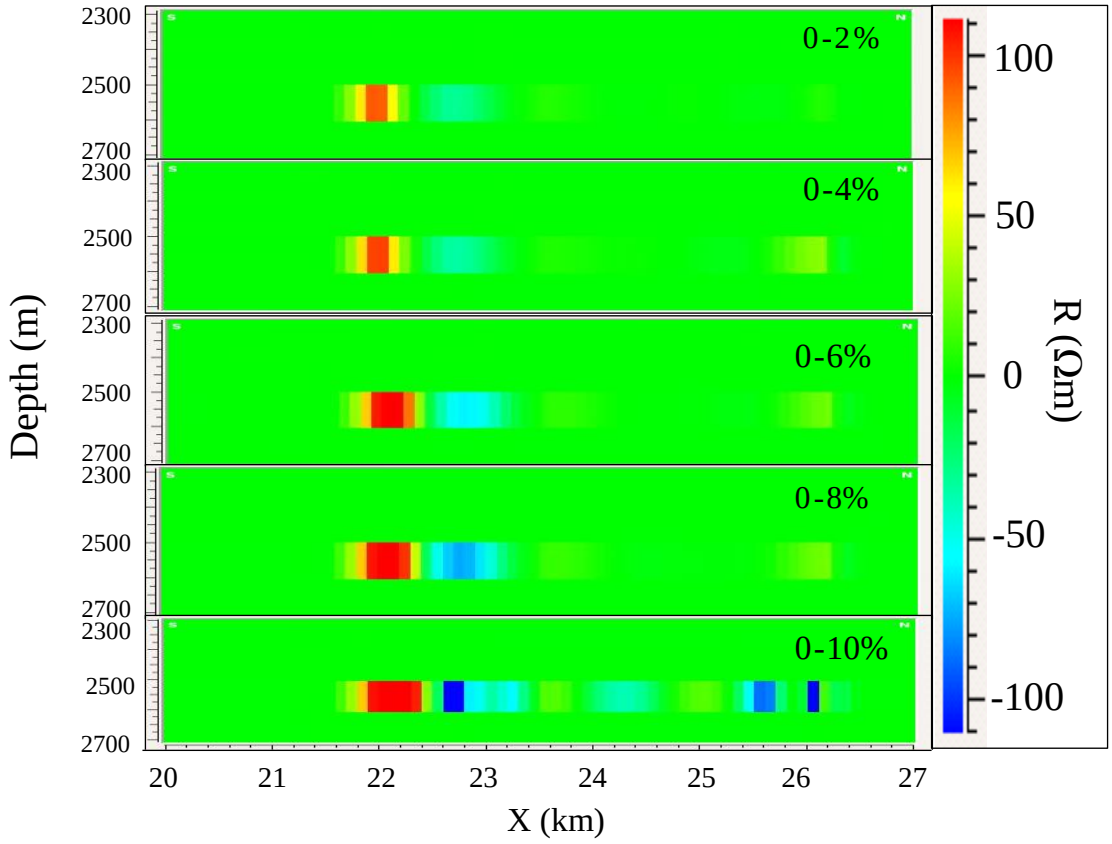

Figure 4. 21: The difference of resistivity between different percentage-depletion and full-reservoir. 0-2%, 0-4%, 0-6%, 0-8%, 0-10%, σ_w = 3.030 S/m.

To detect the minimum depletion the same constrained inversion approach is used when the seawater conductivity has new value of 3.175 S/m. The difference between inversion results of base and monitoring models is shown in Figure 4.22. Comparing results of unconstrained inversion depicted in Figure 4.16 with constrained results of Figure 4.22, one can conclude that Figure 4.22 demonstrates the variations of resistivity in a more understandable way.

Figure 4.22 shows that this variation is up to maximum 10 Ωm while Figure 4.21 shows that the difference between inversion results for full reservoir and 2% depleted reservoir is much larger and is approximately100 Ωm. By analyzing these figures the minimum detectable depletion is approximately 2%. However, assessment base on the image analyzing is uncertain. Therefore, performing numerical analysis based on the average anomalous resistivity, <AR>, is chosen as suitable option here.

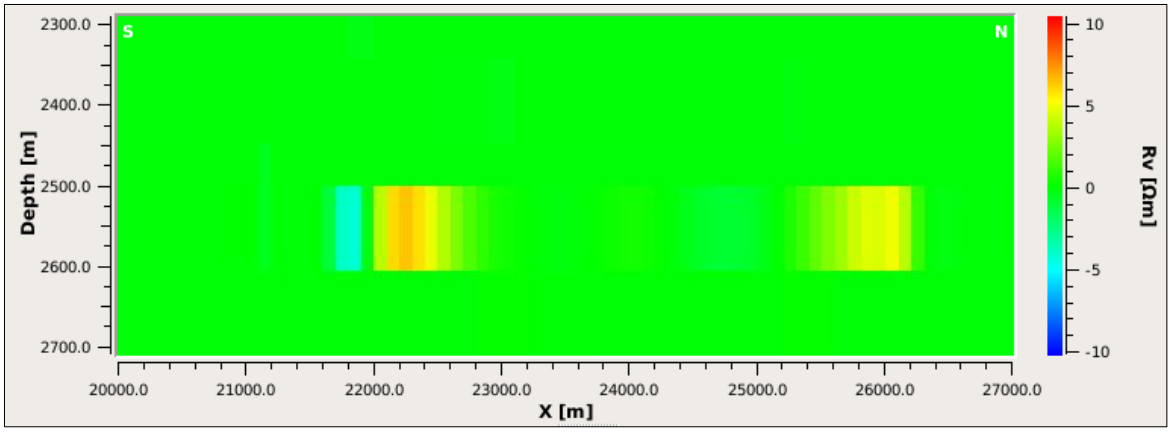

Figure 4. 22: The difference between full-reservoir inversion results for two different water conductivities is computed, (σ_w = 3.030 S/m and σ_w = 3.175) S/m.

Since water would replace the hydrocarbon phase during depletion process, it is therefore expected to observe reduction in resistivity of anomaly. Then the <AR> is computed for the full and depleted models. To get the new values of <AR>, the V_{box} is changed and average anomalous resistivity for the area which only includes the target has been computed. We do so since we already know the resistivity of the target (i.e. 100 Ωm) and the <AR> should be close to 100 Ωm. As might be expected, the average values for resistivity increases substantially. These new values have been plotted in Figure 4.23 where the seawater conductivity is 3.030 S/m. As it is shown, the data are very close to the fitted trend line, except for the 8% depletion. The reason could be due to possible uncontrolled randomness error in inversion results. According to the Figure 4.23, the average anomalous resistivity for cases of full reservoir and 2% depletion is 97.63 Ωm and 96.25 Ωm, respectively. That means there are some changes in <AR> values for different depletion scenarios. Figure 4.24 shows the calculated <AR> when the seawater conductivity is 3.175 S/m. Again a reasonable fit is obtained while the same uncontrolled randomness error is still visible.

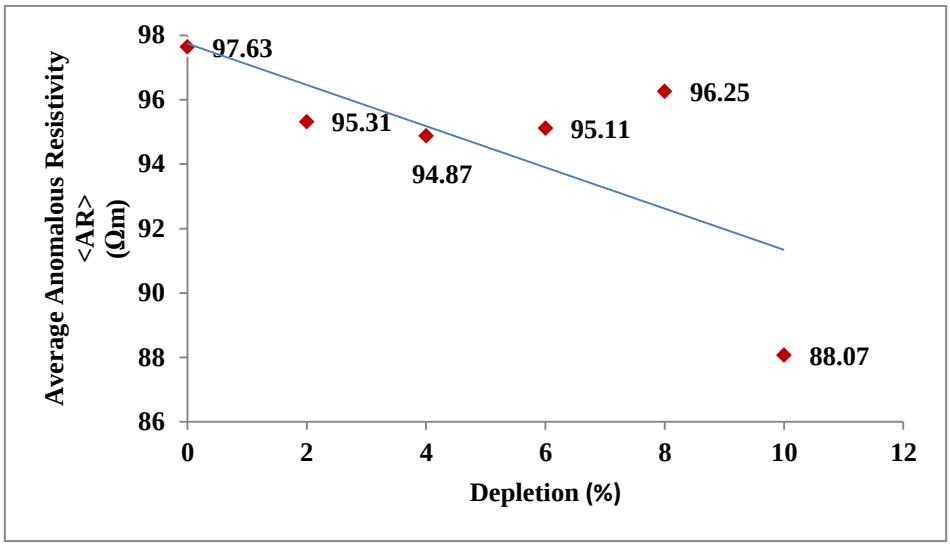

Figure 4. 23: The average anomalous resistivity for different values of depletion, σ_w =3.030 S/m.

Comparison between these two figures indicates that changing the seawater conductivity by 4.5%, would results in only 3% change of average anomalous resistivity.

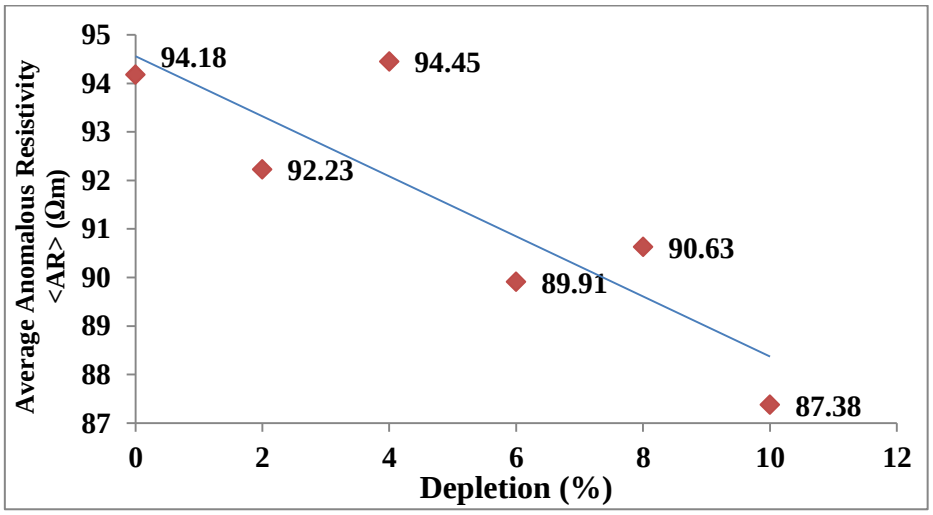

Figure 4. 24: The average anomalous resistivity for different values of depletion, σ_w =3.175 S/m.

The seawater conductivity has a significant impact on inversion results. Basically, in current study, we need to know how much average anomalous resistivity in inverted models would change when the water conductivity changes from 3.030 S/m to 3.175 S/m. Therefore, the difference in average anomalous resistivity for full-reservoir is computed:

$<AR>(\sigma_{w2}) - <AR>(\sigma_{w1}) = 97.63\ \Omega m - 94.18\ \Omega m = 3.45\ \Omega m$

Where:

<AR>(σ_{w1}) and <AR>(σ_{w2}) are average anomalous resistivity for full-reservoir when the sea water conductivity is 3.030 S/m 3.175 S/m, respectively.

These results indicate that applying 4.5% changes in the water conductivity the average anomalous resistivity for full-reservoir changes 3.45 Ωm. However, to detect the minimum depletion this number cannot help us, and another approach has been taken.

Here, more data will be collected and six values of water conductivity will be tested in line with inversions. Then, the average anomalous resistivity values are plotted as a function of water conductivity. The results are shown in Figure 4.25. This plot will look more consistent than the plot with average resistivity versus depletion. However, since the trend is almost perfectly linear, it might be better to ask how much the average anomalous resistivity changes when conductivity changes by

$$\frac{3.175-3.030}{3.175}\times 100 = 4.56\% .$$

To get the minimum detectable depletion, the focus will be on the difference between the variation of resistivity for base when the seawater conductivity is 3.030 S/m and monitoring model when the seawater conductivity is 3.175 S/m. Therefore, the average values form Table 4.6 is generated for these two models and the difference will be computed afterward.

Based on this figure, the relative resistivity difference for two values of water conductivity is computed. Considering the trend line's equation y = -2.1751x + 103.45, the relative difference resistivity according to the Table 4.6 for two different values of water conductivity is:

$$\left|\frac{y_{\sigma w2}-y_{\sigma w1}}{y_{\sigma w2}}\right| = \left|\frac{(-2.1751\times 3.175+103.45)-(-2.1751\times 3.030+103.45)}{(-2.1751\times 3.175+103.45)}\right| = 3.31\times 10^{-3}$$

$1-(3.31\times 10^{-3}) = 0.996$

It means a 0.004 (0.4%) change in resistivity values compare to the reference model. This value (i.e. 0.996) corresponds to depletion of less than 1% as shown in Figure 4.26.

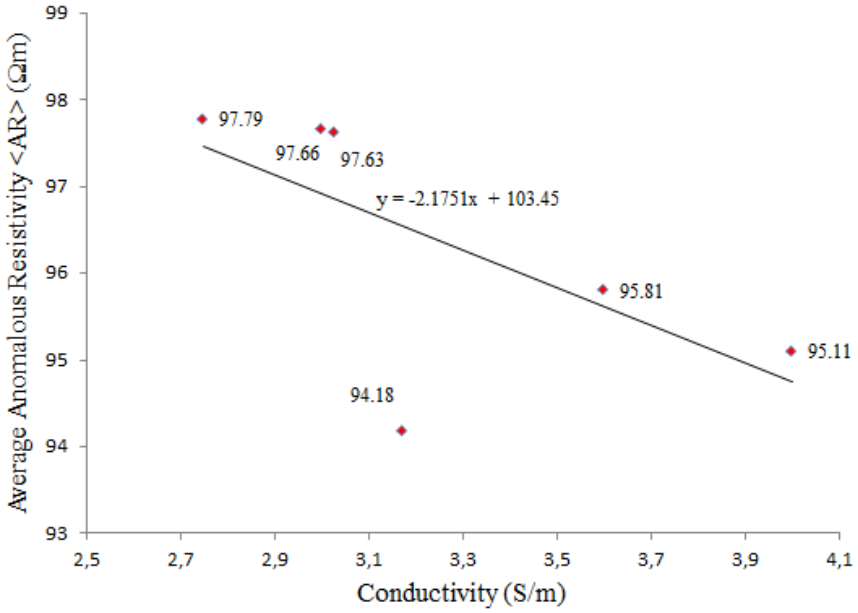

Figure 4. 25: Average anomaly resistivity as a function of seawater conductivities for six different values of seawater conductivity.

Table 4. 6: The average resistivity for different values of depletion, for two different water conductivities.

Depletion (%)	**<AR>(σ_{w1}) (Ωm) σ =3.030 (S/m)**	**<AR>(σ_{w2}) , (Ωm) σ = 3.175 (S/m)**
0	97.63	94.18
2	95.31	92.23
4	94.87	90.45
6	95.11	89.91
8	96.25	90.63
10	88.07	87.38

To determine the minimum detectable depletion, the normalized average anomaly resistivity is required. Thus normalized average anomaly resistivity is computed as following;

$< AR_n > / <AR_1>$

n= 1-7 and $<AR_1> = 97.63$ Ωm

The calculated normalized average anomalous resistivity for all depletion scenarios are also listed in Table 4.7.

Table 4. 7: Calculated normalized average anomalous resistivity.

n	Depletion (%)	Water Conductivity (S/m)	<AR>	Normalized Average Anomalous Resistivity (AR_n / AR_1)
1	0	3.030	97.63	1
2	2	3.030	95.31	0.976
3	4	3.030	94.87	0.972
4	6	3.030	95.11	0.974
5	8	3.030	96.25	0.986
6	10	3.030	88.07	0.910
7	0	3.175	94.18	0.964

Again, in this section the results show that the minimum detectable depletion is 1% which is close to our expectation.

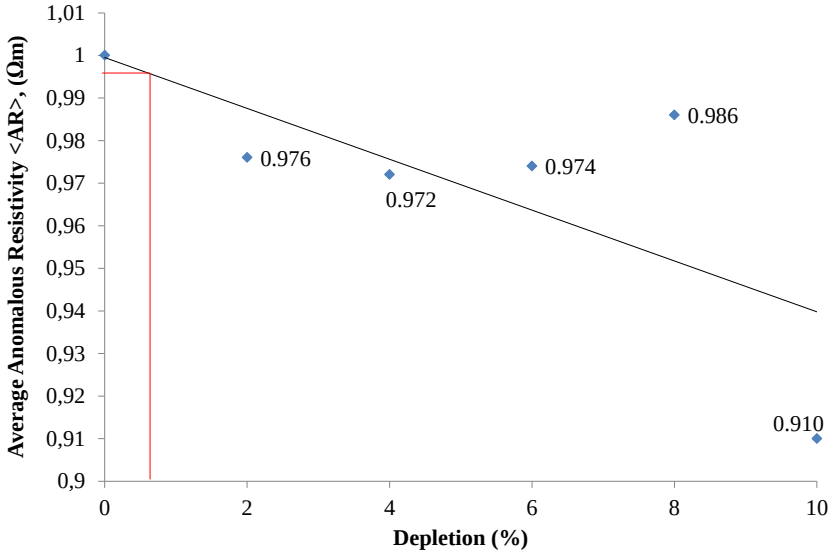

Figure 4. 26: The normalized average anomaly resistivity vs depletion plot to detect the minimum depletion where this shows that the minimum detectable depletion is less than 1%.

4.2.3.3 Fixed Background

During the depletion of the target, the resistivity of the target varies. At the same time, the resistivity of the background is untouched. The data for the base model which has been inverted here are same as previous jobs. In the previous inversion runs, the conductivity of all model constituents including formation and hydrocarbon layer (except water) were used to achieve the least possible minimum detectable depletion. In the new inversion runs, we do not allow inversion workflow to modify the background resistivity which is the biggest part of the

model. To provide the mapping between the conductivity of the model grid cells and the inversion parameters, another model mask must be provided here. Indeed, we can see that the resistivity does not change in the red region in Figure 4.27. That means the resistivity will change only in blue region.

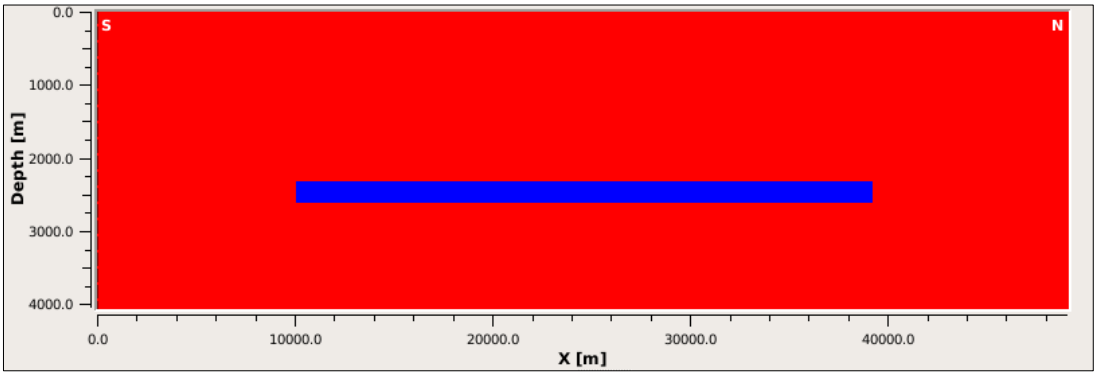

Figure 4. 27: The schematic of mask which has been used in this inversion job.

This region has the shape of the reservoir or at least a few cells bigger. In this case, it is only a few cells bigger in vertical (z) direction, but much wider in horizontal (x) direction. If the final model of full-reservoir inversion is acceptable, it should be used to prepare the start model for all subsequent inversions. This is the right way to create start model for "monitoring" inversions, which in practice will be run few years after the "base" inversion. However, these monitoring inversions should take data for depleted reservoirs, because the reservoir would deplete after few years. In addition, one more inversion that addresses the effect of water conductivity variations should be ran. By inverting the base model with constrained background, the Figure 4.20 is obtained. Then, the target is erased and used as the start model for inversion. This start model is shown in Figure 4.28. The reason was that we had no change in the background. Then the inversion is applied for full reservoir, and final result is shown in Figure 4.29 for the fixed background case. Likewise, the inversion is applied for small depletion steps also and the difference of resistivity between inversion results for full reservoir and small depletion is shown in Figure 4.30. From this figure one can understand that the depletion process occurs from the left. Moreover, the yellow spot in case of 2% depletion indicates some resistivity changes during the depletion.

The variation between seawater conductivity from base model to monitoring model is 4.5%. This new start model (Figure 4.28) is used for monitoring inversion job with the new values of sea water conductivity which varies over the time. The difference between the inverted

resistive models is shown in Figure 4.31 when the sea water conductivity is changed from the base model to the monitoring model. A result presented in figures 4.30 and 4.31 indicates that 4% depletion is more distinguishable than 2% depletion. But because of different color scale on these figures the comparison is difficult. Then, computing of average anomalous resistivity is required.

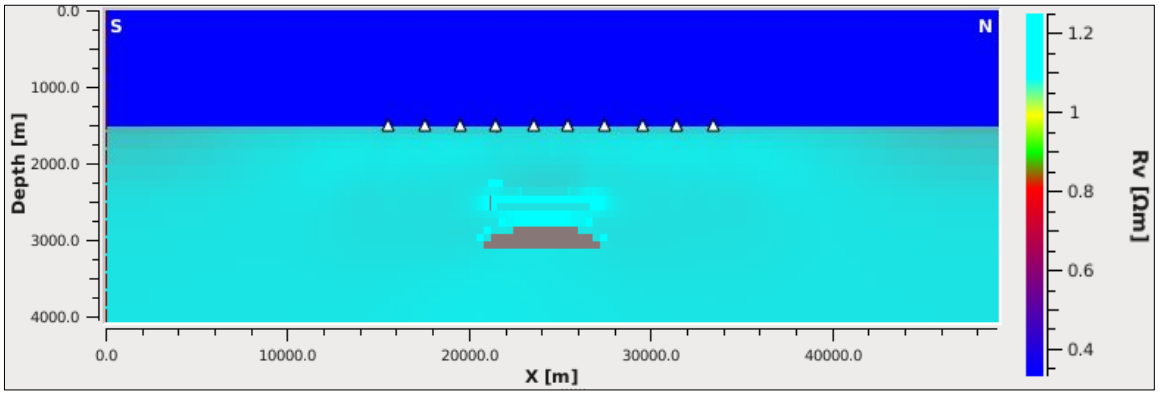

Figure 4. 28: The new start model for fixed background inversion. The target is erased from constrained inversion result.

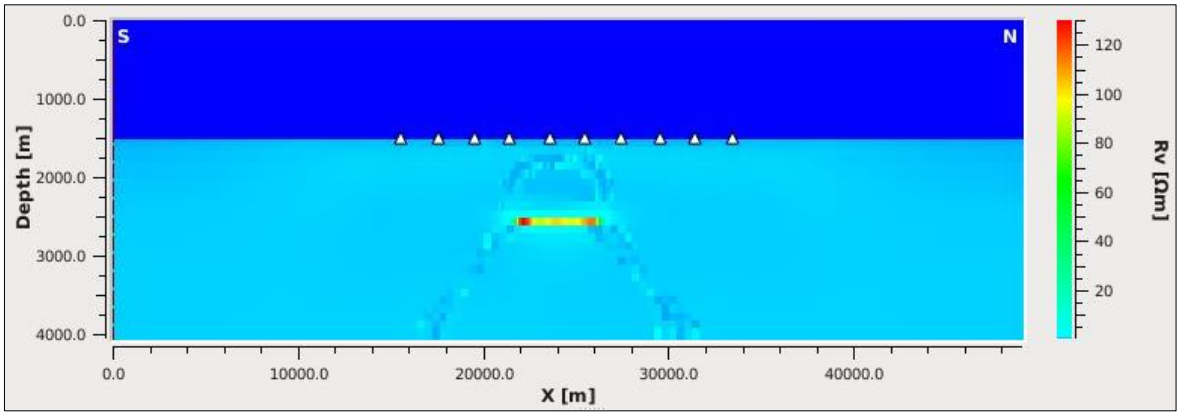

Figure 4. 29: The resistive model after inversion when the background has been fixed.

Again it is tried to find the minimum detectable depletion based on all of these new results. Table 4.8 shows <AR> for the full reservoir with two different values of seawater conductivity and depleted reservoir.

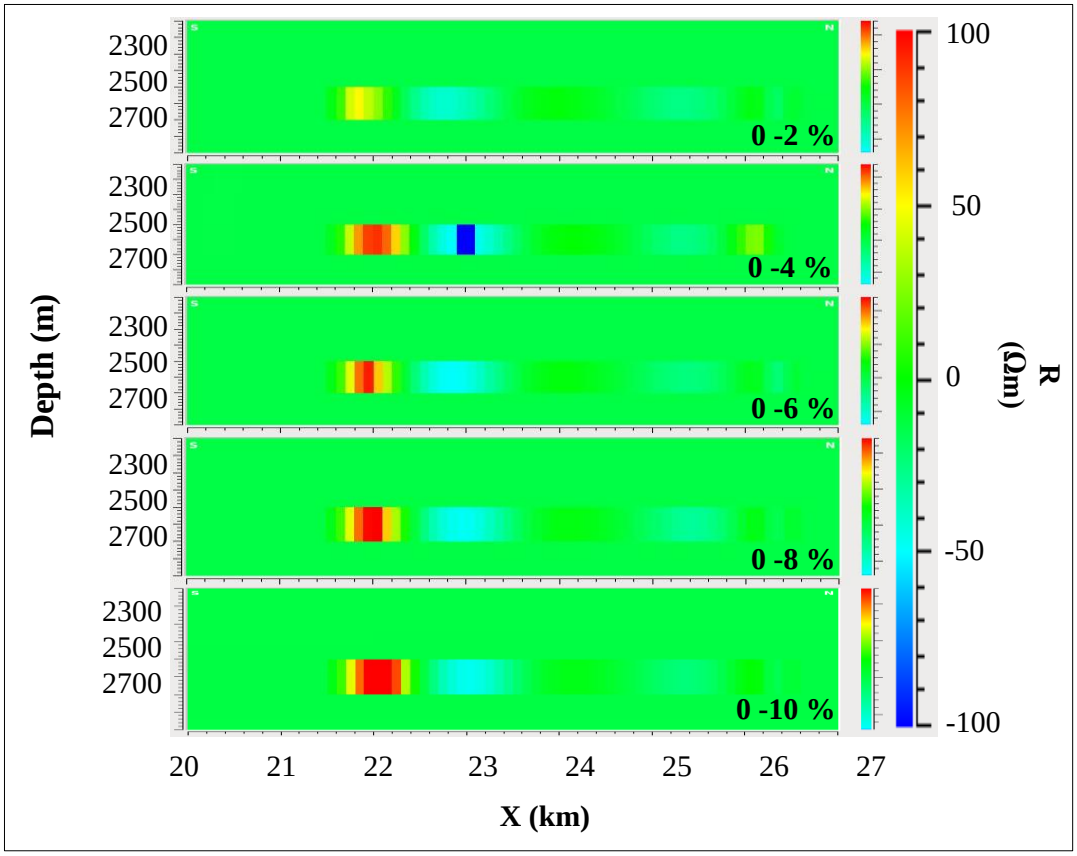

Figure 4. 30: The relation between different percentage-depletion and full-reservoir, for fixed background inversion.σw = 3.030 S/m.

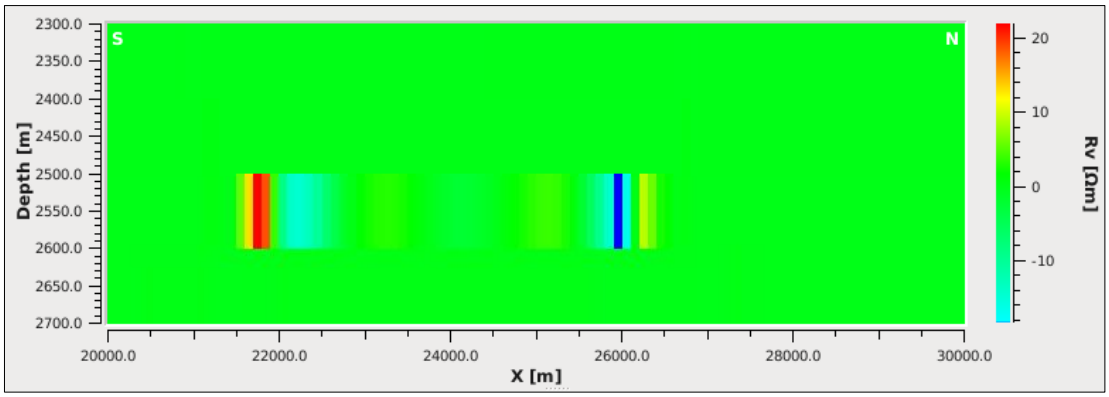

Figure 4. 31: The difference between full-reservoir inversion results for two different values of water conductivity is computed, (σ_{w1} = 3.030 S/m and σ_{w2} = 3.175) S/m.

Table 4. 8: The average resistivity anomalous for different values of depletion, for two different values of water conductivity.

Data used for inversion are computed for			Start model for inversion		<AR> (Ωm)
Background (Ωm)	Target	Water conductivity (S/m)	Background (Ωm)	Water conductivity (S/m)	
1	Full	3.030	1	3.030	90.37(*)
1	Full	3.030	Final model from inversion (*), target erased	3.030	**92.94**
1	2% depleted	3.030	Final model from Inv (*), target erased	3.030	89.50
1	4% depleted	3.030	Final model from Inv (*), target erased	3.030	88.65
1	6% depleted	3.030	Final model from Inv (*), target erased	3.030	86.34
1	8% depleted	3.030	Final model from Inv (*), target erased	3.030	85.02
1	10% depleted	3.030	Final model from Inv (*), target erased	3.030	83.22
1	Full	3.175	1	3.175	91.31
1	Full	3.175	Final model from Inv (*), target erased	3.175	**92.47**

To determine the minimum detectable depletion the same approach as has been used in section 4.2.3.3 is applied here and the for every steps of depletion and for different values of water conductivity also computed. However, in this section the focus is only on between two values of water conductivity. In another word, the normalized average anomalous resistivity for base model when σw1 = 3.030 S/m and monitoring model when σw2 = 3.175 S/m is investigated and then, the minimum detectable depletion is calculated.

$<AR>(\sigma_{w2}) \ / <AR>(\sigma_{w1}) = 92.47/ 92.94= 0.995$

1-0.995= 0.005

Having 0.5% difference in resistivity values compared to the reference model, the minimum depletion will be detectable when depletion is almost 1% as shown in Figure 4.32. By comparing the figures 4.26 and 4.32 one can realize that the detectability of minimum depletion is improved substantially. This improvement is because of the fixing of background. Obviously, with depletion of the reservoir the data would change too. However, we did not allow that changing of the reservoir resistivity affects the background resistivity. Because of this, the variation of resistivity occurs in a specific region where there is hydrocarbon only.

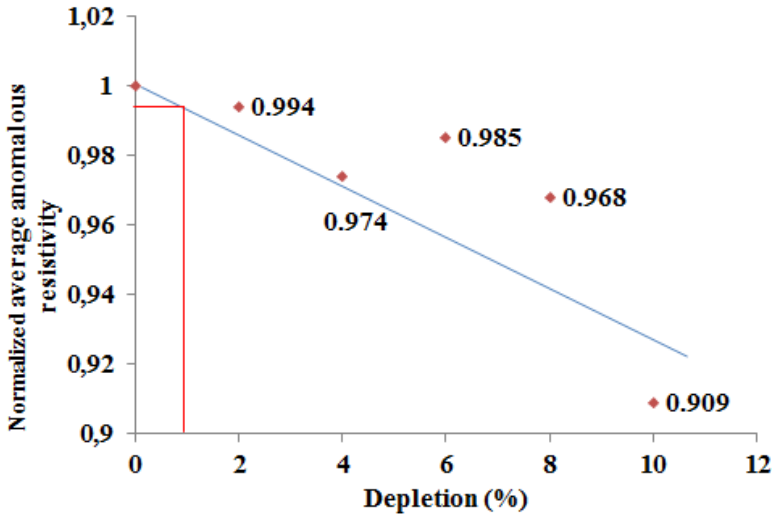

Figure 4. 32: The normalized average anomaly resistivity vs depletion plot to detect the minimum depletion.

4.2.3.4 Wrong background in the start model

So far the start model for the base survey of the full-reservoir was a uniform half-space model (water layer + uniform half-space below seafloor) with resistivity 1 Ωm which is the correct background resistivity. In reality, we do not know the background resistivity accurately and therefore our start model would always be slightly wrong. Therefore, the inversion will be run where the start model is a uniform half-space with resistivity 0.9 Ωm. We run the inversion scenarios which are listed on the Table 4.9. The inversion for these models is run and the last result for full reservoir with σ_w = 3.030 S/m is shown in Figure 4.33. Again, the target should be erased and the new start model is applied for new inversion as it is shown in Figure 4.34.

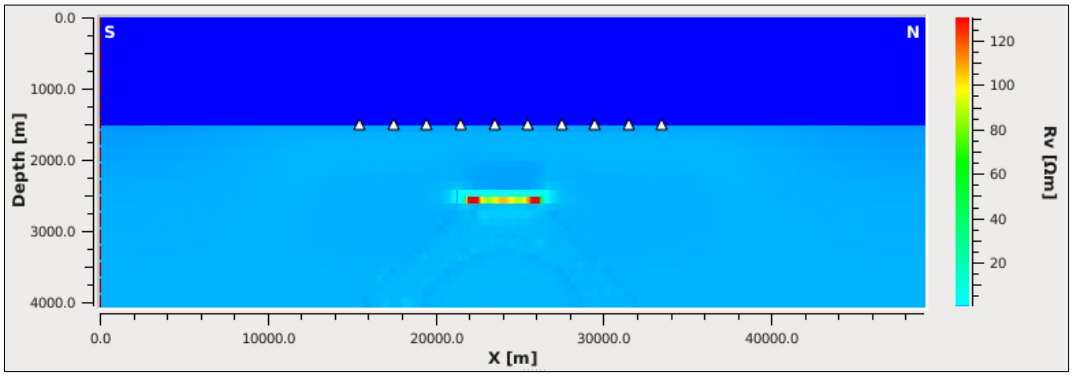

Figure 4. 33: The last inversion result (inversion Nr.1, according to the Table 4.9) for full reservoir with σ_w = 3.030 S/m with wrong background.

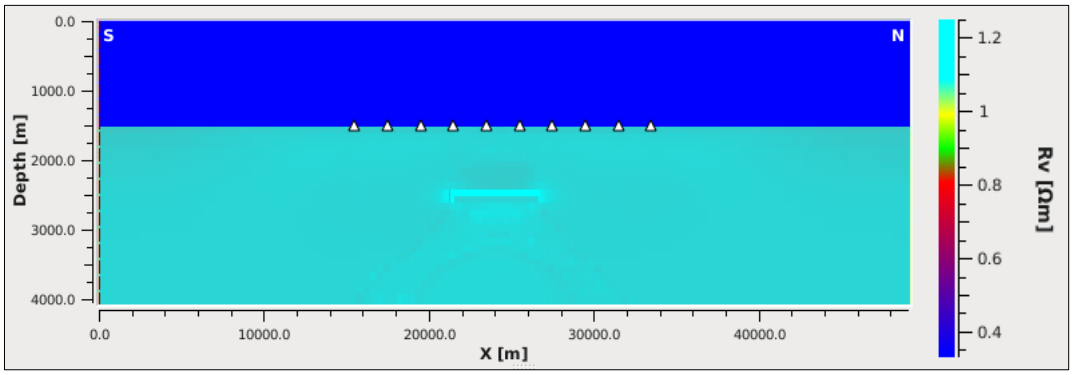

Figure 4. 34: The new start model for wrong background inversion. The target is erased from inversion Nr.1 when the background has wrong value.

Figure 4.35 shows the result of inversion when the background has wrong value of 0.9 Ωm. Comparing to the correct background i.e. 1 Ωm, the new background value is deacresed 10%.

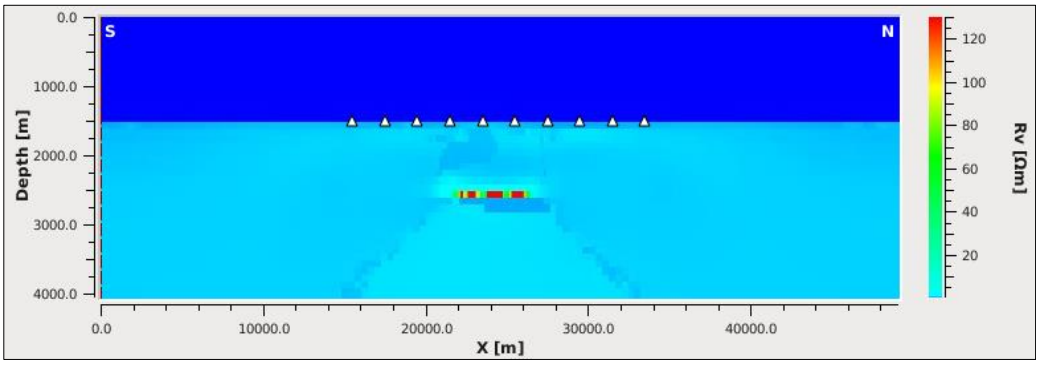

Figure 4. 35: Final inversion result (inversion Nr.2) for full reservoir with σ = 3.030 S/m and wrong background.

The whole process is repeated for 4.5% variation in the seawater conductivity. In addition, the inversion for depleted reservoir is run to detect the minimum depletion. The results are listed in the Table 4.9. By comparing this table with Table 4.8, the variation of <AR> is evident. The reason is the wrong value of background which is 10% difference.

Table 4. 9: The average resistivity for different values of depletion, for two different values of water conductivity with wrong background.

Inversion No.	Data used for inversion are computed for			Start model for inversion		<AR> (Ωm)
	Background (Ωm)	Target	Water conductivity (S/m)	Background (Ωm)	Water conductivity (S/m)	
1	1	Full	3.030	0.9	3.030	101.36 (*)
2	1	Full	3.030	Final model from Inversion (*), target erased	3.030	**111.25**
3	1	2% depleted	3.030	Final model from Inversion (*), target erased	3.030	98.62
4	1	4% depleted	3.030	Final model from Inversion (*), target erased	3.030	97.26
5	1	6% depleted	3.030	Final model from Inversion (*), target erased	3.030	94.90
6	1	8% depleted	3.030	Final model from Inversion (*), target erased	3.030	95.87
7	1	10% depleted	3.030	Final model from Inversion (*), target erased	3.030	93.91
8	1	Full	3.175	0.9	3.175	101.25
9	1	Full	3.175	Final model from Inversion (*), target erased	3.175	**110.39**

Table 4.9 leads to estimate the minimum detectable depletion when the formation has wrong value. The same approach is used here as well and the normalized average anomalous resistivity for two full reservoirs with two different values of seawater conductivity is calculated by following equation:

$<AR>(\sigma_{w2}) \ / <AR>(\sigma_{w1}) = 110.39 / 111.25 = 0.992$

1-0.992= 0.008

It is expected that the average anomalous resistivity deviated more from true model (100Ωm-1Ωm=99Ωm). The average anomalous resistivity is 111.25 Ωm and 110.39 Ωm when the seawater conductivity is 3.030 S/m and 3.175 S/m, respectively. This increasing of <AR> is because of the 10% error of background. And by having 0.8% change in inverted reservoir

resistivity, the minimum detectable depletion is less than 2% as shown in Figure 4.36. The wrong background resistivity contains 10% error. The 10% error in the background resistivity of the synthetic model did not affect the minimum detectable depletion significantly. This claim can be approved through comparing the figures 4.32 and 4.36.

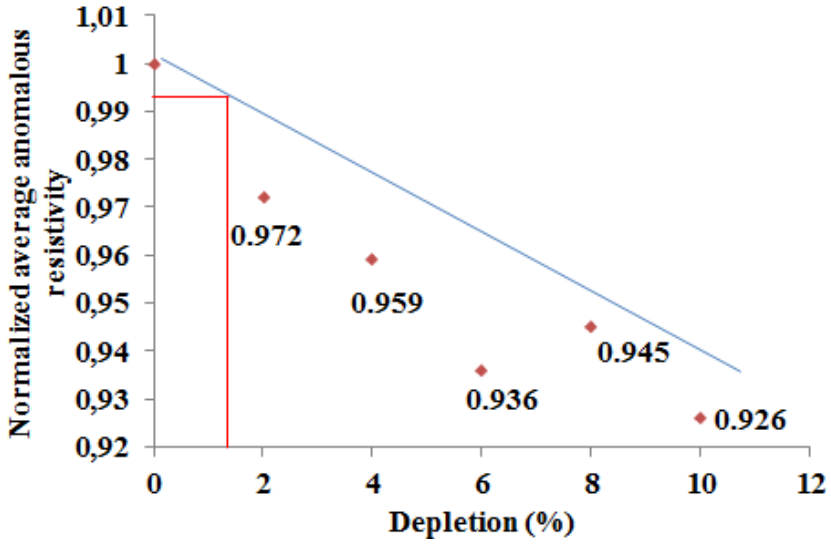

Figure 4. 36: The normalized average anomaly resistivity vs depletion plot to reach the minimum detectable depletion for wrong background.

4.3 Variation of receiver positions

One of the most significant sources of uncertainty in CSEM data is the errors in the position of the receivers. Again, in this section, the applicability of the CSEM method to the reservoir-monitoring problem will be examined by analyzing the ability of the representative 2.5D model to detect the minimum depletion of a reservoir. The 4D capability of the recorded data will be evaluated and one of the most probable sources of non-repeatability which is receiver position (Rx) will be discussed. Ocean current influences the operation of receiver dropping in the seawater. Therefore, the receiver position will not be the same for base and monitoring models. Thus, the recoded data will be different. The aim in this section is to compare the inline electric data for such situation.

4.3.1 Sensitivity analysis

In this section the receiver position variations, effect of target depletion, relative difference in Ex for different depletion scenarios and minimum depletion detectability will be investigated.

The model which has been used here is exactly same as one used by Orange et al. (2009) and is shown in Figure 4.1.

First, we investigate the effect of shifting in the lateral location of the receiver for inline electric field. The CSEM response variation for the third receiver from the left is calculated according to the Figure 8.1. The following formula is used and the results are shown in Figure 4.37.

$$relative\,difference\,in\,Ex = \left| \frac{E_{(new\ receiver\ position)} - E_{(original\ receiver\ position)}}{E_{(new\ receiver\ position)}} \right|_{peak}$$

Where E is inline electric field.

We move the receivers 25, 50 and 100 m away from their original position along the receiver lines. According to this figure, one can see that 25 m variation in lateral position would result in 1.88% relative difference in Ex. For 50 m and 100 m, the corresponding relative difference in Ex is 4.91% and 7.42%, respectively. In these calculations the frequency is set to 0.1 Hz.

The same approach has been done for other values of frequencies and the results are listed in Table 4.9. Moreover, the receivers were moved by 200 m and 500 m along the receiver lines direction to assess the effect of mismatch in receiver locations. Different acquisitions for base and monitoring models are performed. Since, the 100 m shifting of the receiver position gives almost high values of relative difference for Ex, the results for 200 m and 500 m shifting are not evaluated.

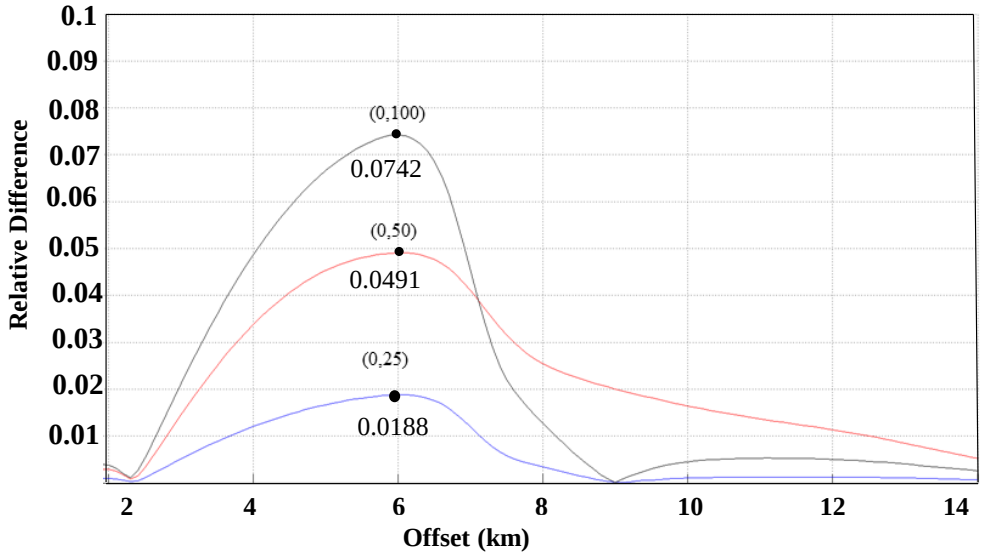

Figure 4. 37: Effect of error in receiver location. Relative difference of Ex with receiver at -2 km to response with receiver at 25m, 50m and 100m and frequency = 0.1 Hz.

Table 4. 10: False anomaly results for different values of receiver positions and frequencies.

Relative Difference in Ex (%)	Receiver position (E,N)	Frequency (Hz)
1.88	(0,25)	0.1
4.91	(0,50)	0.1
7.42	(0,100)	0.1
2.66	(0,25)	0.25
7.05	(0,50)	0.25
10.34	(0,100)	0.25
3.77	(0,25)	0.50
9.90	(0,50)	0.50
14.46	(0,100)	0.50
4.61	(0,25)	0.75
12.18	(0,50)	0.75
17.50	(0,100)	0.75
4.90	(0,25)	0.85
12.94	(0,50)	0.85
18.18	(0,100)	0.85
5.30	(0,25)	1.0
13.97	(0,50)	1.0
19.96	(0,100)	1.0

Now, the goal is to compute the minimum detectable depletion in the sensitivity analysis.. The effect of target depletion and relative difference in Ex for different stage of depletions is investigated.

The focus will be on 100 m shifting. The lateral depletion again is assumed from the left. Different frequencies have been investigated here. Figure 4.38 shows that by increasing the frequency, the absolute relative change of Ex increases as well. Here, 10% depleted reservoir has been investigated and this figure is obtained using following formula:

$$relative\,difference\,in\,Ex = \left| \frac{E_{(10\%\,depleted\,reservoir)} - E_{(Full\,reservoir)}}{E_{(10\%\,depleted\,reservoir)}} \right|_{peak}$$

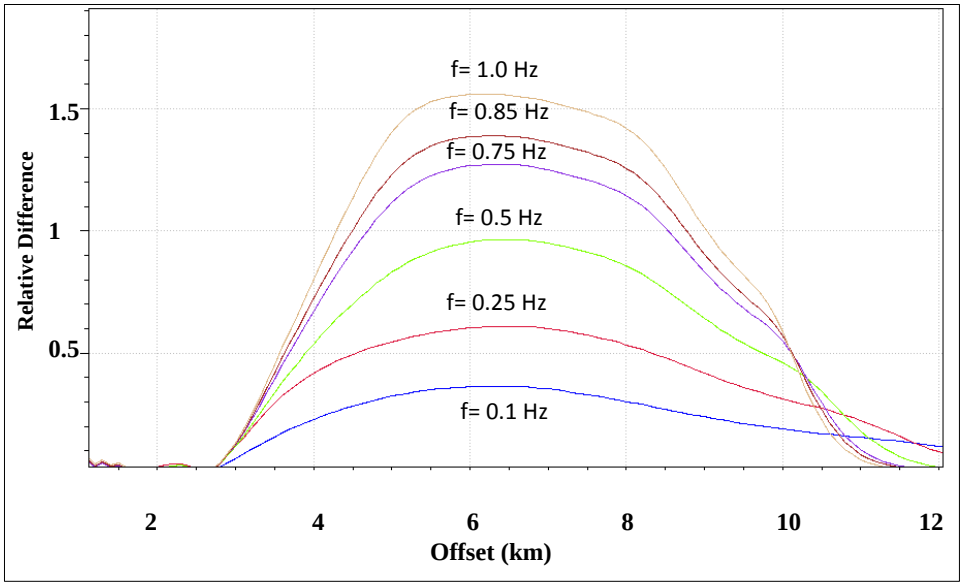

Figure 4. 38: Effect of inline electric field for 10% depletion compare to 0% depletion for different frequencies.

The relative differences in Ex for every step of depletion are calculated by using the following formula and the results are shown in Table 4.11.

$$relative\,difference\,in\,Ex = \left| \frac{E_{(depleted\,reservoir)} - E_{(Full\,reservoir)}}{E_{(depleted\,reservoir)}} \right|_{peak}$$

Table 4. 11: Relative difference values in Ex for small depletion

Depletion (%)	Relative difference in Ex (%)
0	0
2	6.69
4	13.51
6	20.42
8	27.41
10	34.46

Figure 4.37 indicated that by 100 m shifting of receiver positions in monitoring survey, the relative difference in Ex is 7.42% when the frequency is 0.1 Hz. Tables 4.10 and 4.11 are used to get the minimum detectable depletion. Based on these tables, the Figure 4.39 is obtained which indicates a minimum detectable depletion of more than 6% when the frequency is 0.1 Hz.

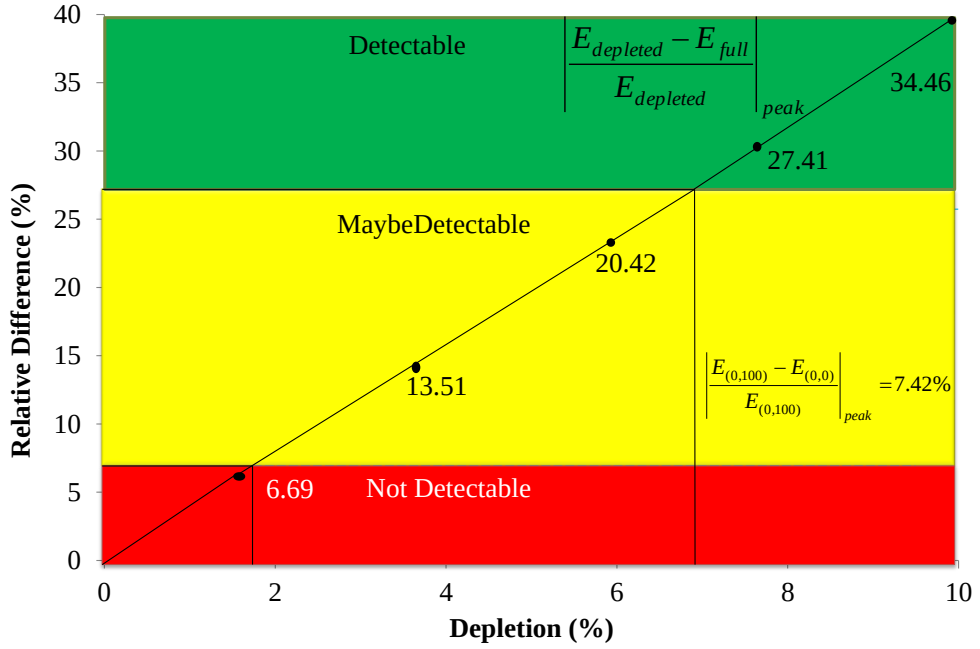

Figure 4. 39: Relative difference in Ex vs depletion, the minimum detectable depletion is more than 6%, frequency = 0.1 Hz.

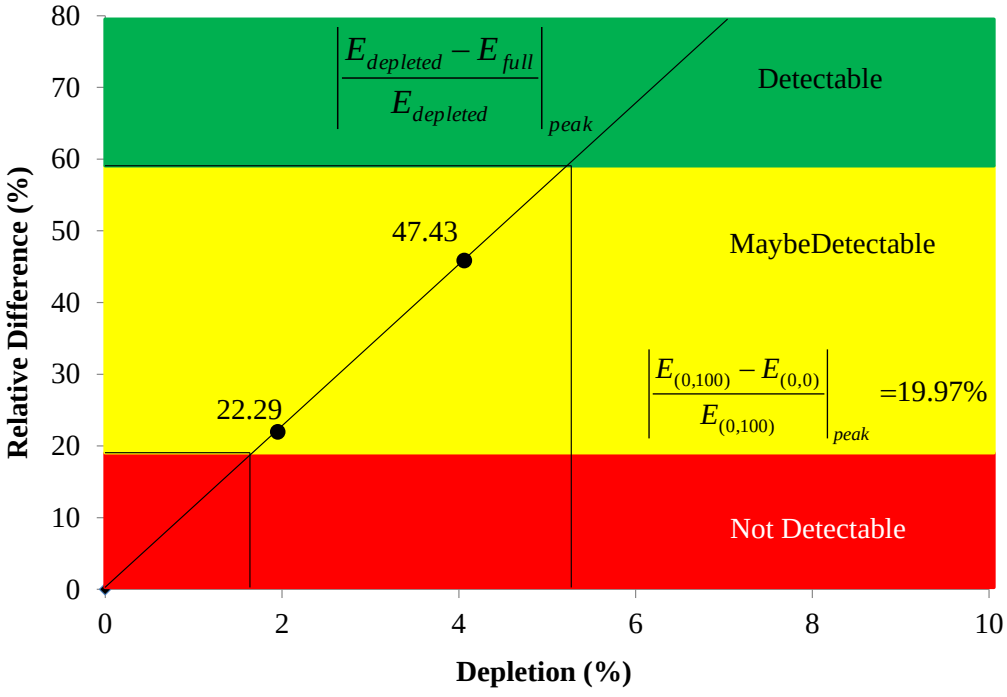

Figure 4. 40: The optimal frequency to detect the minimum depletion is 1.0 Hz and the minimum detectable depletion is 5%.

By evaluating other values of frequencies, the obtained results could be improved. Therefore, this evaluation yields the best result when the frequency is 1.0 Hz, as shown in Figure 4.40. Figure 4.40 indicates that the minimum detectable depletion is 5% when the receivers have been moved by 100 m along receiver lines. It is worth to mention that in this study, the upper frequency values of 2 and 3 Hz have been studied also. However, the relative differences in Ex for these frequencies are smaller than 1 percent. The reason is probably because of the strong attenuation of high-frequency electromagnetic waves in the earth.

4.3.2 Inversion-based analysis

So far and in this section, we have seen from sensitivity analysis that the minimum depletion of 5% can be detected if the receivers are moved by exactly 100 m along receiver lines direction and frequency sets to 1.0 Hz. By using the inversion approach, we hope to get better detectability when the reservoir deplete over time. The receivers are shifted by random values which possess a Gaussian distribution with maximum distance of 100 m. Figure 4.41 compares the receiver positions. The left section of this figure shows the location of receivers when they are in original position and the right section shows that they are randomly moved by not more than 100 m.

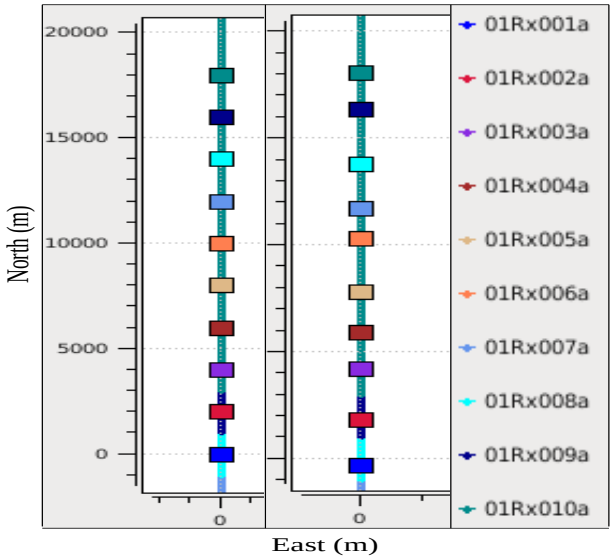

Figure 4. 41: Left) Receivers are located in original position right) Receivers have randomly been moved not more than 100 m.

Then, a fast and rigorous 2.5D inversion approach for the detection of the minimum depletion of reservoir in marine CSEM is applied. The results from the sections 4.2.3.2, 4.2.3.3 and 4.2.3.4 are pretty similar. Fixed background inversion approach is repeated here. The inverted result for full reservoir with the 1Ωm resistivity for start model and Rx as original position is already shown in Figure 4.29. For small depletion the results presented in Figure 4.30 can be used as well. The receivers are 100 m randomly shifted and the model has been inverted again. The result of inversion is shown in Figure 4.42. Figure 4.31 shows the difference between resistivity values for full reservoir with different values of seawater conductivity. Comparing this figure with Figure 4.43, a clear difference could be seen. Figure 4.43 shows that this difference is stronger than the variation of water conductivity effect.

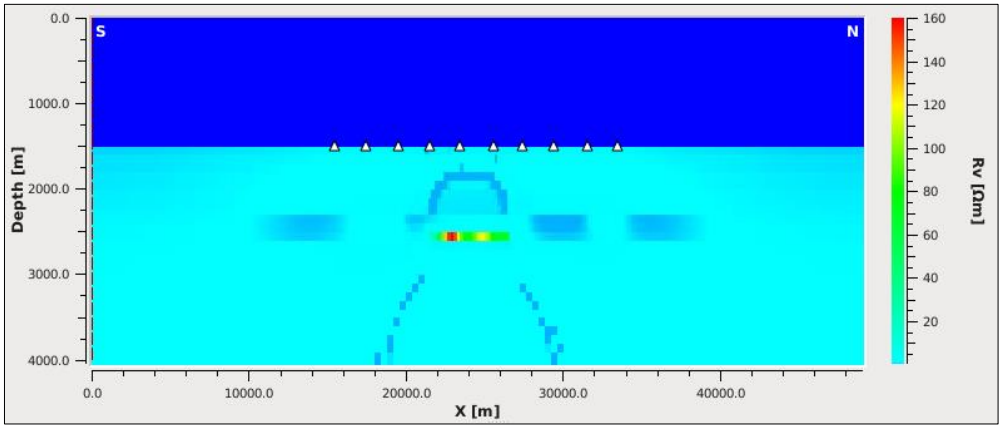

Figure 4. 42: Inverted result model when the receiver positions 100m are randomly shifted.

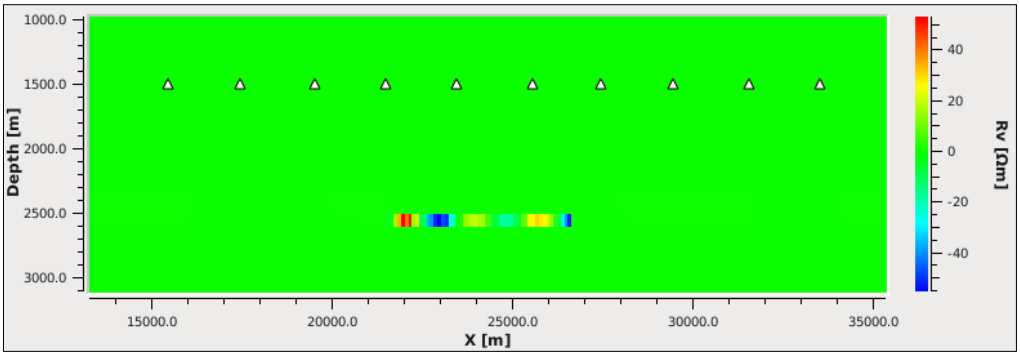

Figure 4. 43: Difference between inverted models when the receivers are in original position with the model when the receivers are randomly shifted by 100 m.

Table 4. 12: The average resistivity for different values of depletion, for two different receiver positions.

Data used for inversion are computed for			Start model for inversion	
Background (Ωm)	Target	Receiver positions (E,N)	Background (Ωm)	<AR> (Ωm)
1	Full	(0,0)	1	90.37(*)
1	Full	(0,0)	Final model from Inversion (*), target erased	**92.94**
1	2% depleted	(0,0)	Final model from Inversion (*), target erased	89.50
1	4% depleted	(0,0)	Final model from Inversion (*), target erased	88.65
1	6% depleted	(0,0)	Final model from Inversion (*), target erased	86.34
1	8% depleted	(0,0)	Final model from Inversion (*), target erased	85.02
1	10% depleted	(0,0)	Final model from Inversion (*), target erased	83.22
1	Full	50 m randomly shifted	Final model from Inversion (*), target erased	93.92
1	Full	100 m randomly shifted	1	98.85
1	Full	100 m randomly shifted	Final model from Inversion (*), target erased	**92.57**
1	Full	200 m randomly shifted	Final model from Inversion (*), target erased	94.85
1	Full	500 m randomly shifted	Final model from Inversion (*), target erased	97.78

The same process will be repeated here and the depleted reservoirs are inverted as well. The average anomalous resistivity values are calculated and are listed in Table 4.12. Table 4.12 shows that five different models with five different positions of Rx. Then, the inversion for full-reservoir with different positions of Rx is run. The average anomalous resistivity values are plotted as a function of maximum shifting of receiver position as shown in Figure 4.44. According to this figure the variation between the base model when the receivers are in the original position and the monitoring model when the receivers are randomly moved by not more than 100 m is investigated to calculate the minimum detectable depletion.

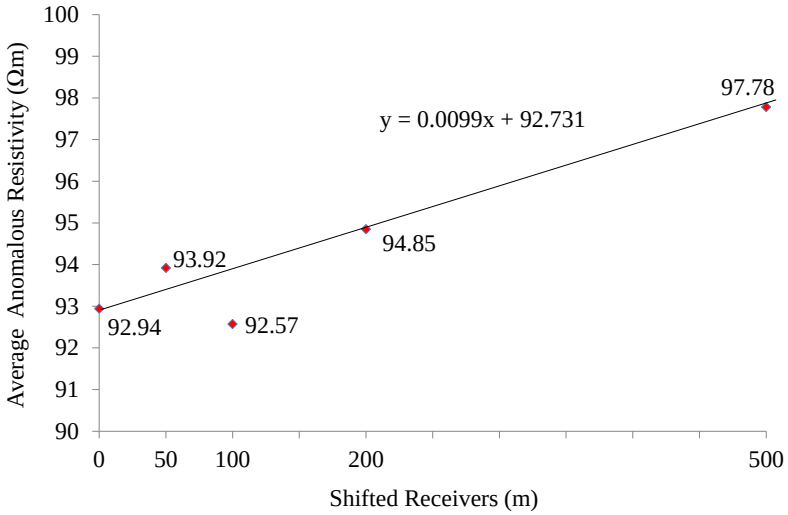

Figure 4. 44: Average anomalous resistivity values vs receiver position.

The relative resistivity difference obtained from the fitted trend line y = 0.0099x + 92.731 , is

$$\left|\frac{y_{100}-y_0}{y_{100}}\right| = \left|\frac{(0.0099\times 100+92.731)-(0.0099\times 0+92.731)}{0.0099\times 100+92.731}\right| = 0.0105$$

1-0.0105= 0.9895

The minimum detectable depletion can be obtained as shown in Figure 4.45. This figure shows that by having 0.1% difference in resistivity values compared to the reference model, the minimum depletion will be detectable when depletion is less than 1%.

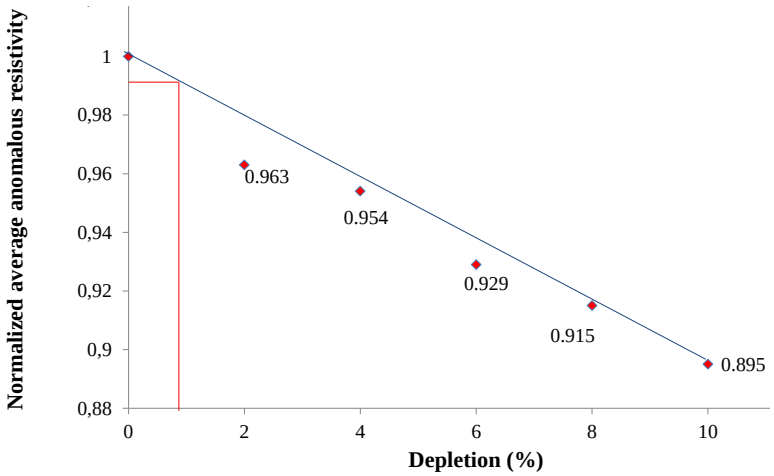

Figure 4. 45: The normalized average anomaly resistivity vs depletion plot to detect the minimum depletion when the receivers have randomly been moved by 100m.

Chapter 5 Conclusions and Recommendations

The potential and applicability of 4D (time-lapse) CSEM as a reservoir monitoring tool is investigated with respect to quantitative mapping of resistivity within large hydrocarbon reservoirs. The time-lapse CSEM data recorded over a producing reservoir for the base and monitoring surveys can be combined to detect and estimate the production-induced changes in the subsurface rock and fluid properties. The main purpose of this study is to obtain the minimum detectable depletion (MDD) of a hydrocarbon reservoir for the 4D CSEM when the water conductivity or the receiver positions are varied in the monitoring survey compared to the base survey. To achieve this, following two different approaches were utilized; (1) sensitivity analysis in the data domain and (2) inversion analysis in the model domain.

Following Orange et al. (2009), a 2.5D synthetic model is used for the simulations. The reservoir is 100 m thick and is buried1000 m below the seafloor. The synthetic model is gridded 491 square cells in X-direction and 81cells along the Z-direction. The size of each cell in the X-direction is 100 m, whereas the size of each cell in the Z-direction is 50 m.

The Estimation of MDD with Respect to Variation in the Seawater Conductivity

The sensitivity analysis with respect to the water conductivity shows that, in a marine environment, a 4.5% variation in the ocean water conductivity would bring about 6.52-8.38 % relative changes in the electrical field magnitude for the frequencies in the range 0.1-1 Hz. Considering this variation, the corresponding MDD is estimated to be about 2-7%. However, estimations based on the inversion method show different results because the incorporated background conductivities are not similar. In fact, three different conductivities are assumed including constrained, fixed, and wrong backgrounds. First, an inversion for a constrained background is performed. The estimated MDD (≈1%) shows a relative improvement compared to the results from sensitivity analysis. For fixed background, the MDD of less than 2% is obtained when the resistivity is assumed 1Ωm. A MDD of 2% is obtained for the wrong background when 10% error is applied for the fixed background resistivity. However, it should be noticed that there is also some error in these calculations due to uncontrolled randomness in inversion results. In summary, the estimations shows a higher potential for using inversion since 4.5% water conductivity variation gives only 0.8% variation in the inverted average reservoir resistivity, despite the measured fields change by as much as 6-8%

as follow from the sensitivity analysis. Moreover, the estimated MMD using inversion method (~1-2%) is very much less than the estimation from sensitivity analysis (~2-7%).

The Estimation of MDD with Respect to Variation in the Receiver Position

The same procedure is used to investigate the effect of variations in the receiver position in the monitoring survey compared to the base survey. The receivers are moved along the receiver line by 25, 50, 100, 200 and 500 meter relative to their original location. The performed sensitivity analysis using frequencies of 0.1-1 Hz shows 7.42-19.97% relative difference in the electrical filed magnitude. The corresponding MMD is estimated 5-7%. For the inversion analysis, we find a relative change of 0.1% in the average reservoir resistivity due to random shifting of the receiver positions within 100 m, and the estimated MDD in this case was less than 1%.

The current study can be extended in the following ways:

- By considering the effect of noise added to the data has been investigated partly in this thesis. A better analysis requires using field data including noise. In addition, it is necessary to repeat the same procedure using
- By considering different reservoir models (see e.g. Appendix A)
- By considering more complicated geological models, in particular, 3D models instead of 2.5D.
- By using field data

References

BARKER, N., MORTEN, J. & SHANTSEV, D. 2012. Optimizing EM data acquisition for continental shelf exploration. *The Leading Edge,* 31**,** 1276-1284.

BLACK, N., WILSON, G. A., GRIBENKO, A. V., ZHDANOV, M. S. & MORRIS, E. 3D inversion of time-lapse CSEM data based on dynamic reservoir simulation of the Harding field, North Sea. 81st SEG Annual International Meeting, 2011.

CONSTABLE, S. 2006. Marine electromagnetic methods—A new tool for offshore exploration. *The Leading Edge,* 25**,** 438-444.

CONSTABLE, S. 2010. Ten years of marine CSEM for hydrocarbon exploration. *Geophysics,* 75**,** 75A67-75A81.

CORUH, E. S. R. C. 1988. *Basic Exploration geophysics*, Iran, Ferdowsi University Press.

EIDESMO, T., ELLINGSRUD, S., MACGREGOR, L., CONSTABLE, S., SINHA, M., JOHANSEN, S., KONG, F. & WESTERDAHL, H. 2002. Sea bed logging (SBL), a new method for remote and direct identification of hydrocarbon filled layers in deepwater areas. *First break,* 20.

ELLINGSRUD, S., EIDESMO, T., JOHANSEN, S., SINHA, M., MACGREGOR, L. & CONSTABLE, S. 2002. Remote sensing of hydrocarbon layers by seabed logging (SBL): Results from a cruise offshore Angola. *The Leading Edge,* 21**,** 972-982.

EMGS 2011. SBLwiz 2.5D Inversion User Manual. emgs.

ENVCOGLOBAL. 2014. *Environmantal Equipment Suppliers* [Online]. HTTP://www.Envcoglobal.com/.

ESPELAND, M. 2014. Introduction to SBLwiz. Norway.

FILLOUX, J. H. 1967. Oceanic electric currents, geomagnetic variations and the deep electrical conductivity structure of the ocean-continent transition of central California. DTIC Document.

FONAREV, G. 1982. Electromagnetic research in the ocean. *Surveys in Geophysics,* 4**,** 501-508.

GELIUS, L. J., TA 2010. *Petroleum geophysics*.

GELIUS, L. J. & WANG, Z. 2008. Modelling production caused changes in conductivity for a siliciclastic reservoir: a differential effective medium approach. *Geophysical Prospecting,* 56**,** 677-691.

HANSEN, K. R. 2014. Introduction to Inversion.

KEY, K. 2009. 1D inversion of multicomponent, multifrequency marine CSEM data: Methodology and synthetic studies for resolving thin resistive layers. *Geophysics,* 74**,** F9-F20.

LIEN, M. & MANNSETH, T. 2008. Sensitivity study of marine CSEM data for reservoir production monitoring. *Geophysics,* 73**,** F151-F163.

LOVATINI, A., KUMAR, R., AL-SAEED, M., KHALID, A., PEZZOLI, M., BATTAGLINI, A., CECI, F. & ROTH, J. Land Controlled-source Electromagnetic Surveying for Viscous Oil Characterization in Kuwait. 75th EAGE Conference & Exhibition incorporating SPE EUROPEC 2013, 2013.

LØSETH, L. O. 2007. *Modelling of controlled source electromagnetic data.* NTNU.

MEHTA, K., NABIGHIAN, M., LI, Y. & OLDENBURG, D. Controlled Source Electromagnetic (CSEM) technique for detection and delineation of hydrocarbon reservoirs: an evaluation. 2005 SEG Annual Meeting, 2005. Society of Exploration Geophysicists.

MORTEN, J., FANAVOLL, S., MROPE, F. & NGUYEN, A. Sub-basalt Imaging Using Broadside CSEM. 73rd EAGE Conference & Exhibition, 2011.

MUSSETT, A. E. & KHAN, M. A. 2000. *Looking into the earth: an introduction to geological geophysics*, Cambridge University Press.

NORMAN, T., ALNES, H., CHRISTENSEN, O., ZACH, J., EIKEN, O. & TJÅLAND, E. Planning time-lapse CSEM-surveys for joint seismic-EM monitoring of geological carbon dioxide injection. First EAGE CO2 Geological Storage Workshop, 2008.

ORANGE, A., KEY, K. & CONSTABLE, S. 2009. The feasibility of reservoir monitoring using time-lapse marine CSEM. *Geophysics,* 74**,** F21-F29.

PANKRATOV, O. V. & GERASKIN, A. I. On processing of controlled source electromagnetic (CSEM) data. Geologica acta, 2010. 0031-49.

PARK, J., BJØRNARÅ, T. I. & FARRELLY, B. A. Absorbing boundary domain for CSEM 3D modelling. Proceedings of COMSOL conference, November, 2010. 17-19.

SCHLUMBERGER. 2014. *Schlumberger* [Online]. [Accessed 05.12.2014 2014].

SHAHIN, A., KEY, K., STOFFA, P. L. & TATHAM, R. H. Time-lapse CSEM analysis of a shaly sandstone simulated by comprehensive petro-electric modeling. 2010 SEG Annual Meeting, 2010. Society of Exploration Geophysicists.

TEHRANI, A. M. & SLOB, E. 2013. Applicability of 1D and 2.5 D marine controlled source electromagnetic modelling. *Geophysical Prospecting,* 61**,** 602-613.

TIAB, D. & DONALDSON, E. C. 2011. *Petrophysics: theory and practice of measuring reservoir rock and fluid transport properties*, Gulf professional publishing.

WANG, M., DENG, M., ZHANG, Q. & CHEN, K. The study on synchronization technology for marine controlled source electromagnetic survey. Electronic Measurement & Instruments, 2009. ICEMI'09. 9th International Conference on, 2009. IEEE, 1-491-1-495.

WANG, Z. & GELIUS, L.-J. 2007. Modeling of seabed logging data for a sand-shale reservoir. *Piers online,* 3**,** 236-240.

WANG, Z., GELIUS, L. J. & KONG, F. N. A sensitivity analysis of the sea bed logging technique with respect to reservoir heterogeneities. 2008 SEG Annual Meeting, 2008. Society of Exploration Geophysicists.

WAXMAN, M. H. & THOMAS, E. 1974. Electrical conductivities in Shaly Sands-I. The relation between hydrocarbon saturation and resistivity index; II. The temperature coefficient of electrical conductivity. *Journal of Petroleum Technology,* 26**,** 213-225.

WIRIANTO, M., MULDER, W. & SLOB, E. 2010. A feasibility study of land CSEM reservoir monitoring in a complex 3-D model. *Geophysical Journal International,* 181**,** 741-755.

ZACH, J., FRENKEL, M., RIDYARD, D., HINCAPIE, J., DUBOIS, B. & MORTEN, J. Marine CSEM time-lapse repeatability for hydrocarbon field monitoring. 2009 SEG Annual Meeting, 2009. Society of Exploration Geophysicists.

Appendices

Appendix A

To increase the confidence we have another model as well.

A1 Effect of Perturbation of receiver

In this appendix it will be examined applicability of the CSEM method to the reservoir-monitoring problem by analyzing representative 2.5D model for several cases. The difference between these cases is only the location of receivers.

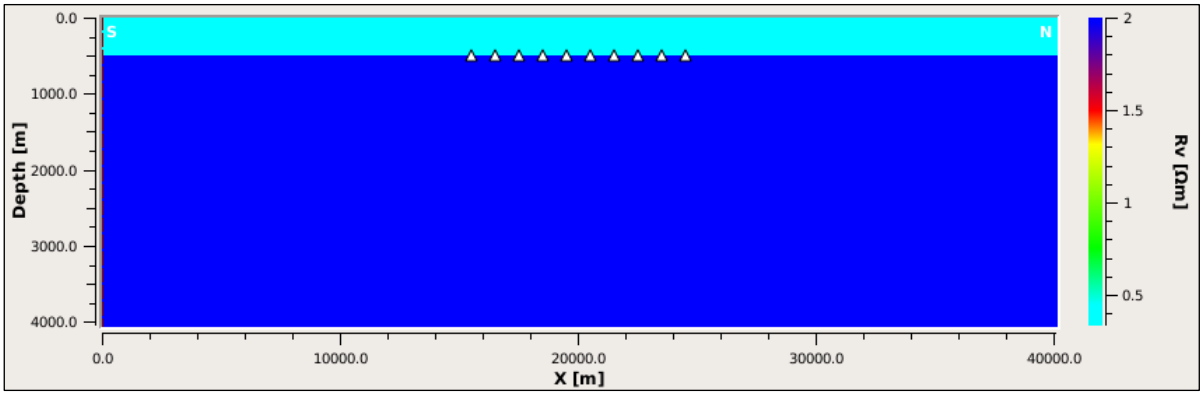

Figure A1: 1D model without target (half-space model).

A1.1 Case 1

The base model for our simulation is a 1D model, shown in Figure A1 which is representing the sea and sub-sea. Figure A2 shows structure which incorporates a thick, higher resistivity hydrocarbon filled layer. This model is the 2D analog of our 1D canonical reservoir and consists of a 300-m thick, 5-km wide, 50 Ωm reservoir buried 1000 m below the seafloor with an ocean depth of 500 m. This model will allow us to evaluate more realistically under what conditions such a thick layer can be detected.

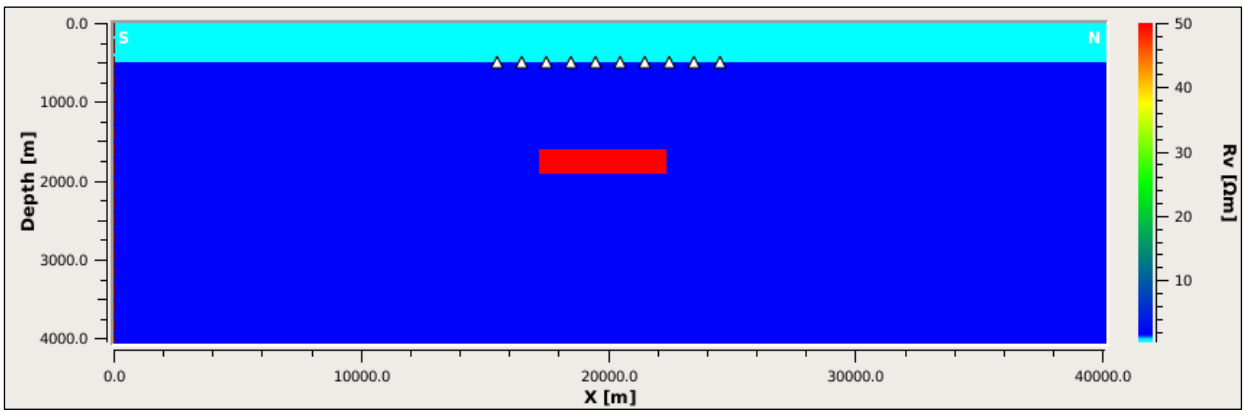

Figure A2: 2D model (with target).

Magnitude of electric fields is measured as a function of source-receiver offset (Figure A3) which shows the response of the inline electric field for the third located receiver. The breaks in slope in the response give clear indications of edges of the resistive layer. The relative increase in signal strength in the presence of a resistive layer is obvious and becomes more prominent with larger sea depth.

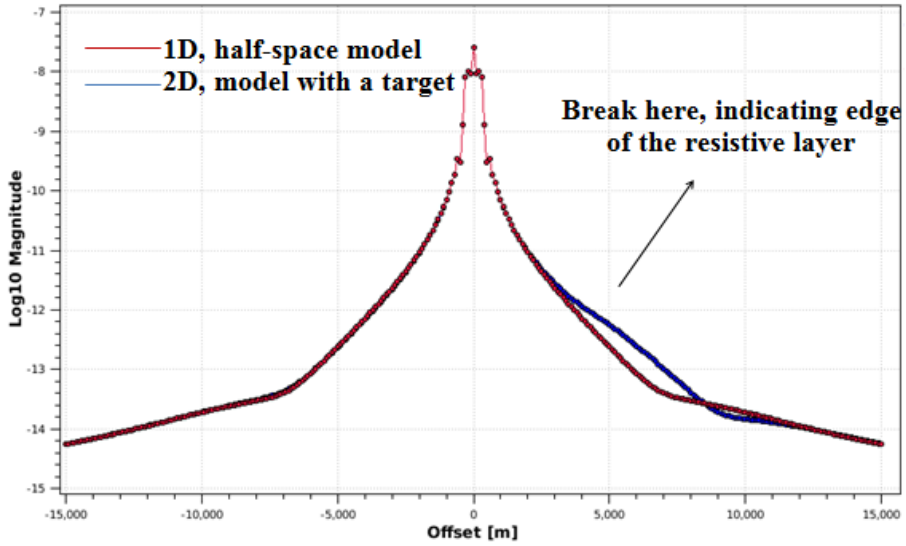

Figure A3: CSEM response for the 1D and 2D models for the electric field Ex, (Source frequency of 0.25 Hz and third receiver has been chosen).

The principle has been demonstrated for 10 receivers where the distance between two receivers is 1 km and then the receivers have been moved 200 m along receiver line direction.

The response of the inline electric fields for these cases has been shown in Figure A4 (left). There are two different results from the same area but with different positions of receivers. For both, it has been tried to have a plot and based on that, these results can be compared as

shown in Figure A4 (left). In this figure the magnitudes have been compared directly to identify the probably difference during the changing of receivers location. It is clear there is really very little differ and it will be difficult to detect if there is any difference at the all. However, there are certainly differences between these two results, but the values are relatively small and seem to be very small. But in the analysis, the relative plots of magnitude have usually been used. Figure A4 (right) shows the response variation. That means a 200 m moving of receivers yields approximately 2% error. This misfit can reach by using fallowing formula:

$$\left| \frac{E_{(0,200)} - E_{(0,0)}}{E_{(0,200)}} \right| \times 100\%$$

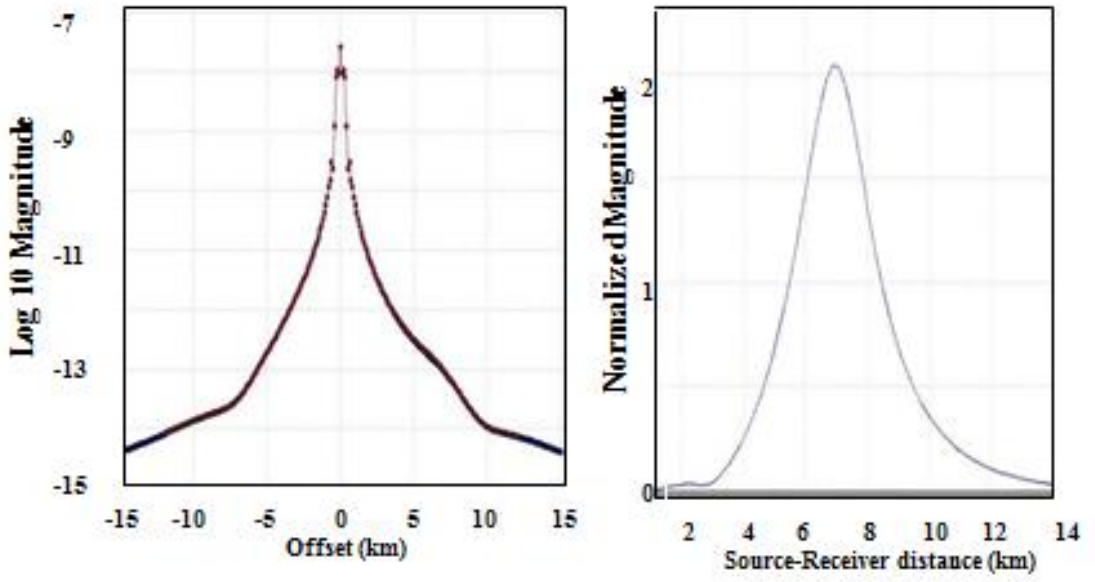

Figure A4: The response of the inline electric field, left), the magnitudes have been compared directly to identify the probably difference during the changing of receiver location, right) the relative plots of magnitude, frequency=0.25 Hz.

The inversion attempts to minimize the error function. Based on that, for the first and second attempts when 10 receivers have been applied and the distance between two receivers was 1 km and then the receivers have been moved along receiver line by 200 m, respectively. For each of them, we have ten iterations. Comparing between these two attempts occurs for the last one (iterations number 10) of them which gives the best result. Figures A5a (inversion of the reference model) and A5b (the inversion of the model when the receivers have been moved along receiver line direction by 200 m) show the inversion results. It will be difficult

to detect the difference of resistivity between inversion models which has been down by 2.5D modeling in terms of resistivity or its invers, conductivity.

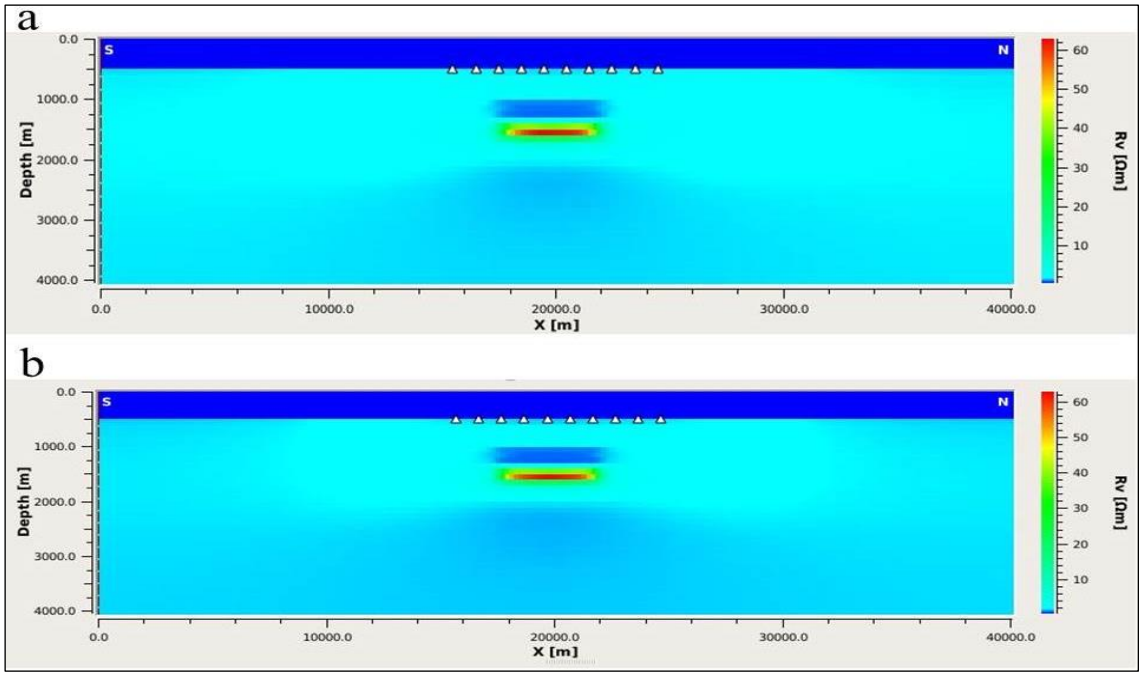

Figure A5: a) Inversion of base model, b) inversion of the monitoring model when the receivers have been moved by 200m along receiver lines.

At the same time, the Figure A6 shows the difference between these two iterations. This result indicates that the difference of the resistivity between these two receiver positions is more than 1Ωm.

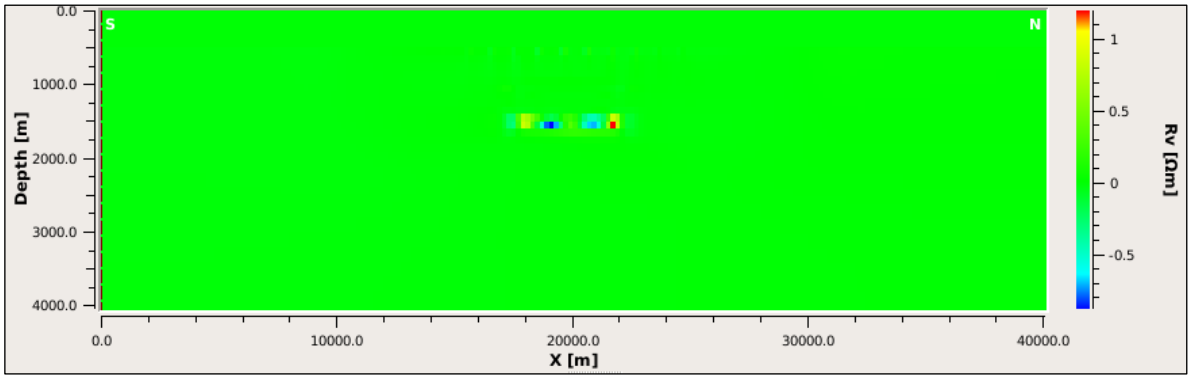

Figure A6: The difference of resistivity between two inversions results for two difference location of receivers.

To handle variation in the anomalous resistivity the average anomalous resistivity, <AR> is introduced. By having good inversion results, it will be possible to quantify their accuracy. One possibility is to integrate the anomalous resistivity over the volume of anomaly detected by inversion. Ideally, it should match the integrated anomalous resistivity of the true model. The resistivity of observed anomaly will be measured where the resistivity of target has given as 50 Ωm and the resistivity of formation is 2 Ωm. The average resistive anomaly for both cases is computed.

The average resistivity anomaly, R_{box} has been calculated in a specific area including the target in interval 17000m < X < 23000m and 1300m < Z< 2000m and this value is 12.91 Ωm.

By following the work done by Gabrielsen et al. (2013) it was necessary to apply a correction factor of 1.28 in order to obtain a correct volume estimate.

The results will be compared together and shown in Table A.2. But let just do this approach in other cases.

A1.2 Case 2

For this attempt, where the figures of base models, not shown here, the base model uses as has already been used. Then, the receivers will be moved 50 0m along receiver line direction and the results will be compared as shown in Figure A7. The results of the relative plot of magnitude yields approximately more than 3% error. At the same time, the average resistivity of observed anomalous will be measured where the resistivity of target has given as 50 Ωm at the same interval as case 1. Then this model will be inverted as well and the measuring gives a value of the average anomalous resistivity by 12.85 Ωm.

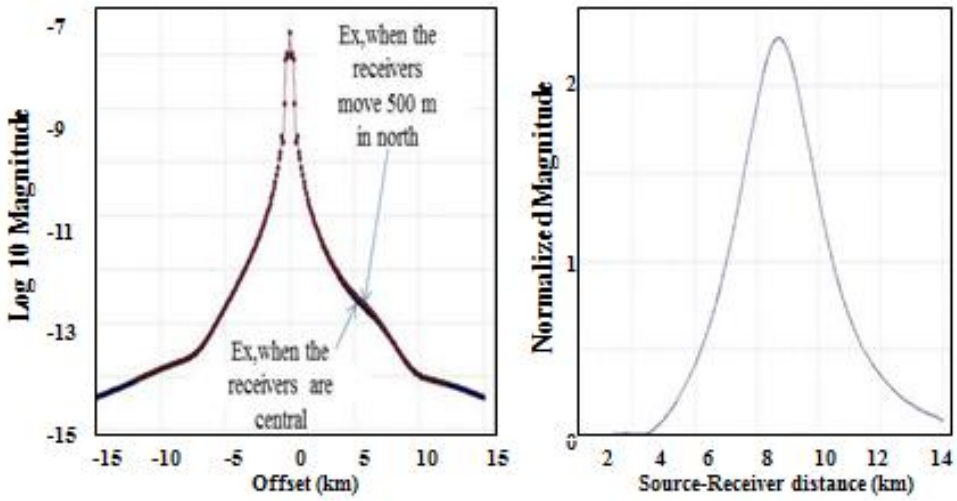

Figure A7: The response of the inline electric field, a) the magnitudes have been compared directly to identify the probably difference during the changing of receiver location, 500 m in north b) the relative plots of magnitude, frequency=0.25 Hz.

A1.3 Case 3

The inline electric field can detect where the hydrocarbon filled layer is, and it will be easier to find the location of hydrocarbon layer's edge if the receivers are outside of the target (Mehta et al., 2005). It means if the receivers are outside of the target, only the existence of the hydrocarbon layer will be depicted.

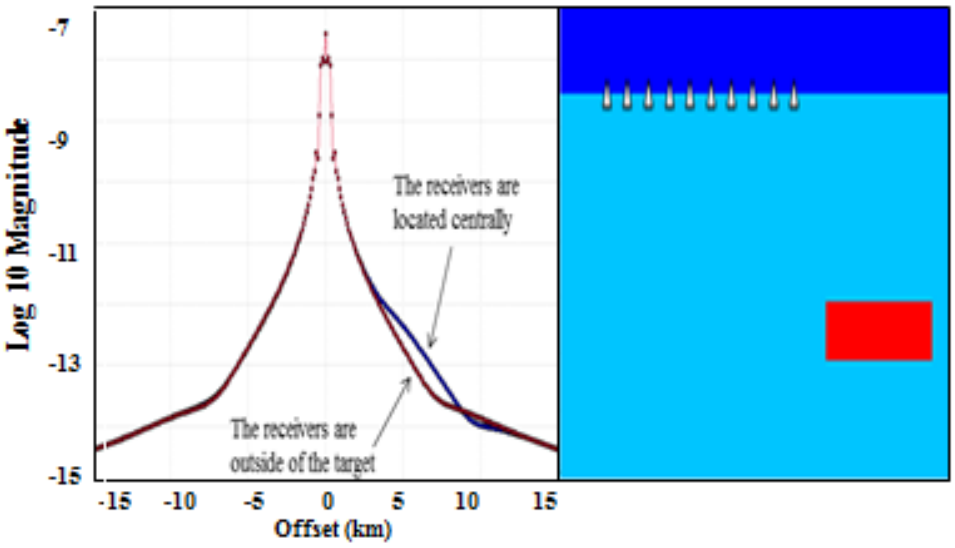

Figure A8: The receivers are located out from the right edge,(right) and comparing between the inline electric field for the base model (Blue line) and the model when a part of receivers are outside of target or monitoring (Red line), frequency=0.25 Hz, the third receiver from the right is selected.

The results of the relative plot of magnitude yield approximately around 6% error, as shown in Figure A9.

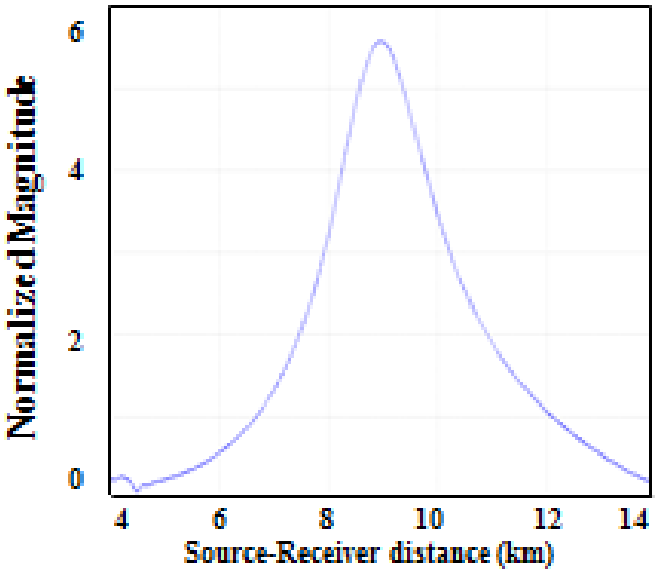

Figure A9: The relative plots of magnitude, based on Figure 5.11, Frequency=0.25 Hz and third receiver is selected.

In this case too, the resistivity of target like 50 Ωm would be kept and to take the average anomalous resistivity, the intervals for both in vertical and horizontal direction is kept as in case1. The new measuring gives <AR> = 9.04 Ωm. It shows that the misfit is very large and is around 8.75%. This indicates that in practice, the probability of error is very high.

Main observation of Case 1, Case 2 and Case 3

Table A1 shows the result from three attempts which has been done with the value of the relative plot of magnitude in present.

Table A1: The results from three differences location of receivers with the value of the relative plot of magnitude in present.

Case	Location of Receiver(E-N)	New Location of Receiver(E-N)	Measurement Uncertainty (%)
1	(0,0)	(0,200)	2
2	(0,0)	(0,500)	2.5
3	(0,0)	The receivers are outside of the target	6

According to the table A1, if the measurement uncertainty is close to 0, that means changing of the recorded Ex data is not so much and the volume's determination of HC layer can be

detected (Mittet and Morten, 2013). The correction factors for these cases have been calculated where the correction factor for true model and invert model in location (0, 0) is 1.57.

Table A2: The calculated <AR> and correction factor from three different receiver positions.

Case	New Location of Receiver(E-N)	Resistivity of base model (Ωm)	Average resistive anomalous <AR> (Ωm)	Correction Factor
1	(0,200)	50	12.85	1.58
2	(0,500)	50	12.76	1.59
3	The receivers are outside of the target	50	9.14	2.40

It will be characterized that by increasing the amount of this deviation, placement of receivers compared with their initial position has changed more.

By comparing the result from the base and monitored models, it can be found out, aside from the inversions results, only the location of receivers had been changed. That means this factor has more effect than another factors (Orange et al., 2009).

In this appendix the effect of receiver location on CSEM is investigated. But another important factor which has influence the marine CSEM is the location of the transmitter. In term of transmitter, when the transmitter is close to the receiver and the target, the signal will be dominated by direct field and the time-lapse signal will be masked. This approach has been used in this thesis and the distance between source and receivers varies between 30-50 m. However, when the distance is too large, detecting of the time-lapse signal will be difficult because this signal is weak in this position. It means the correct distance between source and receivers gives better result in CSEM method and this gives that the acquisition can be improved for a given target shape. Position of the source varies also because of the sail line to the vessel. Therefore, the sail line is also a factor affecting the results of CSEM method. Because in terms of repeatability, vessel must take this line which had taken the data from and it means the same location and the same line before. Otherwise, the position of the source will be changed and the recorded data will be different.

Appendix B: Source codes

After logging to your home workspace the following command could be used:

B1. Layout Input Parameters

Northing:	[Northing (N0) coordinate of model coordinate system origin]
Easting:	[Easting (E0) coordinate of model coordinate system origin]
Depth:	[Depth (D0) coordinate of model coordinate system origin]
Phi:	[Angle (deg, clockwise) between navigation north axis and model x axis]
UTM Zone:	[UTM zone which the model is in. 0 is unknown]
Hemisphere:	[The hemisphwere where the model is]
Source type:	[The underlying file format the model is read from]

B2. Data description

Property:	[What the data is]
Unit:	[The unit of the data]
Origin x:	[Origin x in the model coordinate system (x0)]
Origin y:	[Origin y in the model coordinate system (y0)]
Origin z:	[Origin z in the model coordinate system (z0)]
Cell size x:	[Cell size in the x direction (dx)]
Cell size y:	[Cell size in the y direction (dy)]
Cell size z:	[Cell size in the z direction (dz)]
Cells x:	[Number of cells in the x direction (nx)]
Cells y:	[Number of cells in the y direction (ny)]

Cells z :	[Number of cells in the z direction (nz)]

B3. Target Input Parameters

B3.1. elregrid [OPTIONS]

USAGE:	elregrid [OPTIONS]
Options:	
insp=off	Inspect header and terminate if insp=yes
File options:	
ginfil=gin.Rom	Input grid file
gutfil=gut.Rom	Output grid file
utf=qad	Output format can be qad or cbin (without header)
Smoothing options:	
flt=off	Perform model smoothing
findwdepth=off	Find x,y dependent water depth above which no smoothing occurs
minwcond=2	Parameter to identify water, minimum S/m
zmin=0	No smoothing above this depth (obsolete)
lx=	Filter length in number of cells, x direction
ly=	Filter length in number of cells, y direction
lz=	Filter length in number of cells, z direction
px=	Keep x wavenumbers up to this percentage (specify either lx or px)
py=	Keep y wavenumbers up to this percentage (specify either ly or py)
pz=	Keep z wavenumbers up to this percentage (specify either lz or pz)
Regridding options:	
dx=	New cell size in x direction (meter)
dy=	New cell size in y direction (meter)
dz=	New cell size in z direction (meter)

dir=def	Can be def or tra (default/transposed)
ysize=	Increase to new size in y-direction if given
Coordinate change (only in header):	
x0new=	Change origin header value x0 if given
y0new=	Change origin header value y0 if given
z0new=	Change origin header value z0 if given
dxnew=	Change cell size dx without regridding
dynew=	Change cell size dy without regridding
dznew=	Change cell size dz without regridding
Adding anomalous region:	
anom=off	Add anomalous region to existing model
x0res=0	Smallest x-value for anomaly
y0res=0	Middle y-value for anomaly
z0res=0	Smallest z-value for anomaly
tetres=0	Rotation angle for anomaly
lenres=0	Length of anomaly
widres=0	Width of anomaly
higres=0	Height of anomaly
resres=0	Resistivity for anomaly (Ohm m)
Program info:	
usage=	For more help, type 'elregrid --usage'
version=	Use --version to print the program version.

B3.2. Submodel " to crop the anomalous region

USAGE: submodel [OPTIONS]	
Options: Model options:	
input=	File containing the input model.
output=	File containting the output file name. Extension must be the same as input.
Data file options:	
datainput=	Comma separated list of files containing the input data (nc format).
coordconv=off	Convert coordinates in input data to model coordinate system. Only relevant if datainput is given [on,off].
minrxdist=0	Minimum distance from receiver to the edge of the submodel. Only relevant if the input is a 3D model, and datainput is given.
min_xy_ratio	Force the output model's XY-geometry to be within a given ratio. Value between 0 and 1.
only_extrapolate=off	Only extrapolate and don't cut model. Only relevant if datainput given. See usage for details [on,off].
Submodel extent options:	
x1=	First corner of submodel, x-coordinate, in local coordinate system.
y1=	First corner of submodel, y-coordinate, in local coordinate system.
z1=	First corner of submodel, z-coordinate, in local coordinate system.
x2=	Last corner of submodel, x-coordinate, in local coordinate system.
y2=	Last corner of submodel, y-coordinate, in local coordinate system.
z2=	Last corner of submodel, z-coordinate, in local coordinate system.
modeltemplate=	Use the XY corners of this model instead of specifying the coordinates.
Pad/crop options:	
xadd=0	Symmetrically extend submodel in x-direction by +/- xadd.

yadd=0	Symmetrically extend submodel in y-direction by +/- yadd.
zaddbottom=0	Asymmetrically extend bottom of submodel in z-direction by +/- zadd.
Extrapolation options:	
extrapolate=off [on,off].	Extrapolate output model. Must be set if output is bigger than input
extlimit=	Extrapolation limit in xy [m]. Program will exit with error if extrapolation distance is above this limit.
Logging:	
version=	Use --version to print the program version.
verbose=0	Verbose level.
logfile=	Log file
Configuration:	
config=	Configuration file containing parameters.

B3.3. USAGE: elmodmath [OPTIONS] *(To get the difference between several models also)*

Options:	
m1=	Input model 1
m2=	Input model 2
m3=	Input model 3
m4=	Input model 4
m5=	Input model 5
alignlimit=	Alignment limit among input models in meters.
expr=	Mathematical expression
outmodel=	Output: name of output model.
Logging:	

version=	Use --version to print the program version.
verbose=0	Verbose level.
logfile=	Log file
Configuration:	
config=	Configuration file containing parameters.

B3.4. elmoddump [OPTIONS]

USAGE: elmoddump [OPTIONS]	
Options:	
ifel=>>	Input file
Information to display:	
geometry=on	Show model geometry information
grid_ticks=off	Grid axes tick values ('on', 'off')
verify=off	Inspect values and print occurrences of nans and infs. Min and max values are also displayed ? ('on', 'off')
unique=off	Print unique values of cells?('on', 'off')
all=off	Print values for all calls / voxels? ('on', 'off')
Logging:	
version=	Use --version to print the program version.
verbose=0	Verbose level.
logfile=	Log file
Configuration:	
config=	Configuration file containing parameters.

B3.5. elmodconvert [OPTIONS]

File options:	
ifel=	Filename of the input model.
ofel=	Filename of the output file.
General options:	
inputhandedness=	Set handedness for files where this is unknown. Valid values are (right,left).
Options for model file output:	
outputversion=	Output file version. Default is newest. If you need old style newrom, use 0.1
phi=	Force phi angle of output model to this. Must be in the interval (0, 360). Useful for rom -> newrom/rmsrom.
proptype=	Set property type. Can only be stored in newrom >=1.0. Valid values are (cond,cond_h,cond_v,res,res_h,re s_v,bath).
utmzone=	Set UTM zone. Can only be stored in newrom >= 1.0.Must be in the interval [1,60].
hemisphere=	Set the hemisphere. Can only be stored in newrom >= 1.0. Valid values are (north,south).

B4. Options for segy file output:

ep=100	Energy source point number in trace header.
invert=on	Invert trace data values. Can be set to 'on' or 'off'.
ibmfloats=off	Write IBM instead of IEEE floats in SEG-Y (GeoFrame needs this!). Can be 'on' or 'off'.
Logging:	
version=	Use --version to print the program version.
verbose=0	Verbose level.
logfile=	Log file

Configuration:	
config=	Configuration file containing parameters.

SEGy :

addpath SegyMAT
addpath SegyMAT/GUI
[Data,SegyTraceHeaders,SegyHeader]=ReadSegy('INVERSION23_acceptedmodel_it012.segy');

B5. USAGE : elmath [options]

ifel=>>:	Input file.
ofel=<<:	Output file.
op=noop:	Operation flag. abs, add, mult, norm, (s)power, sin, cos, log, log10, exp. All data are scaled by Escale/Hscale before operation, ex: add;data->(data*Xscale)+fac
fac=1.0:	Factor for operations that requires it (add, mult and power)
cfac=0.0:	Complex part of fac (only for add and mult)
Escale=1.0:	Scale factor E field. For op=noop (default), only scaling will be done
Hscale=1.0:	Scale factor H field.
cur=off:	Process current, on or off. NB! if cur=on all other traces are ignored

B6. Receivers moved randomly:

~/addNavNoise

Program needs at least one argument to start

Default arguments:

ifel=ifel.nc:	names for input NC file OR folder name
ofel=ofel.nc:	names for output NC file OR folder name
rxNoise=0:	white noise in receiver x
ryNoise=0:	white noise in receiver y
sxNoise=0:	white noise in source x
syNoise=0:	white noise in source y
szNoise=0:	white noise in source z
spitchNoise=0:	white noise in source pitch
sxShift=0 :	systematic shift in source x
syShift=0:	systematic shift in source y
szShift=0:	systematic shift in source z
spitchShift=0:	systematic shift in source pitch
alenShift=0 :	systematic shift in source length (all fields are proportional to it)
wavelength=0 :	wavelength (m) of shift. If <1e-2 then performs parallel shift
nsin=4:	number of sines to represent pseudorandom variation
mult=0:	multiplicative noise in all fields, uncorrelated, e.g. 0.05
eta=0:	additive noise in E fields, uncorrelated, e.g. 1e-15, can be comma-separated
etaH=0 :	additive noise in H fields
multtype=gauss:	mult noise amp distribution: gauss/fixed(amp is mult)
etatype=gauss:	additive noise amp distribution: gauss/uni(uniform)/fixed(amp is eta)

seed=1:	random seed
plot=0 :	plot noisy navigation? 0 or 1
verbose=1:	Level of controll output.
Version:	Unknown

B7.Convert data to use in matlab:

sblwiz -shell

Options:		
version	show program's version number and exit	
listconfig	Print valid config values and exit	
ifel=	Input file	
ifel_noise=	None	Input noise file
ifel_mask=	None	Input mask file
ofel=	Output file	
config=	AllInOne	Output configuration
cat outputfile.txt | gawk '(print $1 , $2)' > outputfile		
gedit outputfile		

B8. To drew the difference data together in matlab:

dlmread : Read ASCII-delimited file of numeric data into matrix
M = dlmread(filename)
M = dlmread(filename, delimiter)
M = dlmread(filename, delimiter, R,C)
M = dlmread(filename, delimiter, range)
M = dlmread(filename) readsthe ASCII-delimited numeric data file filename,and returns the data in output matrix M. The filename inputis a string enclosed in single quotes. dlmread infersthe delimiter from the formatting of the file.
M = dlmread(filename, delimiter) readsdata from the file, using the specified delimiter.Use '\t' to specify a tab delimiter.
M = dlmread(filename, delimiter, R,C) reads data whose upper left corner is at row R andcolumn C in the file. Values R and C arezero-based, so that R=0, C=0 specifiesthe first value in the file.
M = dlmread(filename, delimiter, range) readsthe range specified by range = [R1 C1 R2 C2] where (R1,C1) isthe upper left corner of the data to read and (R2,C2) isthe lower right corner. You can also specify the range using spreadsheetnotation, such as range = 'A1..B7'.